UNIVERSITY OF SOUTHAMPTON

Development of Bi-doped Fibre Amplifiers and Lasers & Broadband Er-doped Multi-Element Fibre Amplifiers

by

Naresh Kumar Thipparapu

A thesis submitted in fulfillment for the
degree of Doctor of Philosophy

in the
Faculty of Physical and Applied Sciences
Optoelectronics Research Centre

March 2018

Declaration of Authorship

I, Naresh Kumar Thipparapu, declare that this thesis titled, 'Development of Bi-doped Fibre Amplifiers and Lasers & Broadband Er-doped Multi-Element Fibre Amplifiers' and the work presented in it are my own. I confirm that:

- This work was done wholly or mainly while in candidature for a research degree at this University.
- Where any part of this thesis has previously been submitted for a degree or any other qualification at this University or any other institution, this has been clearly stated.
- Where I have consulted the published work of others, this is always clearly attributed.
- Where I have quoted from the work of others, the source is always given. With the exception of such quotations, this thesis is entirely my own work.
- I have acknowledged all main sources of help.
- Where the thesis is based on work done by myself jointly with others, I have made clear exactly what was done by others and what I have contributed myself.

Signed:

Date:

UNIVERSITY OF SOUTHAMPTON

Abstract

Faculty of Physical and Applied Sciences

Optoelectronics Research Centre

Doctor of Philosophy

by Naresh Kumar Thipparapu

The demand for fibre optic communication is continuously increasing over the years. This is due to the increased accessibility to the World Wide Web using internet of things. The capacity of current fibre optic communication through the single mode fibre is limited by the amplification bandwidth of Er-doped fibres. To increase the capacity of fibre optic communication research community around the world are proposing different approaches. One of them is to use the low loss window (1260-1625nm) of silica optical fibres by developing efficient fibre amplifiers and lasers. Another one is to use novel fibres such as multi-core fibres, multi-mode fibres and multi-element fibres (MEFs) for space division multiplexing in the C-band (1525-1565nm).

In this thesis, we developed amplifiers and lasers within the wavelength band from 1150-1625nm using Bi-doped and multi-element Er-doped fibres. Here, we investigated the fabrication of Bi-doped optical fibres in different glass hosts (aluminosilicate and phosphosilicate) using MCVD-solution doping technique. Bi-doped aluminosilicate fibres are used to develop an amplifier with 12dB gain at 1180nm. Bi-doped phosphosilicate fibres are used to develop amplifiers and lasers in the second telecommunication band from 1300-1360nm. An all-fibre Bi-doped phosphosilicate amplifier with a 25dB flat gain in a 40nm bandwidth from 1320-1360nm is reported. Also, a Bi-doped fibre laser operating at 1360nm with an output power of 110mW, and a picosecond pulsed mode-locked fibre laser operating at 1340nm with a peak power of 1.15W, are demonstrated. These amplifiers and lasers have important applications in medicine, astronomy and optical fibre communication. In addition, we also discussed the novel fibres known as MEFs and developed core and cladding pumped broadband amplifiers covering 1500-1620nm using multi-element Er and Er/Yb-doped fibres, respectively.

Acknowledgements

I consider this opportunity to express my deepest gratitude to my supervisor Prof. Jayanta Sahu for his guidance and continuous encouragement during this work. I wish to thank the UK Engineering and Physical Sciences Research Council (EPSRC) for providing support to my research through the Hyperhighway project.

I also thankful to the Optoelectronic Research Centre (ORC), University of Southampton, UK for offering me PhD and providing me all the facilities required to successfully complete it. I also thank Prof. Dan Hewak and Dr. Morten Ibsen for their valuable time for evaluating eighteen-month and sixteen-month reports, respectively.

I also express my sincere thanks to T. C. May-Smith, A. S. Webb and Rob. J. Standish for their time to train me in operating different systems in the silica fibre fabrication group. It gives me a great pleasure in acknowledging the support and help of Dr. Pranabesh Barua, Dr. Andrey A. Umnikov, Dr. Saurabh Jain and Dr. Deepak Jain for their friendly nature and helping me all the way during this work.

I would also like to thank the ORC staff for spending their valuable time in discussions and providing me equipment from their labs whenever needed. I also thank the academic staff of the University of Southampton for providing me required documents to attend conferences.

I also thank all my friends around the world especially from India and England who are part of this journey.

At the most, I express my sincere thanks to my father and mother and also to my beloved brother and sister for their tremendous support and motivation throughout my life.

Contents

Declaration of Authorship i

Abstract iii

Acknowledgements iv

List of Figures viii

List of Tables xii

Abbreviations xiii

1 Introduction 1
- 1.1 Motivation . . . 1
  - 1.1.1 Introduction to Bi-doped fibres . . . 4
  - 1.1.2 Luminescence characteristics of Bi-doped fibres . . . 6
  - 1.1.3 Origin of near-infrared luminescence . . . 7
- 1.2 Unsaturable loss and excited state absorption . . . 11
  - 1.2.1 Unsaturable loss . . . 11
  - 1.2.2 Excited state absorption . . . 12
- 1.3 State of the art of Bi-doped fibre lasers and amplifiers . . . 15
  - 1.3.1 Bi-doped fibre lasers and amplifiers from 1150-1250nm . . . 15
  - 1.3.2 Bi-doped fibre lasers and amplifiers from 1280-1500nm . . . 16
  - 1.3.3 Bi-doped fibre lasers and amplifiers from 1600-1800nm . . . 18
- 1.4 State of the art of Bi-doped pulsed fibre lasers . . . 19
  - 1.4.1 Bi-doped pulsed fibre lasers from 1150-1250nm . . . 19
  - 1.4.2 Bi-doped pulsed fibre lasers from 1280-1500nm . . . 20
  - 1.4.3 Bi-doped pulsed fibre lasers from 1600-1800nm . . . 22
- 1.5 Superfluorescent sources (SFS) in different wavelength bands using Bi-doped fibres . . . 22
- 1.6 Multi-element fibres . . . 23
- 1.7 Lay out of the thesis . . . 25

2 Fabrication and characterisation of Bi-doped optical fibres 27
- 2.1 Introduction . . . 27
- 2.2 MCVD-solution doping method . . . 27

2.3 Fibre drawing process . . . 30
2.4 Characterisation techniques . . . 31
2.4.1 Cut-back technique . . . 31
2.4.2 Unsaturable loss measurement . . . 32
2.4.3 Gain and noise figure measurement . . . 33
2.5 Fabrication of Bi-doped preforms . . . 34
2.5.1 Bi-doped aluminosilicate preforms . . . 35
2.5.2 Bi-doped phosphosilicate preforms . . . 36
2.5.3 High concentration Bi-doped phosphosilicate preforms . . . 36
2.6 Electron probe microanalysis of Bi-doped fibres . . . 38
2.6.1 EPMA of Bi-doped aluminosilicate fibre . . . 39
2.6.2 EPMA of Bi-doped phosphosilicate fibres . . . 39
2.7 Conclusion . . . 42

3 Development of Bi-doped aluminosilicate fibre amplifier 44
3.1 Introduction . . . 44
3.2 Laser guide star . . . 45
3.3 Bi-doped aluminosilicate fibre amplifier . . . 47
3.3.1 Experimental setup . . . 49
3.3.2 Results . . . 50
3.4 Conclusion . . . 53

4 Bi-doped fibre laser and amplifier in the second telecommunication wavelength band 55
4.1 Fibre fabrication and characterization . . . 55
4.2 Bi-doped fibre laser . . . 57
4.2.1 Introduction . . . 57
4.2.2 Experimental setup . . . 58
4.2.3 Results . . . 58
4.3 Bi-doped fibre amplifier with a flat gain of 25dB, operating in the wavelength band 1320-1360nm . . . 62
4.3.1 Introduction . . . 62
4.3.2 Experimental setup . . . 63
4.3.3 Results . . . 64
4.4 Conclusion . . . 68

5 Bismuth-doped all fibre mode-locked laser operating at 1340nm 70
5.1 Introduction . . . 70
5.1.1 Dispersion . . . 71
5.1.2 Spectral sidebands . . . 72
5.1.3 Autocorrelation . . . 73
5.2 Mode-locked Bi-doped fibre laser . . . 74
5.2.1 Experimental setup . . . 74
5.2.2 Results . . . 75
5.3 Master oscillator power amplifier . . . 79
5.3.1 Experimental setup . . . 79
5.3.2 Results . . . 79
5.4 Autocorrelation . . . 81

5.5 Conclusion 83

6 Core and cladding pumped wideband multi-element Er-doped fibre amplifiers in C+L bands 84
6.1 Core pumped wideband multi-element Er-doped fibre amplifier 84
6.1.1 Introduction 84
6.1.2 Experimental setup for 3-MEF characterisation 85
6.1.3 Results 86
6.1.4 Experimental setup for 7-MEF characterisation 89
6.1.5 Results 89
6.2 Cladding-pumped Er/Yb-doped multi-element fibre amplifier for wideband applications 94
6.2.1 Introduction 94
6.2.2 Experimental setup 95
6.2.3 Results 95
6.2.4 Conclusion 96

7 Conclusions and future scope 98
7.1 Bi-doped fibres for lasers and amplifiers 98
7.1.1 Introduction 98
7.1.2 Future scope 100
7.2 MEF fibres for broadband amplifiers 104
7.2.1 Introduction 104
7.2.2 Future scope 104

A Publications 105
A.1 Journal Publications 105
A.2 Conference publications 105

Bibliography 108

List of Figures

1.1 Attenuation spectra of conventional SMF and all-wave fibre 2
1.2 Bar chart showing the increase of internet users per each 10 year gap . . . 3
1.3 Spectral regions covered by various RE doped elements in silica host . . . 4
1.4 Energy level diagram of (a) Yb^{3+}, (b) Er^{3+}, (c) Tm^{3+} 5
1.5 Energy level diagram of (a) Pr^{3+}, (b) Nd^{3+} 5
1.6 Spectral regions covered by various Bi-doped fibres with different hosts . . 6
1.7 (a) Energy level diagram of Si-BAC (b) Energy level diagram of Ge-BAC 7
1.8 Quenching process leading to unsaturable loss in Er^{3+} 11
1.9 Unsaturable absortpion as a function of small signal absorption in various Bi-doped fibres 12
1.10 Er^{3+} energy level diagram, illustrating the process of ESA 13
1.11 (a) ESA of BASF (b) ESA in BASF with different concentration 13
1.12 (a) ESA of BGSF (b) ESA of BPSF 14
1.13 Variation of the output power with the absorbed pump power for Bi-doped fibre lasers at different lasing wavelengths. The lasing wavelength and the output coupling are indicated in each graph 17
1.14 Schematic representation of GT-wave concept 23
1.15 (a) Schematic of 7-MEF preform draw on tower (b) Schematic of 5-MEF (cladding pump) preform 24
1.16 (a) Microscopic image of 7-MEF (b) Microscopic image of 5-MEF 24

2.1 Schematic of MCVD process 28
2.2 Schematic solution doping process 29
2.3 Fibre drawing process 30
2.4 Schematic of cut-back technique 31
2.5 Schematic of unsaturable loss measurement 32
2.6 Experimental set up to measure gain and noise figure 33
2.7 Spectral measurements to determine gain and noise figure 33
2.8 Laser performance in different length of high concentration fibres fabricated 38
2.9 Normalized distribution of Al_2O_3 and Bi_2O_3 in fibre A0621 39
2.10 Normalized distribution of P_2O_5 and Bi_2O_3 in fibre A0623 40
2.11 Normalized distribution of P_2O_5 and Bi_2O_3 in fibre A0625 41
2.12 Normalized distribution of P_2O_5 and Bi_2O_3 in fibre A0787 41

3.1 Laser guide star 45
3.2 Refractive index profile of the fibres L30366-A0621 and L30367-A0647 . . 47
3.3 Absorption spectrum of Bi-doped aluminosilicate fibres 48
3.4 Loss variation with pump power for 1120 and 1047nm pump wavelengths 48

3.5 Schematic of the experimental setup to measure gain in Bi-doped fibre. (The 1047nm pump with dashed line was used for bi-directional pumping; otherwise, that port of the WDM was used to monitor the excess pump). 49
3.6 ASE spectra for 1047 and 1120nm pump wavelengths for 20 and 100m length of the fibre, respectively (Pump power: 350mW). 50
3.7 Gain variation with fibre length at 1180nm for two different pump wavelengths (Pump power: 350mW). 51
3.8 Gain variation with pump power at 1180nm for a 100m long fibre with a signal power of -4dBm 51
3.9 Gain variation with fibre length at 1180nm for bi-directional pumping (total pump power: 700mW) and for an input signal power of -4dBm. . . 52
3.10 Loss variation in Bi-doped fibre for single 1120nm pumping (black line) and for dual pumping (1120nm + 1047nm) by varying the power of 1047nm pump while operating the 1120nm pump at its maximum power of 350mW (violet line) 53

4.1 Refractive index profile of fibre (BPSF-3) measured by Inter Fibre Analyser (IFA) 56
4.2 Absorption spectra of Bi-doped phosphosilicate fibres 57
4.3 Schematic experimental setup of Bi-doped fibre laser 58
4.4 Optimum length of BPSF-2 for 390mW of pump power 59
4.5 Pump power vs. output power of BPSF-2 59
4.6 Optimum length of BPSF-3 for 390mW of pump power 59
4.7 Pump power vs. output power of BPSF-3 60
4.8 Output power vs launched pump power with different output coupling (OC) for 46m long BPSF-3 60
4.9 Optical spectrum of the Bi-doped fibre laser 61
4.10 Slope efficiency of 50m fibre with 50/50 coupling ratio 61
4.11 Optimum length for bi-directional pumping 61
4.12 Schematic experimental setup of Bi-doped fibre amplifier 63
4.13 ASE spectra for 1267nm or 1240nm pump wavelengths for a 100m long Bi-doped fibre when pumped with a maximum available power of laser diodes 64
4.14 Gain and NF characteristics for the maximum available power of 360mW (1267nm) or 400mW (1240nm) with optimum fibre lengths of 100m and 75m, respectively (Signal power: -10dBm) 65
4.15 Amplifier performance with bi-directional pumping by 1267nm (360mW) and 1240nm (400mW) LDs for a signal power of -10dBm 66
4.16 The flat gain characteristics of the amplifier from 1320-1360nm 66
4.17 Variation of gain and NF with pump power for bi-directional pumping at 1267nm and 1240nm for an input signal power of -10dBm and operating at a wavelength of 1340nm) 67
4.18 Characteristics of the amplifier with input signal power at wavelengths of 1300nm and 1340nm, when dual pumping with 1267nm and 1240nm laser diodes operating at their maximum power 67
4.19 Gain and NF characteristics of the amplifier by dual pumping at 1210nm or 1240nm pump in conjunction with 1267nm pump [pump powers: 1210nm or 1240nm @ 300W; 1267nm @ 360mW, signal power: -10dBm] 68

5.1 Pulse evolution in presence of anomalous dispersion and SPM 72
5.2 Experimental setup of the commercially available FR-103XL autocorrelator 73
5.3 Schematic experimental setup of mode-locked Bi-doped fibre laser 74
5.4 Pulse width and Rep.rate variation with different length of Bi-doped fibre for a single 1270nm laser diode pumping 75
5.5 Pulse width variation with pump power of 25m long Bi-doped fibre for a 1270nm laser diode pumping 76
5.6 Pulse train of the ML-BDFL at minimum and maximum pump power of 175 and 335mW, respectively with pulse widths of 1.5 and 3ns 76
5.7 Single pulse width variation with pump power 77
5.8 Optical spectrum of the ML-BDFL at a pump power of 335mW for a 25m long Bi-doped fibre 77
5.9 RF spectrum of the ML-BDFL at a pump power of 335mW for a 25m long Bi-doped fibre 78
5.10 Experimental setup of master oscillator power amplifier (MOPA) 79
5.11 Variation of signal power with pump power of MOPA for a fixed input seed power of 2.5mW (3.95dBm) 80
5.12 Signal power variation of MOPA with seed power for fixed pump power of 420mW 80
5.13 Autocorrelation trace of the mode-locked Bi-doped fibre laser 81
5.14 The $sech^2$ fitting of the autocorrelation trace 82
5.15 Optical spectrum of the ML-BDFL observed over 2hrs of time 82

6.1 3-MEEDFA schematic experimental setup to measure gain and NF of ;a-single fibre element, b-cascaded fibre elements (Inset: cross-sectional view of Er-doped 3-MEF) 85
6.2 Gain and NF of fibre elements S1, S2 and S3 for a pump power of 208mW for an input signal power of (a) -10dBm (b) -23dBm 86
6.3 Gain and NF variation in fibre element S3 of MEF for different input signal and pump powers 86
6.4 Gain and NF variation of 2-cascaded fibre elements for different input signal and pump powers 87
6.5 Gain and NF for cascaded two fibre elements with bi-directional pumping for an input signal of -10dBm, The pump power of one of the laser diodes was varied while the other laser diode was maintained at a fixed power of 60mW 88
6.6 Gain and NF for cascaded two fibre elements with bi-directional pumping for an input signal of -23dBm, The pump power of one of the laser diode was varied while the other laser diode was maintained at a fixed power of 60mW 88
6.7 7-MEEDFA schematic experimental setup to measure gain and NF of ;a-single fibre element, b-cascaded fibre elements (Inset: cross-sectional view of Er-doped 7-MEF) 89
6.8 Gain and NF with wavelength for Er-doped 7-MEF at a pump powers of 250mW for elements f1, f2, f3, f4, f5, f6 and f7 90
6.9 Variation of gain and NF with wavelength for single element of Er-doped 7-MEF at different pump powers 91
6.10 Gain and NF characteristics of 2-element cascade at a maximum pump power of 250mW 91

6.11 Gain and NF characteristics of different cascade configurations for bi-directional pumping with a total pump power of 320mW, input signal power: -10dBm 92
6.12 Gain and NF characteristics of different cascade configurations for bi-directional pumping with a total pump power of 320mW, input signal power: -23dBm 92
6.13 Performance of a split-band MEEDFA in the wavelength region of 1520 to 1600nm (Pump powers used: f1-250mW, f2+f3-250mW, f4+f5+f6+f7-320mW) 93
6.14 Schematic of experimental setup for gain and noise figure measurement (Inset shows the microscope image of the 5-MEF) 95
6.15 Performance of a split band MEFA with gain >20dB (1545-1615nm) using 12m MEF at 10W of pump power (-10dBm input signal) 96

List of Tables

1.1 ITU-T definition of telecom optical wavelength bands 2
1.2 Bi active centres (BAC) theories for NIR emission 9
1.3 Bi active centres (BAC) theories for NIR emission 10
1.4 Parameters of BPGSF lasers 17

2.1 Absorption, UL and laser performance in Bi-doped phosphosilicate fibres (A0746, A0745) 37
2.2 Absorption, UL and laser performance in high concentration Bi-doped phosphosilicate fibres (A0787, A0792 and A0795) 37
2.3 EPMA in Bi-doped aluminosilicate fibre 39
2.4 EPMA in Bi-doped phosphosilicate fibres 40

3.1 Small signal loss and UL at 1120 and 1047nm pumps 49

4.1 Absorption and UL of BPSFs at two different pump wavelengths 55

5.1 Relation between T_{FWHM} and t_p for commonly used pulse shapes 74

6.1 Gain of different fibre elements in 6m 5-MEF at different wavelengths for a pump power of 6.4W, Input signal power;-23dBm 95

Abbreviations

EDFA	Erbium doped fibre amplifier
WDM	Wavelength division multiplexing
CWDM	Course wavelength division multiplexing
DWDM	Dense wavelength division multiplexing
SMF	Single mode fibre
MCF	Multi core fibres
MMF	Multi mode fibres
MEF	Multi element fibres
PMD	Polarization mode dispersion
Bi	Bismuth
RE	Rare earth
Er	Erbium
Yb	Ytterbium
Tm	Thulium
Ho	Holmium
Pr	Praseodymium
Nd	Neodymium
BASF	Bi-doped aluminosilicate fibres
BPSF	Bi-doped phosphosilicate fibres
BGSF	Bi-doped germanosilicate fibres
BPGSF	Bi-doped phosphogermanosilicate fibres
Al	Aluminium
P	Phosphorous
Ge	Germanium
Si-BAC	Silica bismuth active centres

Ge-BAC	Germania bismuth active centres
NIR	Near infrared
UL	Unsaturable loss
ESA	Excited state absorption
FWHM	Full width at half maximum
FBG	Fibre Bragg grating
Nd:YAG	Neodymium-doped yttrium aluminium garnet
CW	Continues wave
$LiNbO_3$	Lithium niobate
MgO-PPLN	Periodically poled MgO-doped lithium niobate crystal
OC	Output coupling
NF	Noise figure
SESAM	Semiconductor saturable absorber mirror
CNT	Carbon nano tube
NPR	Non-linear polarisation rotation
CFBG	Chirped fibre Bragg grating
ML-BDFL	Mode-locked Bi-doped fibre laser
MOPFA	Master oscillator power fibre amplifier
BDFA	Bi-doped fibre amplifier
MOPA	Master oscillator power amplifier
SWNT	Single walled carbon nano tube
SA	Saturable absorber
DCF	Dispersion compensating fibre
NALM	Non-linear amplifying loop mirror
NOLM	Non-linear optical loop mirror
AOM	Acoustic optic modulator
EDFL	Er-doped fibre laser
SDM	Space division multiplexing
UV	Ultra-violet
MO	Microscopic objective
OSA	Optical spectrum analyser
FUT	Fibre under test
LD	Laser diode

ASE	Amplified spontaneous emission
BAS	Bi-doped aluminosilicate
BPS	Bi-doped phosphosilicate
WLS	White light source
Nd-YLF	Neodymium-doped yttrium lithium fluoride
TLS	Tunable laser source
ISO	Isolator
OSNR	Optical signal to noise ratio
BDFL	Bi-doped fibre laser
AC	Autocorrelation
SNR	Signal to noise ratio
BW	Bandwidth
C-band	Conventional band
O-band	Ordinary band
L-band	Long wavelength band
MEEDFA	Multi element Er-doped fibre amplifier
MUX	Multiplexer
MEFA	Multi element fibre amplifier

Dedicated to my family

Chapter 1

Introduction

In Chapter 1 we give an overview of the motivation behind this work. We also present the literature review of Bi-doped fibres to understand the host dependent absorption and emission characteristics of Bi-doped fibres and also their active luminescence centres. We also discuss the major theories regarding nature of the Bi NIR emission. Detrimental effects such as UL and ESA are explained in Bi-doped fibres. We also present the state of the art of Bi-doped fibres to give an idea of the field and where it stands in developing Bi-doped fibre amplifiers and lasers (both CW and pulsed). Moreover, we also discuss both core and cladding pumping MEF fibre geometries and brief fabrication aspects of MEF fibres. Further, the advantages of MEF geometry to develop wideband amplifiers are mentioned.

1.1 Motivation

In the year 1966 C. Kao et al., reported that the loss in a dielectric waveguide can be 20dB/km and further possible to reduce by using suitable di-electric material without impurities [1]. This statement made researchers put efforts in finding ways to reduce the loss in silica optical fibres. Silica was chosen as the material to develop optical fibres due to its favourable optical and mechanical properties. As a result, immediately after a few years in 1970, the first low-loss fibre was made by Corning with a loss of 20dB/km [2].

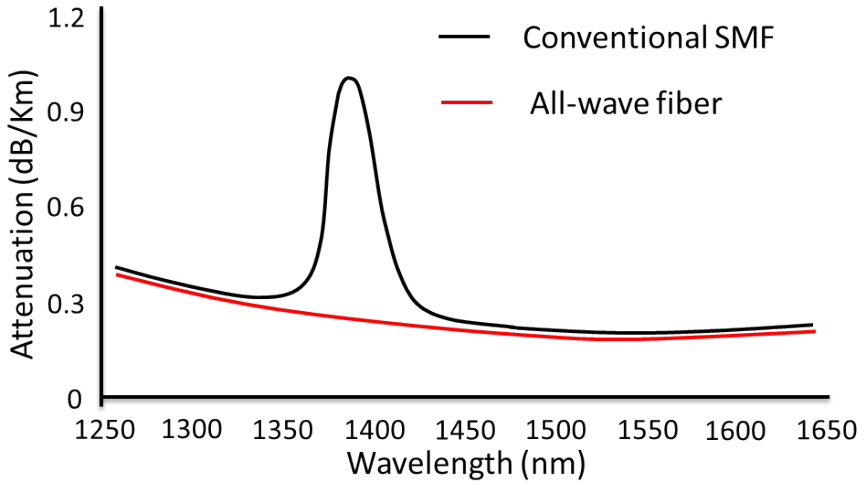

FIGURE 1.1: Attenuation spectra of conventional SMF and all-wave fibre [3]

Further, with ultra-pure precursors having impurities of the order of ppb (parts per billion) it is proved that the development of a low-loss (0.2dB/km) single mode fibres around 1.55μm are possible [4]. The attenuation spectrum of conventional single mode fibre is shown in Fig 1.1. This wavelength band from 1260-1625nm is divided into several sub wavelength bands. Each band is allocated a certain wavelength range by ITU-T as shown in Table 1.1

Band	O	E	S	C	L
Wavelength (nm)	1260-1360	1360-1460	1460-1530	1530-1565	1565-1625

TABLE 1.1: ITU-T definition of telecom optical wavelength bands

After the development of low-loss fibre, in 1987 (less than 10 years), erbium (Er)-doped fibre amplifier (EDFA) technology emerged as a breakthrough to revolutionize optical fibre communication and made transatlantic optical fibre communication possible [5]. The advancement of fibre fabrication process to develop low-loss fibres in combination with the EDFA technology helped to use the low-loss spectrum from 1530-1625nm (C+L band) for optical fibre communication. Over the years various techniques such as wavelength division multiplexing (WDM), dense wavelength division multiplexing (DWDM) and coarse wavelength division multiplexing (CWDM) with novel modulation formats such as quadrature phase shift keying (QPSK), 16-QPSK, 64-QPSK etc., were used to increase the capacity of existed silica optical fibres in the C+L band. However, the record reported transmission capacity of standard single mode fibre (SMF) is now approaching the non-linear Shannon limit [6].

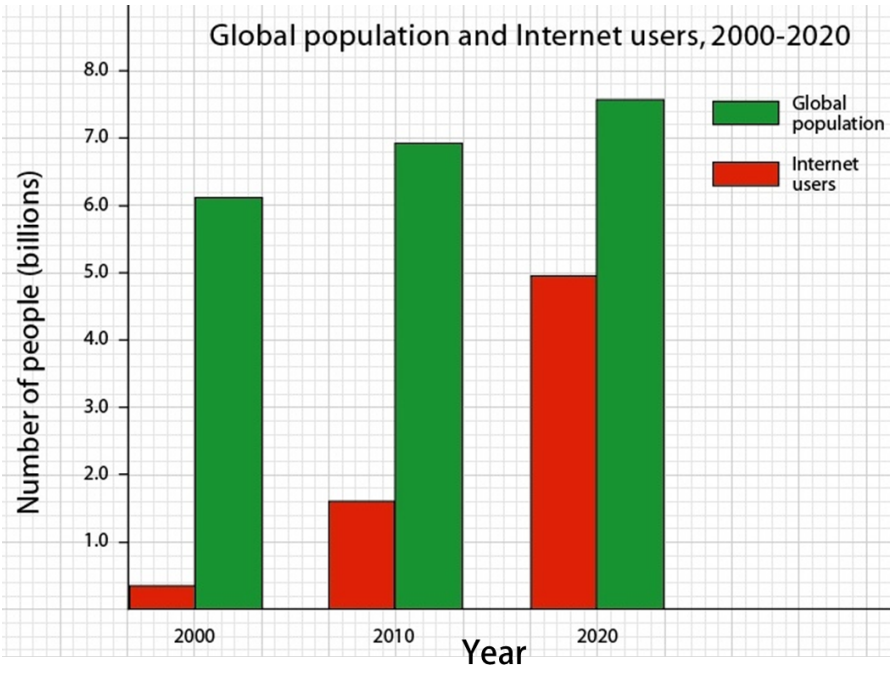

FIGURE 1.2: Bar chart showing the increase of internet users per each 10 year gap [7]

Fig 1.2 shows growth of the internet users in global population per every 10-years. It is predicted that by the year 2020 over 60% of the global population will be connected to the internet. The increased accessibility of the internet and extensive internet-based applications such as social media, cloud computing, e-commerce and e-learning etc. are the factors leading to a huge demand in fibre transmission capacity. Therefore, it is necessary to consider new approaches to boost the capacity of existing optical fibre networks in a cost-effective manner rather than simply installing more conventional single mode fibres to cope with end-user needs. Different approaches have been proposed by the research community around the world. One of them is to use the low-loss window (1260-1625nm) of silica optical fibres by developing efficient fibre amplifiers and lasers. Other one is to fabricate novel fibres such as multi-core fibres (MCF), multi-mode fibres (MMF) and multi-element fibres (MEF) for space division multiplexing (SDM) in a C-band from 1530-1565nm. Another one is to explore a new transmission band around the 2μm wavelength region using new transmission fibres [6].

As mentioned earlier, the early days of fibre optic communication used silica fibres that have a loss of 0.2dB/km in the C-band around 1.55μm and a water peak around 1.38μm as shown in Fig 1.1. Recent years, companies like OFS and Lucent technologies are offering optical fibres with low-loss in the complete 1260-1625nm wavelength band. These ultra-low loss fibres are called dry fibres and offer almost 53THz bandwidth for optical fibre communication. The attenuation of these ultra-low loss fibres in the wavelength band from 1260-1625nm is less than 0.4dB/km as presented in Fig 1.1 [3, 8].

Moreover, they have been used in recent years to build up new optical networks and offer dramatically improved performance in almost every characteristic over conventional single-mode fibre, including increased available spectrum, superior macro bend performance and ultra-low polarization mode dispersion (PMD). In 53THz bandwidth offered by these dry fibres, 10THz belongs to Er amplification band from 1530-1625nm. Hence by using the dry fibres, one can offer four times more bandwidth. All these features of dry fibres provide ultimate network design flexibility and enable cost-effective solutions to help maximize the data transfer capacity. However, to use this complete low-loss band for optical communication, the industry needs efficient fibre amplifiers and lasers, which are the critical part of an optical fibre communication link. Unfortunately, there are no efficient rare earth (RE)-doped fibre amplifiers and lasers that can cover the band from 1260-1530nm. Despite many efforts to adopt different RE-dopants in silica fibres to develop lasers and amplifiers in this wavelength range, there is still a shortage of potential devices available for practical implementation. In this thesis, we will discuss the development of amplifiers and lasers in the wavelength band from 1260-1625nm to utilize the low-loss window of ultra-low loss optical fibres by using bismuth (Bi) and Er-doped fibres.

1.1.1 Introduction to Bi-doped fibres

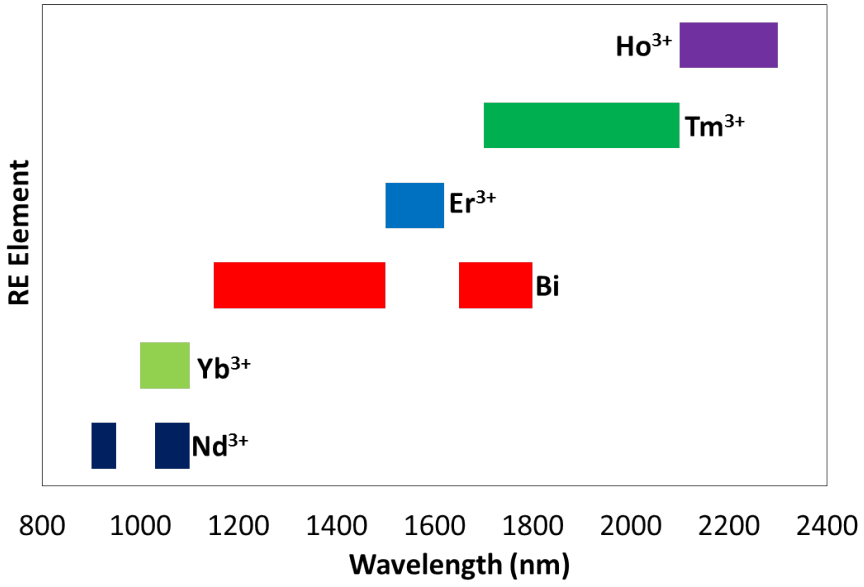

FIGURE 1.3: Spectral regions covered by various RE doped elements in silica host

For an optical fibre fabricated for the purpose to develop amplifiers or lasers, doping of core region with RE material is essential. Fig 1.3 shows different RE elements and their preferred emission bands in silica host. Conventional RE elements such as Er, ytterbium

(Yb) and thulium (Tm), or holmium (Ho) can cover the wavelength bands around 1, 1.5, and 2μm [9] but the band between Er and Yb is not covered by any RE-doped silica fibre. The Energy level diagram of Yb, Er, Tm are given in Fig 1.4

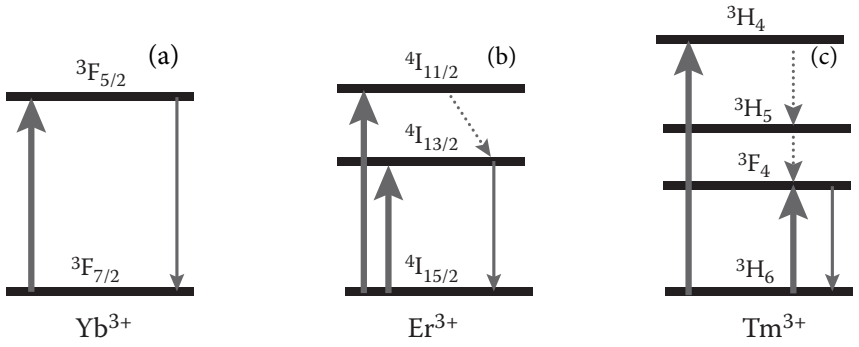

FIGURE 1.4: Energy level diagram of (a) Yb^{3+}, (b) Er^{3+}, (c) Tm^{3+} [9]

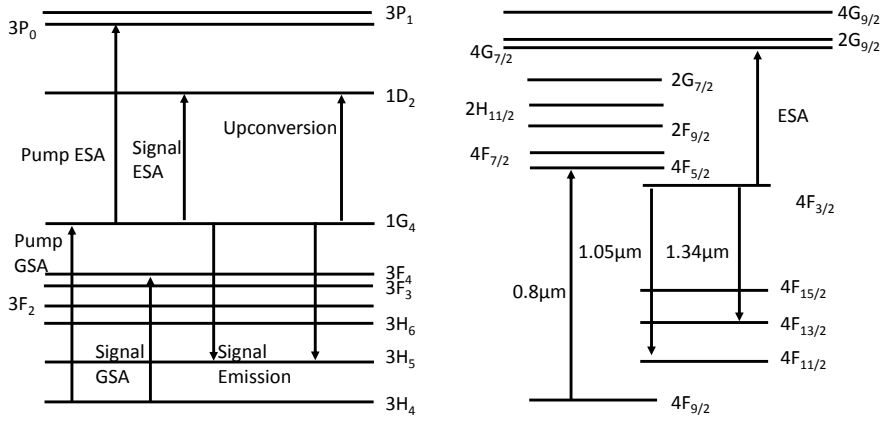

FIGURE 1.5: Energy level diagram of (a) Pr^{3+}, (b) Nd^{3+} [10]

Praseodymium (Pr) and neodymium (Nd)-doped fibres were studied extensively in silica host to develop amplifiers and lasers around 1.3μm. However, high phonon energy in a silica host made these dopant's inefficient. Changing to a low phonon energy host such as fluoride glass made them comparatively efficient but fluoride glasses are unsuitable to splice with conventional silica fibres as required in many applications for compact all-fibre devices. Nevertheless, the fabrication of these fibres is complex and not mature enough as compared to conventional modified chemical vapour deposition (MCVD)-solution doping technique. Further, as presented in Fig 1.5, in case of Pr, ground state absorption ($3H_4$-$3F_4$), excited state absorption (ESA) ($1G_4$-$1D_2$) at signal wavelength and pump ESA ($1G_4$-$3P_0$) are detrimental to develop efficient Pr-doped fibre amplifiers and lasers at 1.3μm. In case of Nd the ESA at signal wavelength ($4F_{3/2}$-$4G_{7/2}$) and the gain competition between 1.05μm ($4F_{3/2}$-$4F_{11/2}$) and 1.34μm ($4F_{3/2}$-$4F_{13/2}$) are detrimental to develop 1.3μm amplifiers and lasers [10]. Recently, Bi as a dopant in fibres has proven its capability to develop efficient amplifiers and lasers in 1150-1800nm

wavelength range except the band covered by Er. Here, we investigate Bi-doped fibres to develop amplifiers and lasers in the wavelength band from 1150-1500nm. In the following section, we discuss the luminescence characteristics of Bi-doped fibres.

1.1.2 Luminescence characteristics of Bi-doped fibres

The broadband near-infrared (NIR) luminescence properties of Bi-doped silica fibres were found to be very sensitive to the glass composition as well as fabrication conditions. In RE ions, the partial shielding of unfilled 4f subshell by fully filled 5s and 5p prevents significant interaction from the host environment. In contrast to RE elements, Bi has inner subshells that are completely filled and the outer 6s and 6p electrons have significant interaction with host thereby showing host dependent absorption and emission properties. Hence co-dopants can significantly alter the luminescence spectra as shown in Fig 1.6.

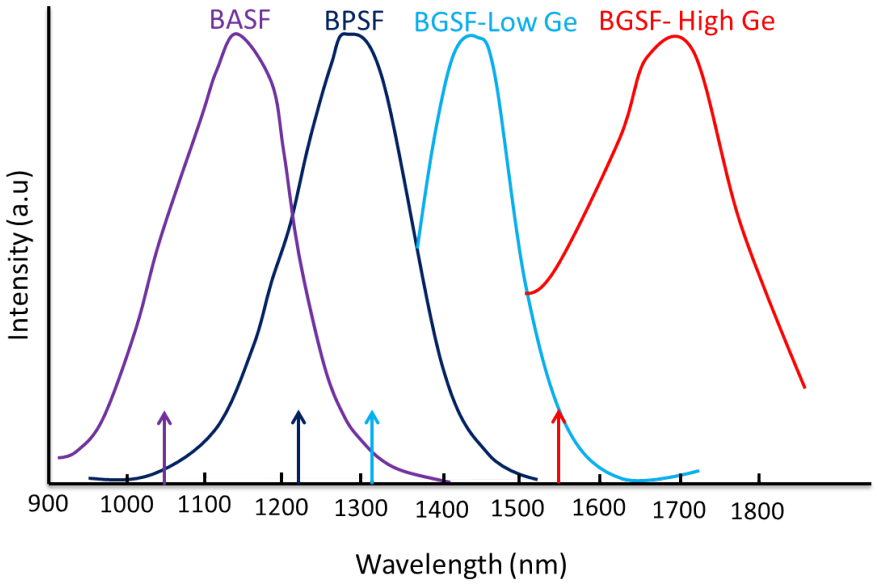

FIGURE 1.6: Spectral regions covered by various Bi-doped fibres with different hosts [11]

Bi-doped fibres with aluminosilicate host from here onwards represented as Bi-doped aluminosilicate fibres (BASFs) have shown luminescence peak around 1150nm, whereas Bi-doped fibres with phosphosilicate and germanosilicate core composition (here onwards represented as Bi-doped phosphosilicate fibres (BPSFs) and Bi-doped germanosilicate fibres (BGSFs) have been known to push the emission band towards longer wavelength side around 1300 and 1450nm, respectively. Recently, the Bi emission window was extended further to cover 1600 to 1800nm wavelength band by using high GeO_2 concentration (50mol%) within the fibre core. Luminescence in Bi-doped phosphogermanosilicate

fibres (BPGSFs) is broad compared to other Bi-doped fibres co-doped with germanium (Ge) and phosphorous (P). This makes it possible to use Bi-doped optical fibres to demonstrate amplifiers and lasers for covering the entire spectral region from 1150 to 1800nm by varying the fibre core composition. The pump wavelength bands are indicated by arrow marks in Fig 1.6. The pump wavelength bands around 1050, 1230 and 1310nm for BASFs, BPSFs and BGSFs, respectively are typically used. In case of BGSFs with high GeO_2 concentration the pump wavelength band is around 1550nm [11, 12].

1.1.3 Origin of near-infrared luminescence

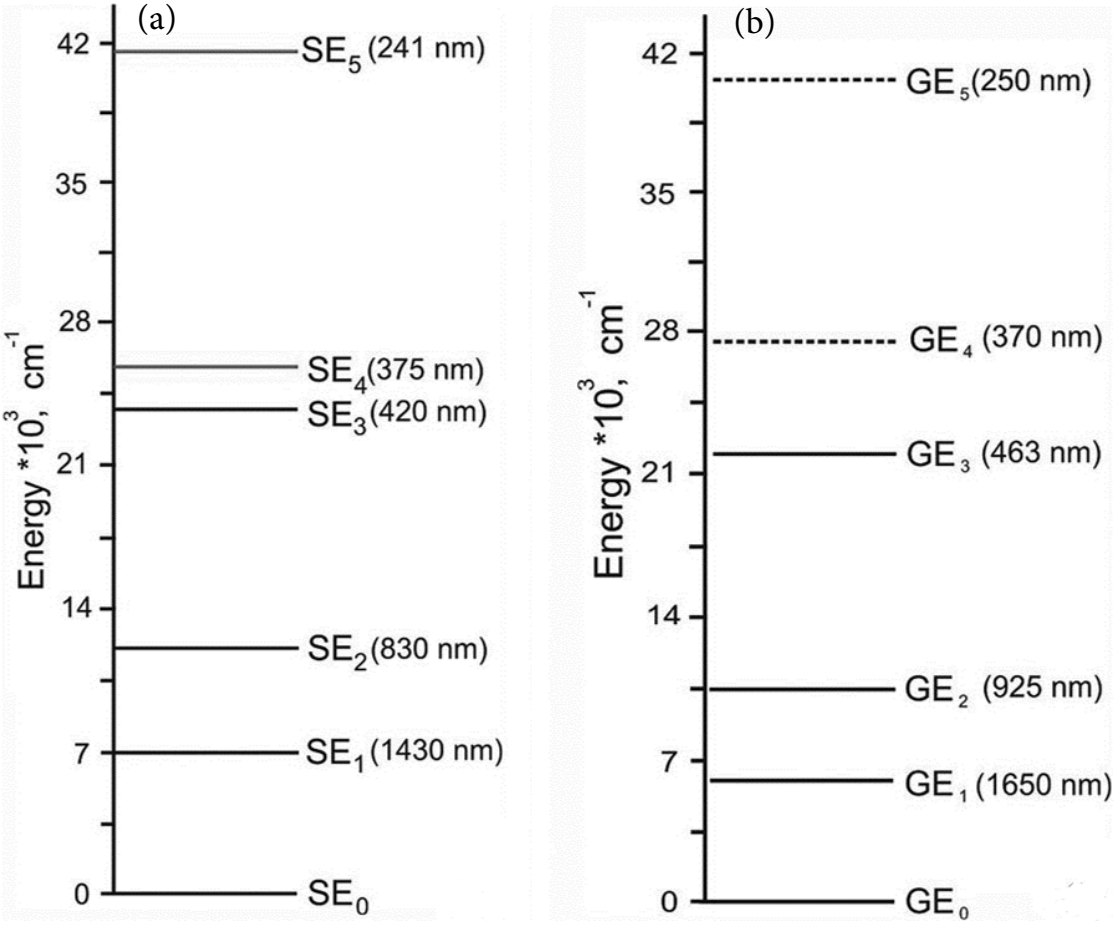

FIGURE 1.7: (a) Energy level diagram of Si-BAC (b) Energy level diagram of Ge-BAC [13]

Near-infrared emission has been observed in Bi-doped fibres with different silica hosts such as Al, P and Ge. However, the state involved in the origin of NIR luminescence is still unknown. The difficulty comes from the fundamental chemistry involved with Bi. Bismuth is a polyvalent element with four oxidation states Bi^{+}, Bi^{2+}, Bi^{3+}, Bi^{5+}.

During the fabrication process, Bi can go towards oxidation (higher valance state) or reduction (lower valence state). This makes it difficult to control and identify the state of Bi in the desired form. If the rapid reduction happens then the formation of Bi clusters and metal colloids can form and will induce the unsaturable loss and reduce the efficiency of Bi-doped fibre lasers and amplifiers [14]. Moreover, the performance of Bi-doped fibres so far reported with only low concentration of Bi, this also made it complicated to determine the state of Bi by using conventional methods [15]. A study on measurement of the luminescence intensity (I_{lum}) depending on both emission and excitation wavelength in the spectral range from 250-1700nm was performed in Bi-doped fibres with only silica host and then in more complex host glasses such as aluminium-silica, phosphorous-silica and germanium-silica and predicated the energy level diagram for Bi active centres in pure silica host and in germanium-silica host glass composition as shown in Fig 1.7 [16–24]. Here it is considered that the active centres in Bi-doped silica fibres are represented as Si-BAC and in case of Bi-doped germanosilicate fibres as Ge-BAC. Further, a number of hypothesis have been proposed to explain the NIR luminescence but none of them are confirmed yet [25–35].

Table 1.2 and Table 1.3 presents major theories regarding nature of the Bi NIR emission.

Bi NIR-luminescence	Host	Reference	Note
Metallic Bi clusters	SiO_2	[36]	Bulk glass
Bi^{5+}	SiO_2-Al_2O_3	[25]	alumosilicate bulk glass
Bi^{+}	Bi_2O_3-BaO-Al_2O_3	[37]	barium-aluminum-borate bulk glass
Bi Clusters	GeO_2-Ta_2O_5	[38]	Tantalum co-doped germanium oxide bulk glass
Bi^{2+} or Bi^{+}	Germanosilicate multicomponent glass	[27]	Bulk glass
Bi_2/Bi_2^{-}	Aluminosilicate multicomponent glasses	[28]	Bulk glass
Point defects in glasses	Germanate glasses	[39]	Bulk glass
Bi^{+}	SiO_2-Al_2O_3-GeO_2-P_2O_5 and SiO_2-GeO_2-P_2O_5 fibre preforms	[40]	Optical fibre
Bi_2 or Bi_4 clusters	M_2O-Al_2O_3-SiO_2 (M=Li, Na) and Li_2O-Ta_2O_5-SiO_2	[41]	Bulk glass
Bi_2^{-} and Bi_2^{2-}	Alumosilicate glass	[42]	Bulk glass
Bi_2 dimers	Mg-Al-silicate glasses (MgO-Al_2O_3-SiO_2)	[30]	Bulk glass
Bi^{2+}-Bi^{3+} dimers	Silicate glasses and silica fibre preforms	[35]	Bulk glass and optical fibre
Bi^{0}-Bi^{+}	SiO_2-Al_2O_3-GeO_2 fibre preforms	[43]	Optical fibre
Bi^{2+}-Bi^{3+} dimer, two Bi ions with a total charge of +5	$10Al_2O_3$-30MgO-$60SiO_2$ glass	[44]	Bulk glass

Table 1.2: Bi active centres (BAC) theories for NIR emission

Bi NIR-luminescence	Glass composition	Reference	Note
Bi^{+}-Bi_2^{4+} and Bi_5^{3+} ions	$AlCl_3$-$ZnCl_2$-$BiCl_3$ glass	[45]	Bulk glass
Bi^{+} and defect	Gallium silicate glass	[46]	Bulk glass
UV absorption in glasses is explained by Bi^{3+}	Magnesium-aluminosilicate glass, silica-free calcium-aluminate glass, silica glass and lead-aluminosilicate glass	[47]	Bulk glass
Bi^{2+} and Bi_n clusters	Bi^{-} and Pb^{-}doped oxide and chalcogenide glasses	[48]	Red and NIR photoluminescence was investigated in Bi- and Pb-doped oxide and chalcogenide glasses
Existence of atomic Bi	Germanosilicate glass optical fibres	[49]	Upconversion emission in Bi-doped germanosilicate optical fibres and the origin of this luminescence were discussed
Bi in a low valence state and oxygen (anion) vacancies	SiO_2, SiO_2-Al_2O_3, SiO_2-GeO_2, and SiO_2-P_2O_5 fibre preforms	[50]	It was concluded that Bi-related centres of near-IR luminescence in Bi:SiO_2 and Bi:GeO_2 glasses are mainly represented by the $Bi^0\cdots\equiv$Si-Si$\equiv$ and $Bi^0\cdots\equiv$Ge-Ge$\equiv$ complexes formed by interstitial bismuth atoms and intrinsic defects of glass, $\equiv$Si-Si$\equiv$ and $\equiv$Ge-Ge$\equiv$ oxygen vacancies

TABLE 1.3: Bi active centres (BAC) theories for NIR emission

However, few of the possible Bi states are omitted based on experimental facts, for example, Bi^{3+} and Bi^{2+} ions observed to emit only visible luminescence hence they might not be the cause for NIR luminescence. The observed NIR luminescence bands of Bi-doped fibres are located in the same spectral region of thallium(Tl) and lead (Pb)-doped crystals and it was found that the NIR emitting centres in these materials consist of definite Tl or Pb ions and adjacent anion vacancies. Based on this grounds and also considering the isoelectronic nature of Tl^0, Pb^+ and Bi^{2+} one can consider that the NIR luminescence centres in Bi-doped fibres are Bi-ions and adjacent oxygen deficiency centres but not Bi-ions themselves [51]. In recent experiments, the research group (FORC) from Russia reported that the oxygen deficiency centres in combination with Bi in low oxidation state is the active centre in BGSFs and leading to NIR luminescence. [52, 53]. Despite of all these experimental and theoretical predictions, the topic is still an interesting puzzle that needs to be solved in order to develop efficient Bi-doped fibres for amplifiers and lasers.

1.2 Unsaturable loss and excited state absorption

Other important aspects of Bi-doped fibres are the unsaturable loss (UL) and excited state absorption(ESA). UL and ESA are two detrimental effects that can reduce the efficiency of amplifiers and lasers. In the following section, we will discuss the UL and ESA in Bi-doped fibres in more detail.

1.2.1 Unsaturable loss

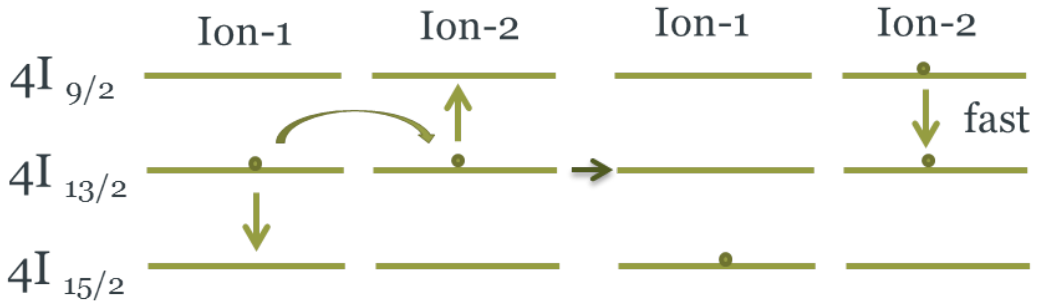

FIGURE 1.8: Quenching process leading to unsaturable loss in Er^{3+} [54]

UL is a well-known phenomenon, which occurs due to the ion-ion interaction when the concentration of RE-dopant is high. In case of low RE concentration fibres, this could happen because of the interaction between ions and defect centres or impurities (hydroxyl (OH^-) molecule, iron etc.). The presence of UL will induce additional losses by reducing

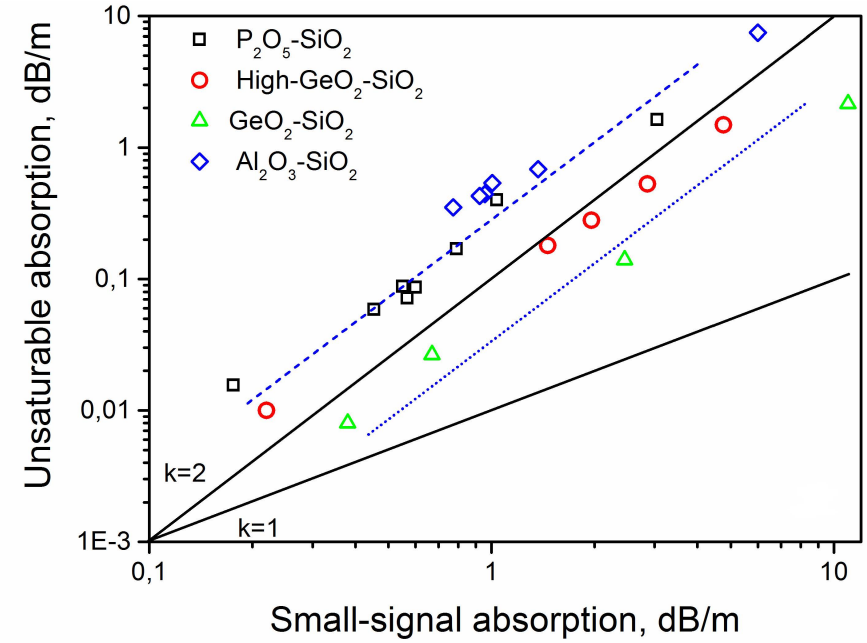

FIGURE 1.9: Unsaturable absortpion as a function of small signal absorption in various Bi-doped fibres [55]

the population inversion of the laser gain media. The concept of UL is explained with the help of Er^{3+} energy level diagram as shown in Fig 1.8. When two ions (ion-1 and ion-2) sits close to each other in the lasing energy level ($4I_{13/2}$) ion-1 will transfer energy to ion-2 and then comes to the ground energy state ($4I_{15/2}$). At the same time, ion-2 excited to the upper energy level ($4I_{9/2}$) and will come back to the lasing energy level by fast non-radiative relaxation. In this process, we will lose one excited ion in the lasing level. Having unsaturable loss in the fibre will lead to increased pump threshold for lasing to start and also lead to poor efficiency. Recently, unsaturable absorption as a function of small signal absorption was investigated in Al_2O_3-SiO_2, P_2O_5-SiO_2, GeO_2-SiO_2, high-GeO_2-SiO_2 for different Bi-concentrations and is presented in Fig 1.9. The straight lines in Fig 1.9 show the linear function (in log-log scale) with a slope of 1 and 2. It is observed that the unsaturable absorption grows with increase of Bi concentration. Therefore it is necessary to optimise the Bi fabrication process to achieve high Bi concentration with low UL to develop highly efficient fibre amplifiers and lasers [54–56].

1.2.2 Excited state absorption

ESA in fibres is wavelength dependent and is due to the presence of possible electron transition from the lasing level, with energy equivalent to electron transition from ground to laser level. In Fig 1.10, the process of ESA is described by considering the Er^{3+} energy level diagram. Er^{3+} has possible electron transition from $4I_{11/2}$ to $4F_{7/2}$ whose energy corresponds to the electron transition from $4I_{15/2}$ to $4I_{11/2}$. When pumped at 980nm

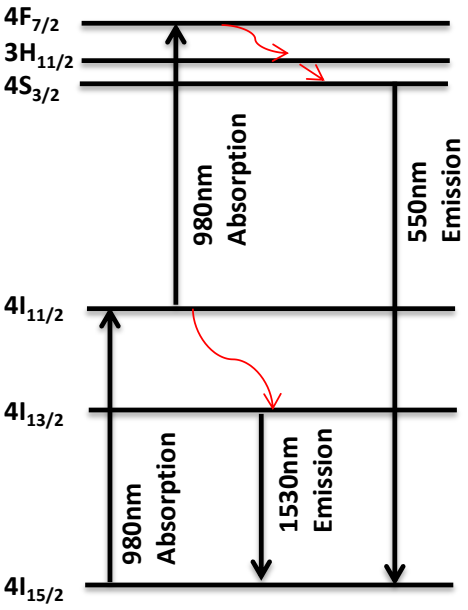

FIGURE 1.10: Er^{3+} energy level diagram, illustrating the process of ESA [57]

this causes the excited atoms in the energy level $4I_{11/2}$ to excite to the upper energy level $4F_{7/2}$ instead of participating in the laser action. From the $4F_{7/2}$ level, the ions come down to the energy level $4S_{3/2}$ by fast non-radiative relaxation. The ions in the $4S_{3/2}$ energy level can emit 550nm radiation by radiative relaxation to the ground level of $4I_{15/2}$. The green emission observed when pumping Er-doped fibres with 980nm pump wavelength is due to the presence of ESA in these fibres. In this process we lose ions from the lasing energy level without contributing for the laser action corresponds to 1530nm emission and will reduce the laser efficiency [57].

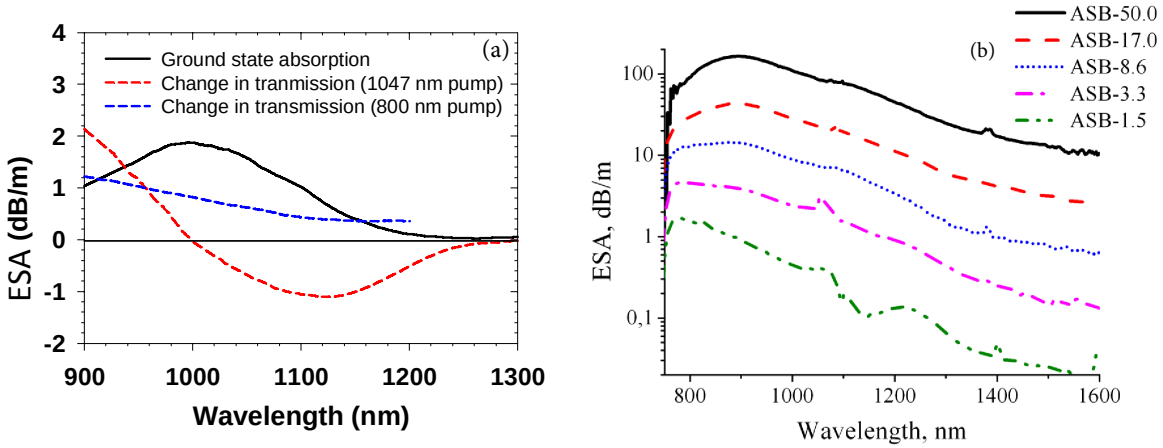

FIGURE 1.11: (a) ESA of BASF (b) ESA in BASF with different concentration [58–60]

ESA has been measured for the first time in BASFs in the wavelength range from 900-1300nm under pumping at 800 and 1047nm. ESA was observed in the whole spectrum

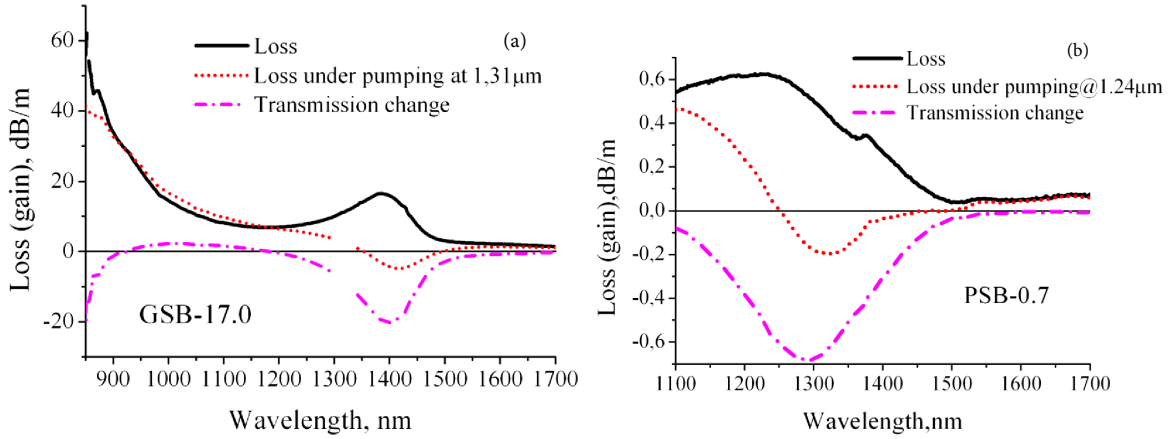

FIGURE 1.12: (a) ESA of BGSF (b) ESA of BPSF [59, 60]

when pumping at 800nm whereas when pumped at 1047nm it was observed only from 900-1000nm range in which high power commercially available laser diodes such as 915nm and 975nm are available. However, no significant ESA was observed at the 1080nm pump band as well as 1160nm emission band when pumped at 1047nm as shown in Fig 1.11 (a) [58]. Later, the ESA in BASFs was reported in the extended band from 750-1700nm with different Bi concentrations. Five different Bi-concentrations were used to measure the ESA. Absorption at around 1μm was used to estimate Bi concentration in each of these fibres. These measurements also showed that considerable ESA was observed in BASFs and ESA was increased as the concentration of Bi increases as shown in Fig 1.11 (b). It was also noticed that the ESA decreases with increasing wavelength. This was the reason to pump the BASFs around 1050nm pump band and also to use relatively low Bi-concentration in the fibre core. In case of Ge host with low Bi-concentration, no significant ESA was observed whereas at high Bi-concentration some noticeable ESA was observed from 950-1200nm as shown in Fig 1.12 (a). Absorption at 1.4μm was used to estimate concentration in these fibres. In case of P host with low Bi-concentration, no significant ESA was observed as shown in Fig 1.12 (b). Pump wavelengths of 1058 or 1085, 1240 and 1320nm were used for BASFs, BPSFs and BGSFs, respectively to measure the ESA from 750-1700nm. The high amount of ESA presented in BASFs is considered as the possible reason for low efficiency achieved in these fibres compared to BPSFs and BGSFs [59, 60].

1.3 State of the art of Bi-doped fibre lasers and amplifiers

1.3.1 Bi-doped fibre lasers and amplifiers from 1150-1250nm

In 2001 K. Murata et al., discovered wideband (200-300nm) NIR luminescence from Bi and Al co-doped silica glass in the spectral region of 1100-1500nm [61]. Subsequently, a large number of glass compositions were investigated to obtain luminescence in the wavelength range from 1-2μm and the details can be found in a review by Fujimoto [62]. After five years in 2005, the first Bi-doped fibre was fabricated by MCVD-solution doping technique [63, 64]. In the same year, the first Bi-doped fibre laser was demonstrated in aluminosilicate host. The fibre exhibits absorption bands at 500, 700, 800 and 1000nm and a luminescence band around 1150nm with a full width at half maximum (FWHM) of 150nm. The measured luminescence lifetime in these fibres was $\sim$1ms. At that point, the motivation to develop these fibres was to access the 1050-1200nm wavelength band and the possible applications are to develop tunable femtosecond lasers and broadband amplifiers. At a later time, the application area was broadened by developing sources in the yellow wavelength range from 575-590nm, which are of great importance in dermatology [65], ophthalmology [66] and in astronomy [67].
Fibre lasers are advantageous to develop efficient, compact and reliable sources for these applications. In the first experiment with BASFs, a linear cavity with fibre Bragg gratings (FBGs) was constructed to develop CW lasers and lasing was obtained at 1146, 1215nm by changing the FBGs. A Nd:YAG laser at 1064nm was used as a pump source with a 5W of pump power. A CW laser generation with a slope efficiency of 10% and 14% was obtained at 1146 and 1215nm, correspondingly [68].
After this, a number of CW BASF lasers were developed at 1150, 1160, 1178, 1205, 1215nm by changing the pump wavelength and FBGs [69–72]. Among them lasing at 1160nm with a maximum efficiency of up to 32% at room temperature and up to 52% at 77K is best so far. These fibre lasers are convenient for the visible light generation by frequency doubling using non-linear crystals. To demonstrate this potential a 580nm laser with 300mW of output power was developed by frequency doubling the 1160nm laser with a commercially available lithium niobate ($LiNbO_3$) crystal. A visible laser at 589nm was also demonstrated by frequency doubling the 1178nm laser by periodically poled MgO-doped lithium niobate crystal (MgO-PPLN) [73, 74].

Although the efforts to develop fibre lasers were appreciated there was much less progress made in developing amplifiers around 1150nm. To the best of our knowledge, up till, a maximum gain of about 5dB was demonstrated in Bi-doped aluminosilicate fibre amplifier at room temperature at a wavelength of 1180nm. As a pump source, a high-power

Yb-doped fibre laser operating at 1060nm with a maximum output power of 6.5W was used [75].

1.3.2 Bi-doped fibre lasers and amplifiers from 1280-1500nm

The successful demonstration of lasers and amplifiers in Bi-doped aluminosilicate fibres elevated the interest to study the Bi-dopant in different host materials and it was found that instead of Al, if co-doped the core with P and Ge then the NIR luminescence will shift towards longer wavelength side. Later, Bi-doped phosphosilicate and germanosilicate fibres were used to demonstrate lasers and amplifiers in the wavelength range from 1280-1400nm and 1400-1500nm, respectively. However, it was observed that the performance of Bi-doped phosphosilicate fibres was better when added a small amount of Ge and also addition of Ge makes the luminescence window broad covering the entire 1280-1500nm band. Here, we will discuss the review of lasers and amplifiers developed by BPGSFs. The lifetime in these fibres was measured to be 600μs at 1300nm by pumping with 808nm laser diode. The first fibre laser in the wavelength band from 1280-1400nm was demonstrated in BPGSF. A Raman fibre laser operating at 1230nm was used as a pump source. A 30m BPGSF was used as an active gain media. Laser at 1310nm was demonstrated by pumping at 1230nm with an efficiency of 3.2% (T=300K) and 5.4% (T=77K). Further, at high pump powers the slope efficiency was different and was 19% (T=300K) and 29% (T=77K). The observed laser slope efficiency was strongly depends on temperature and the pump power. By changing the pump wavelength to 1210nm lasing at 1310nm was also demonstrated. The lasing efficiency was 1.4% (T=300K) and upon cooling to 77K it was 5% [76].
Later lasing at 1280, 1330nm were demonstrated by using the BPGSFs by pumping at 1230nm with efficiencies of 12% and 24%, respectively [77, 78].
In addition, lasers at 1280, 1330, 1340, 1360, 1480nm were demonstrated with 90-100m long BPGSF. Different resonant wavelength Bragg gratings with different output coupling ratio were used to test the laser efficiencies. A Raman fibre laser at 1230nm was used as a pump source to demonstrate lasers between 1280-1370nm and a 1340nm Raman fibre laser was used to demonstrate lasing at 1480nm. The pump power levels of these pump sources were 30 and 10W, respectively. Fig 1.13 shows the slope efficiencies of lasers at 1280, 1330, 1340, 1360nm with different output coupling (OC) ratio of Bragg gratings.

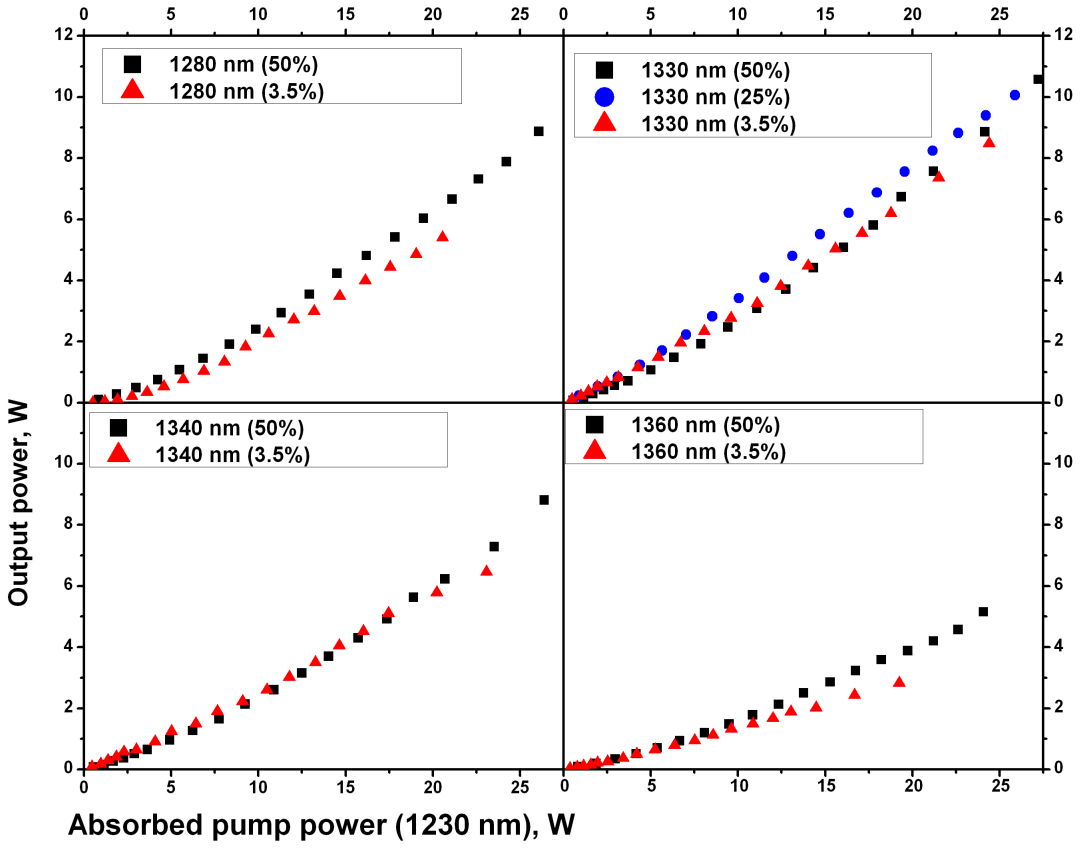

FIGURE 1.13: Variation of the output power with the absorbed pump power for Bi-doped fibre lasers at different lasing wavelengths. The lasing wavelength and the output coupling are indicated in each graph [79]

Lasing wavelength (λ_L) (nm)	R_{OC} (%)	P_{out} (W)	η_{min} (%)	η_{max} (%)
1280	50	8.9	14	31
1280	3.5	5.4	3	19
1330	50	10.6	17	37
1330	25	10.06	22	36
1330	3.5	8.5	19	29
1340	50	8.8	15	31
1340	3.5	6.5	13	23
1360	50	5.23	9.5	18
1360	3.5	2.8	7.1	9.8
1480	50	1.94	9.1	21
1480	3.5	0.95	-	13.3

TABLE 1.4: Parameters of BPGSF lasers

From Fig 1.13, it can be observed that the slope efficiency was different at high pump powers compared to low pump powers. It was also noticed that, the slope efficiency depends on the output coupling of Bragg gratings and the laser wavelength. The threshold for all lasers was around 100mW. Among all these lasers a maximum slope efficiency of 50% was reported in case of 1330nm laser with an output power of 10.6W using 50% OC Bragg grating. The parameters of all BPGSF lasers were mentioned in Table 1.4. Here, R_{OC} is output coupling of the Bragg grating, P_{out} is laser output power and η_{min}, η_{max} are the slope efficiencies at minimum and maximum pump powers.

Compared to Bi-doped aluminosilicate fibre amplifiers at 1180nm higher gain values were reported in Bi-doped phosphogermanosilicate fibre amplifiers in the wavelength range from 1300-1500nm. A conventional experimental setup was used to measure the gain and noise figure (NF). The length of the Bi-doped fibre was 200m. A pump power of 460mW and 190mW at 1230 and 1318nm, respectively were used to measure the gain and NF of the amplifiers. A maximum gain of 24.5 and 20.7dB was measured at 1321 and 1442nm, respectively. A minimal NF of 4-6dB was reported for both amplifiers [79].

1.3.3 Bi-doped fibre lasers and amplifiers from 1600-1800nm

In recent years it was observed that by increasing the GeO_2 concentration to 50mol% in Bi-doped fibres it is possible to access the wavelength range from 1600-1800nm. Conventional MCVD-solution doping technique was used to develop these fibres. The lifetime of these fibres was measured to be 500μs at 1700nm under pumping with 975nm laser diode. In this section, we will review the lasers and amplifiers developed by Bi-doped germanosilicate fibres with high GeO_2 concentration. Using a linear laser scheme with FBGs, inscribed in Bi-doped fibre, lasers operating between 1600-1800nm were demonstrated. An Er-Yb co-doped fibre laser operating at 1568nm was used as a pump source with a pump power of nearly 3.5W. The length of the active fibre was 15-20m. A laser at 1703nm with a slope efficiency of 20% was demonstrated [12].
Further, by optimising the fibre parameters a Watt level laser at 1700nm was demonstrated with a slope efficiency of 33% and with an output power of 1.05W using 25m long Bi-doped fibre [80].

Bi-doped fibre amplifiers were also demonstrated at 1700nm by using Bi-doped germanosilciate fibres with high GeO_2 concentration. A laser diode operating at 1550nm with a pump power of 150mW was used as a pump source. A 50m of Bi-doped fibre was used to build the amplifier. A total pump power of 300mW was used in bi-directional pumping configuration. A maximum gain of 23dB at 1710nm with a NF of 7dB was reported for an input signal power of -20dBm [81].

1.4 State of the art of Bi-doped pulsed fibre lasers

Pulsed fibre lasers in the wavelength band from 1100-1500nm and 1600-1800nm are important for many applications including optical fibre communication, material processing, and spectroscopy. The broad luminescence offered by Bi-doped fibres is a useful property to develop ultra-fast fibre lasers. Various Bi-doped pulsed fibre lasers were demonstrated using saturable absorbers such as semiconductor saturable absorber mirror (SESAM), carbon nano tube (CNT), and non-linear polarization rotation (NPR) etc. Different wavelength bands around 1150, 1300 and 1700nm were covered by using Bi-doped fibres with different hosts. In the following section we will discuss the Bi-doped pulsed fibre lasers in different wavelength bands using aluminosilcate, phosphogermanosilicate and high GeO_2 host Bi-doped fibres.

1.4.1 Bi-doped pulsed fibre lasers from 1150-1250nm

The first Bi-doped pulsed fibre laser was demonstrated using Bi-doped silicate fibre. 50ps pulses at 1161.6nm with an average power of 2mW was demonstrated using 6m long fibre. Mode-locking was achieved by using SESAM as a saturable absorber. The fibre was pumped with an Yb-doped fibre laser operating at 1063.8nm with a pump power of 800mW. The total dispersion of the cavity was in the normal dispersion regime [82]. Later many more demonstrations around 1150nm were reported using Bi-doped aluminosilicate fibres.

A tunable mode-locked Bi-doped soliton fibre laser was demonstrated in the 1153-1170nm range with 0.9ps pulses using SESAM. A chirped fibre Bragg grating (CFBG) was used to compensate the dispersion of the fibre and to change the dispersion from normal to anomalous for soliton operation [83].

Further, a mode-locked laser at 1165nm with 1.9ps pulses using SESAM was demonstrated with 15m long active fibre. Here also a CFBG was used to bring the dispersion to anomalous regime for soliton operation. A 1062nm Yb-doped fibre laser was used as a pump source. The pulse width with length of the fibre was measured and found that it depends on the total dispersion of the cavity [84].

In another experiment, a 1.19ps mode-locked fibre laser from 1158-1168nm was demonstrated using SESAM as a saturable absorber with 10m long Bi-doped fibre. A 1075nm Yb-doped fibre laser with 2.7W pump power was used to pump the ML-BDFL [85].

Further, a picosecond mode-locked Bi-doped master oscillator power fibre amplifier (MOPFA) for frequency conversion was demonstrated in 2011, A three-stage experimental setup was used to develop MOPFA. In the first stage, a mode-locked Bi-doped fibre laser was developed. In the second stage, two Bi-doped fibre amplifiers (BDFAs)

were used to amplify the pulses. In the third stage, a $LiNbO_3$ crystal was used to frequency double the mode-locked laser. The mode-locked laser was constructed with a 5m long Bi-doped aluminosilciate fibre and SESAM. A 1065nm Yb-doped fibre laser was used as a pump source. A CFBG was used to make the dispersion of the cavity to be anomalous. 3.9ps pulses with an output power of -4dBm were demonstrated and then amplified using the second stage amplifiers. In this second stage, a 30m long BASF was used to develop BDFAs. A pump power of 2W and 5W were used for the first and second BDFAs, respectively. Finally, after MOPFA a pulse width of 28ps with an average power of 150mW and a peak power of 580mW was demonstrated. In the third stage, a $LiNbO_3$ crystal was used to generate 588.75nm, with an average power of 13.7mW. Note here that all the active fibre in different stages was cooled to improve the performance [86].
In addition, a single-walled carbon nano-tube (SWNT) was also used to demonstrate Bi-doped mode-locked lasers in both normal and anomalous dispersion regime. A 30m long fibre was used to construct the ML-BDFL. A CFBG was used to modify the dispersion of the cavity. 558ps pulses with a repetition rate of 5.47MHz were demonstrated at 1157nm in the normal dispersion regime with a pump power of 1.5W. The fibre was cooled to 77K to enhance the gain of the fibre. In the anomalous dispersion regime, 4.7ps pulses with 5.13MHz repetition rate were demonstrated at 1177nm. An average power of 10-15μW with a 200mW of pump power was reported [87].

In another experiment, the Bi-doped fibre was also used as a saturable absorber for mode-locking other RE-doped fibres. In an example by using Bi-doped fibre as a SA, an Yb-Bi Q-switched laser was demonstrated. Here it was proved that the Bi-doped fibre can itself work as a saturable absorber (SA) for mode-locking RE-doped fibre lasers [88].

1.4.2 Bi-doped pulsed fibre lasers from 1280-1500nm

A 1320nm mode-locked Bi-doped phosphogermanosilicate fibre laser based on SESAM in both normal and anomalous dispersion regime was studied in 2013 for the first time [89]. A 1220nm semi-conductor disk laser was used to pump the Bi-doped fibre. A 39m long Bi-doped phosphogermanosilicate fibre was used as an active medium. A high reflecting plane mirror and a CFBG were used to change the dispersion of the cavity. In the anomalous dispersion regime, the laser produces 2.51ps pulses with an average power of 0.3mW and corresponding peak power of 40W, for a pump power of 250mW. By replacing the CFBG with a plane reflecting mirror the dispersion of the cavity was changed to normal and the laser produces pulses of 25.5ps. The pulses were compressed down to 580fs by further sending them through a 300m long single mode fibre. In case of normal dispersion regime, the average power was increased to 0.8mW

with corresponding peak power of 470W. The superior performance was achieved in case of net normal dispersion regime [89].
Later a 1440nm all-bismuth fibre master oscillator power amplifier was demonstrated by pumping with 1320nm semiconductor disk laser. The two-stage master oscillator power amplifier (MOPA) has one stage to generate mode-locked pulses in the normal dispersion regime and another stage to amplify and compress the pulses. The first stage of the master oscillator was developed by a 3.4m Bi-doped germanosilicate fibre. The cavity was adjusted to the normal dispersion regime by using an 80m dispersion compensating fibre (DCF). The master oscillator delivered 2.1ps pulses with an average power of 1.5mW using SESAM as a SA, for a pump power of 320mW . The pulses were then forwarded to a power amplifier constructed by 35m long Bi-doped fibre. A pump power of 400mW was used for pumping the amplifier. 240fs pulses with 15mW average power and 3.1kW peak power was demonstrated after the amplifier [90].
Further, a non-linear Kerr effect mode-locking at 1310nm based on figure eight scheme in both non-linear amplifying loop mirror (NALM) and non-linear optical loop mirror (NOLM) configurations was demonstrated using BPSFs. A high Ge-doped fibre was used to provide large positive dispersion and non-linearity to operate the mode-locking in the dispersive soliton regime. 13.8ps pulses with a repetition rate of 3.9MHz were demonstrated based on NALM configuration. Whereas 11.3ps pulses with a repetition rate of 3.5MHz were demonstrated using NOLM configuration with an average power of 6mW. The pulses were further amplified and compressed by a Bi-doped fibre amplifier and a diffraction grating. The average power after Bi-doped fibre amplifier was increased to 30mW and the pulses are compressed down to 530fs [91].

Self Q-switched lasers were also demonstrated at 1460nm by using Bi-doped germanosilicate fibres. 1.8μs pulses at 1463nm wavelength was reported by using 10m BGSF as a saturable absorber. A laser diode operating at 1310nm with a pump power of 130mW was used as a pump source. For pumping the active fibre, bi-directional pumping configuration was used with a total pump power of 260mW [92].
In another experiment, a burst mode pulse generation from Bi-doped germanosilicate fibre was demonstrated. Two 1310nm laser diodes each having 130mW pump power were used in bi-directional laser configuration with an active fibre length of 10m. A passive fibre length in the cavity was varied from 10-90m to adjust the dispersion in the cavity. Burst pulses with a pulse repetition rate of 31.5KHz, 3.088MHz and width of 4.7μs, 1.2ns were demonstrated with a cavity length of 65m [93].

Pulse dynamics in Bi-doped fibres in the anomalous dispersion regime are complicated to understand due to the soliton grouping phenomenon. Recently soliton grouping was observed in Bi-doped germanosilicate fibres. SESAM and frequency shifted feedback technique were used to mode-lock the Bi-doped fibre laser operating at 1450nm. In

both cases a 1320nm semiconductor disk laser was used as a pump source. Fundamental cavity soliton width of 900fs and 1.89ps were reported [94, 95].

1.4.3 Bi-doped pulsed fibre lasers from 1600-1800nm

The emission band of Bi-doped fibres was further extended upto 1800nm using high germania (50mol%) doped fibres. 1.65ps pulses at 1730nm were demonstrated with a fundamental repetition rate of 4MHz. A SWNT was used to initiate the mode-locking and pulse dynamics were studied in both normal and anomalous dispersion regimes. The dispersion of the cavity was adjusted by using different length of single mode fibre (SMF) within the cavity. An Er-doped fibre laser (EDFL) at 1563nm was used as a pump source. A 5m length of the Bi-doped fibre was used as an active medium. 1.4 and 1.65ps pulses were reported in the normal and anomalous dispersion regimes, respectively [96]. Recently another technique based on nonlinear phase shift in figure of eight scheme was also used to develop pulsed fibre laser at 1700nm. The cavity consisted of 15m long active fibre with positive dispersion at 1700nm and a 25m passive silica based fibre with 30mol% Ge content. The passive fibre will introduce extra non linearly into the loop mirror. The laser produces 18ps pulses at 3.57 MHz repetition rate with a pulse energy of 84pJ. The pulses were then amplified by using BDFA operating at 1700nm and increased the pulse energy to 5.7nJ at the expense of pulse elongation to 28ps. Amplified pulses were then compressed to 630fs by using 150m long SMF-28 [97].

1.5 Superfluorescent sources (SFS) in different wavelength bands using Bi-doped fibres

Superfluorescent sources (SFS) were also developed by using Bi-doped fibres. The first SFS was developed at 1.44μm using Bi-doped germanosilicate fibre in 2012. A Raman fibre laser at 1320nm with a pump power of 260mW and a 200m long Bi-doped fibre was used in a single stage. SFS having a bandwidth of 25nm at an output power of 82mW, with an optical efficiency of 31% was reported. Temperature stability of SFS was also studied from -60^{0}C to +60^{0}C. The mean wavelength of the SFS was varied from 1444 to 1440.5nm and the FWHM was changed from 24.4 to 26nm [98]. Further, SFS at 1.34μm was also demonstrated by Bi-doped phosphosilicate fibre. Here the experimental set up consist of two stages, the first stage acts as a signal source and the second stage acts as an amplifier. In the first stage, a laser diode operating at 1240nm with a total pump power of 300mW and a 150m long Bi-doped phosohosilicate fibre was used. Whereas, in the second stage, a laser diode operating at 1240nm with a total pump power of 300mW

and a 120m long Bi-doped fibre was used. The SFS has an output power of 48mW with a FWHM of 26nm [99]. SFS at 1730nm was also developed by using single pass backward pumped configuration with Bi-doped high germania core fibres. A LD or an Er/Yb-doped fibre laser operating at 1.55nm or 1.57nm was used as a pump source. Bi-doped high germania core fibre of 50m was used to construct the SFS. The threshold power of the SFS was 50mW. An output power of 7mW and FWHM of 50nm was generated with a pump power of 650mW [100].

1.6 Multi-element fibres

To develop broadband amplifiers in the wavelength range from 1500-1620nm, we adopted a novel fibre geometry of multi-element fibres (MEF). Er-doped MEF amplifier can cover the wavelength band from 1500-1620nm (C+L band) for optical fibre communication moreover these amplifiers are compatible for SDM applications. The idea of MEF geometry actually developed from the GT-wave concept which was invented and developed by A.B. Grudinin and P. W. Turner from the ORC, University of Southampton, UK and is shown in Fig 1.14 [101]. This invention helped to scale the power levels of high power fibre lasers.

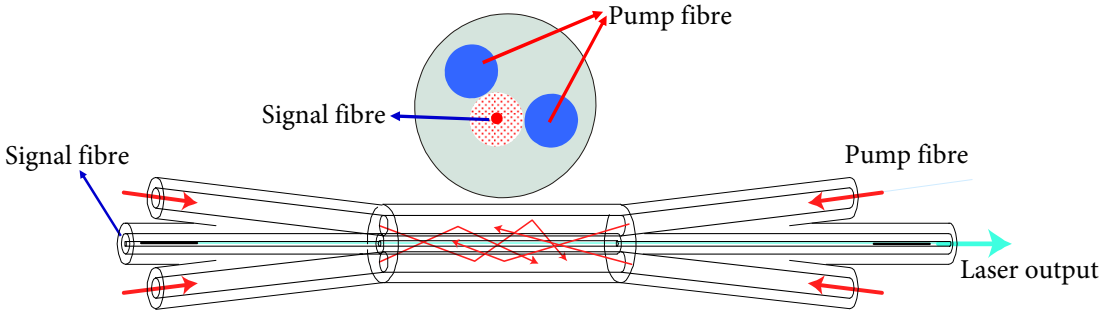

FIGURE 1.14: Shematic representation of GT-wave concept [101]

In GT- wave concept as shown in Fig 1.14 two passive fibres close to the signal fibre (RE-doped) held under common low index coating were used for pump and signal delivery, respectively. The pump light couples to the signal fibre which is doped with RE as it propagates along the length of the fibre.

Similar to GT-wave fibre, MEF basically comprises of multiple fibre elements (fibre with core and clad) under common coating. The cores can be doped with RE elements such as Er, Yb and Tm or Ho depending on the wavelength of amplification required. The preform to develop MEF fibres were fabricated by MCVD-solution doping technique.

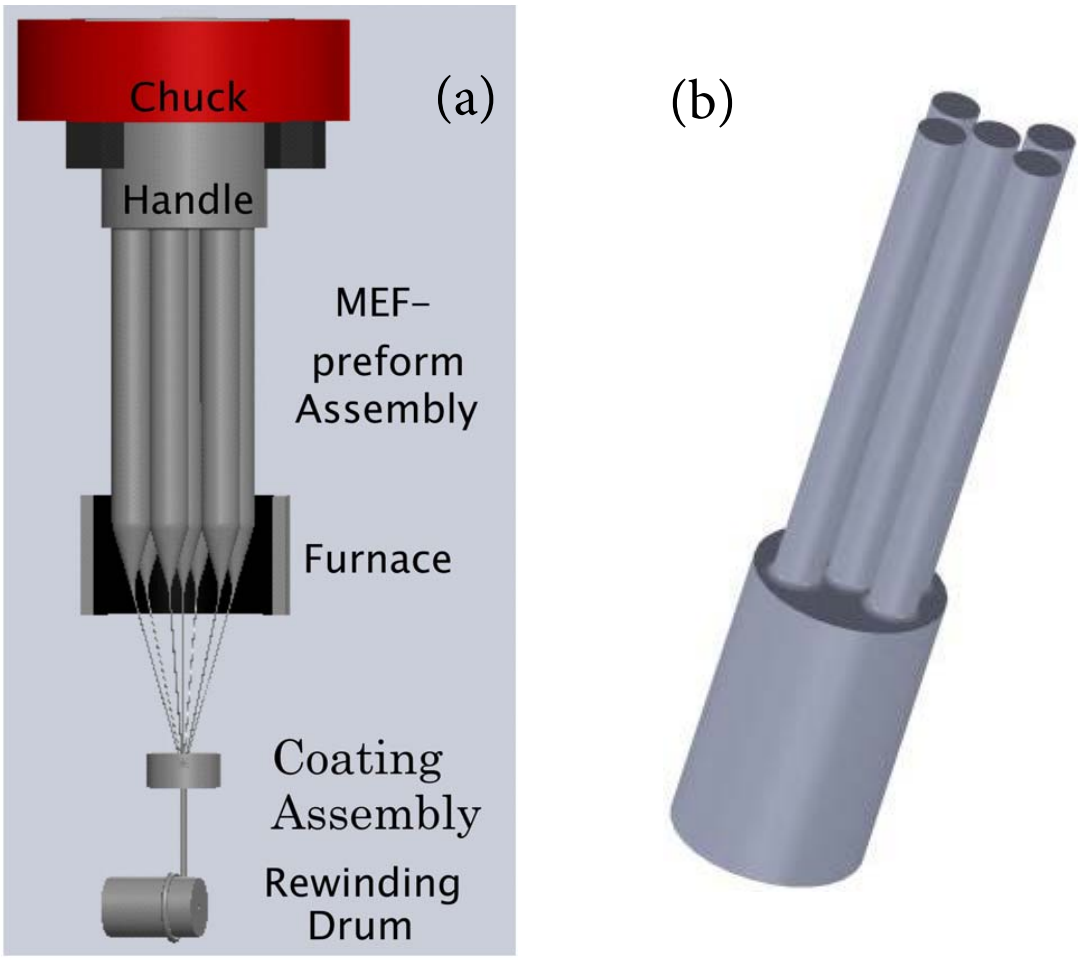

FIGURE 1.15: (a) Schematic of 7-MEF preform draw on tower (b) Schematic of 5-MEF (cladding pump) preform [102]

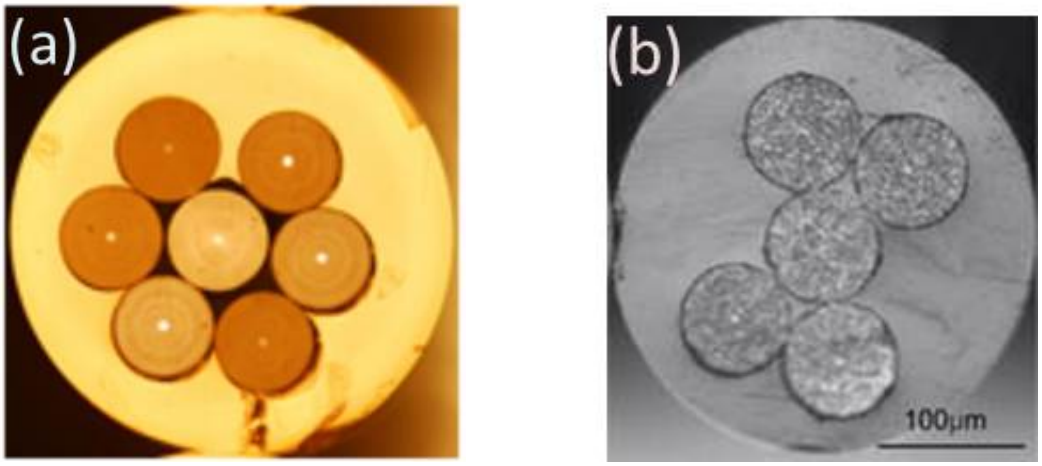

FIGURE 1.16: (a) Microscopic image of 7-MEF (b) Microscopic image of 5-MEF [102, 103]

Once the preform was made with required dopant it is stretched and cut into sections of equal lengths to allow stacking in the required 3-MEF and 7-MEF configurations.

A support handle was joined to the stacks to allow simultaneous drawing of the fibre elements as shown in Fig 1.15 (a). When drawing the MEFs, the fibres were collected together and threaded through a pressurised coating system to enable them to be combined and coated together with a high or low index polymer coating (fabricated by S. Jain and T. C. May-Smith). Note that as opposed to MCF the MEF approach is highly tolerant to any imperfection in fibre geometry due to the independent nature of the individual elements and the means of interconnection [102]. MEF can be operated under the core pump as well as cladding pumping. In case of cladding pumping one of the element of the MEF was replaced with a coreless suprasil F-300 rod for pump delivery and the remaining fabrication process is similar. Schematic of 5-MEF cladding pump preform is shown in Fig 1.15 (b). In the core pumping configuration both pump and signal light guide in the core independently. Whereas in cladding pumping, the pump is guided by a single passive fibre element and all the remaining elements doped with RE share the pump travelling in the passive fibre element. Thus cladding pump configuration reduces the number of pumps required. Fig 1.16 (a) and (b) shows the cross sectional images of MEFs for core and cladding pumping [102, 103]. By using multi-mode MEFs (i.e each element acts as multi-mode) a few mode amplifier for mode division multiplexing was demonstrated [104]. Also a transmission system was built to implement SDM technology [105–107].

There are several advantages of novel MEF geometry to develop amplifiers they are 1. MEF provides convenience in fibre handling as each of the fibres can be accessed independently and conventional splicing techniques can be used. 2. There is no crosstalk between the signals of different fibres. 3. Moreover, the preforms required to develop MEF fibres can be fabricated by using conventional MCVD-solution doping technique.

1.7 Lay out of the thesis

In Chapter 2 we first introduce the conventional MCVD with solution doping and fibre drawing processes to understand the preform and fibre fabrication. Here, we also discuss the fabrication of Bi-doped fibres using MCVD-solution doping process. Characterisation techniques to measure absorption and unsaturable loss in the fabricated fibres are discussed. Elemental compositional analysis of few Bi-doped fibres using electron probe microanalysis (EPMA) is also presented.

In Chapter 3 we discuss the development of Bi-doped aluminosilicate fibres. A 1180nm amplifier is developed by using the fabricated Bi-doped aluminosilicate fibres. Pump optimization to achieve maximum gain at 1180nm is discussed and studied the effect of

UL on gain characteristics. Finally, a 12dB gain Bi-doped aluminosilicate fibre amplifier at 1180nm is demonstrated. This wavelength is suitable for laser guide star application.

Chapter 4 is about the Bi-doped phosphosilicate fibres. These fibres are important to develop lasers and amplifiers for optical fibre communication. Here we discussed the detailed fabrication of Bi-doped phosphosilicate fibre and the effect of fabrication conditions on optical properties such as absorption and unsaturable loss. Further, we discussed the development of Bi-doped fibre laser operating at 1360nm and demonstrated 100mW output power with 50m long fibre. We also discussed the development of Bi-doped fibre amplifier in the O-band for optical communication. Gain dependency on pump wavelength is studied and developed a flat gain Bi-doped phosphosilicate fibre amplifier in the wavelength range from 1320-1360nm.

Chapter 5 discusses the Bi-doped pulsed fibre lasers. Here we studied the pulsing phenomena in Bi-doped fibres using a ring cavity without any saturable absorber. Effect of pump power on pulse width is presented. A mode-locked Bi-doped fibre with an output power of 3mW is developed and a master oscillator power amplifier is constructed to amplify the output power to 18mW. Finally, a picosecond (ps) Bi-doped fibre laser at 1340nm with 1.15W peak power is demonstrated using 25m long Bi-doped phosphosilicate fibre.

Chapter 6 provides the general background of Er-doped 3-MEF, 7-MEF. Gain and NF characterisation of these fibres is presented in single and cascaded configurations in order to develop a wideband multi-element Er-doped fibre amplifier. Also, a brief introduction of Er/Yb-doped MEFs and their application to develop wideband MEF fibre amplifiers using cladding pumping configuration are discussed.

Chapter 7 presents the future scope of work presented in this thesis. Initially, the work discussed in this thesis is reviewed and the future directions of this work on Bi-doped fibre fabrication and development of Bi-doped fibre amplifiers and lasers are mentioned. Also, a brief note on the extension of MEF work to develop broadband amplifiers is presented.

Chapter 2

Fabrication and characterisation of Bi-doped optical fibres

2.1 Introduction

The aim of this chapter is to introduce the Bi-doped preform fabrication approach using conventional modified chemical vapour deposition (MCVD) method in combination with solution doping. The fibre drawing process to fabricate fibres from Bi-doped preforms is also discussed. The characterisation techniques to measure absorption and unsaturable loss (UL) which are used to investigate Bi-doped fibres are discussed. Finally, electron probe microanalysis of few fabricated Bi-doped preforms is presented.

2.2 MCVD-solution doping method

Modified chemical vapour deposition (MCVD) method is a conventional process to fabricate passive preforms with high purity. This method is widely used in industry as well as in research to manufacture a range of high performance optical fibres for optical communication because of reproducible control over refractive index profile and superior process flexibility. In case of MCVD method to produce passive preforms volatile liquid halide precursors such as $SiCl_4$, $GeCl_4$, $POCl_3$, BBr_3 and SF_6, with high vapour pressure at a temperature around 30^oC were used. These chemicals are sent into the rotating silica reference tube (F300) while heating it up using an oxyhydrogen burner. The burner can move along the length of the reference tube and its movement is precisely controlled by the computer. The core composition depends on the chemical flow of the precursors into the tube and the temperature of the burner. Whereas the core thickness can be

controlled by the number of layers deposited. Once the desired number of layers were deposited the preform with a hole in the centre is collapsed to a minimum and follows sealing of the glass tube to get a solid preform. On the other hand, because of low vapour pressure of RE precursors such as $ErCl_3$, $YbCl_3$, $TmCl_3$ it is not possible to incorporate these chemicals using chemical vapour deposition method at low temperatures around 30^oC hence alternative procedures are required to introduce these chemicals within the core of the preform. One of these procedures is called solution doping. MCVD process in combination with solution doping technique is the well-matured method to develop rare earth (RE)-doped fibres with low-loss. Along with standard telecommunication fibres that were used for long-haul optical communication, RE-doped speciality optical fibres (erbium (Er), ytterbium (Yb), neodymium (Nd), thulium (Tm) and holmium (Ho)) are the current driving force of the fibre industry. These RE-doped fibres are used to produce lasers and amplifiers in different wavelength bands of the IR spectrum. The advantage of MCVD with solution doping process is that it is simple and convenient to play with different process parameters during the preform fabrication to develop a range of active preforms. The process coupled with solution doping technique involves two major steps.

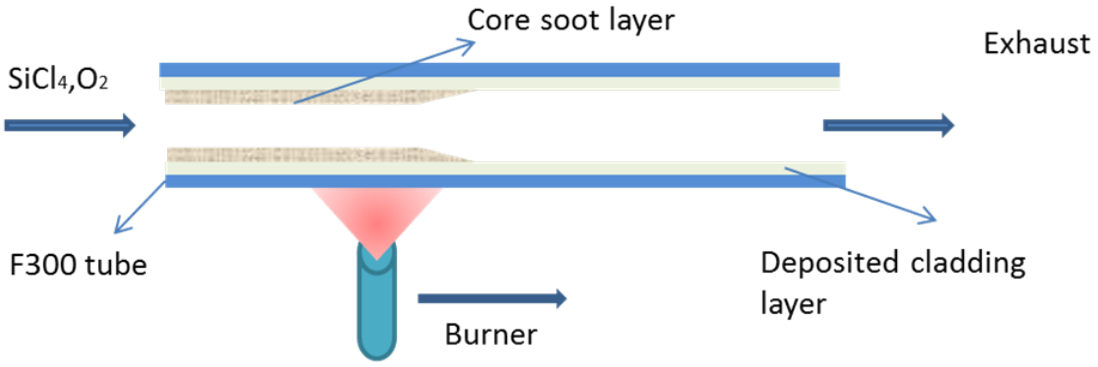

FIGURE 2.1: Schematic of MCVD process

In the first step, an F300 tube was heated up and etched to remove any contamination that can induce the loss by passing through SF_6 gas mixture with oxygen while the outer surface of the tube is heated by the burner. Then several sintered silica cladding layers were deposited at a burner temperature of about 2000^oC to avoid OH^- diffusion into the preform core in the subsequent heating process. After this, a soot layer (partly vitrified silica or silica with phosphorous and germanium) for the RE incorporation into the core is deposited at a low temperature as shown in Fig 2.1.

The second step involves the solution doping technique, in which the soot layer deposited inside the tube as mentioned in the first step was solution doped by keeping the tube within an alcoholic solution (mixture of RE and Al salts in water or alcohol) filled container for approximately an hour as shown in Fig 2.2.

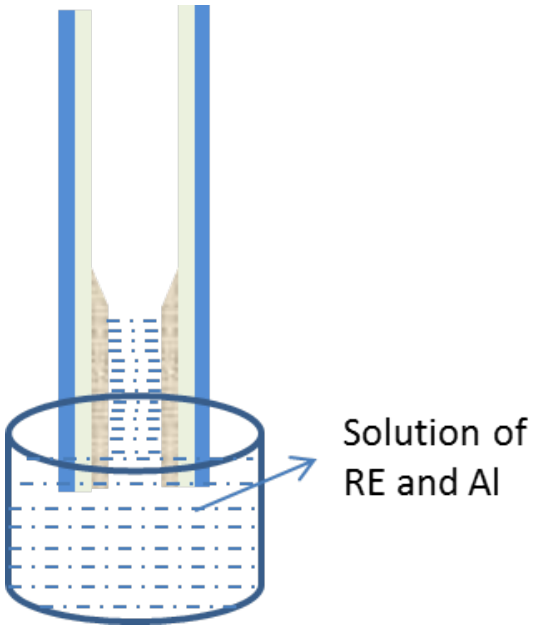

FIGURE 2.2: Schematic solution doping process

After the porous layer impregnation process with desired RE-dopants finished, the preform is again carried on to the MCVD lathe. Then the porous layer is subsequently dehydrated in the presence of N_2/O_2 flow to eliminate traces of solvents and OH^- adsorbed in the soot during solution doping process. Next, the dried porous layer is gently heated in the presence of oxygen (O_2) for the conversion of the RE- and Al-salts into corresponding oxides. A temperature of 800-1200^{o}C is usually maintained at this stage. This is done to avoid evaporation of the salts during subsequent processing steps at high temperature. However, control of temperature at this stage is critical to ensure complete oxidation without evaporation which is strongly dependent on the characteristics of the salts used. The final step is sintering of the porous layer to obtain the RE-doped silica core. The tube containing the RE-doped core is finally collapsed to produce the preform. At this step due to increasing burner temperature and slower burner traverse speed, the preform with a central hole will be collapsed under surface tension and eventually sealed into a solid preform. The same process was implemented to fabricate Bi-doped preforms with slight modifications. Since the Bi-doped fibre absorption and emission characteristics depend on the co-dopants, different co-dopants such as aluminium (Al) and phosphorous (P) were used to form the guiding structure and to change the absorption and emission bands of the resulted Bi-doped fibres. Al was incorporated through solution doping whereas P was introduced into the core of the preform during porous layer deposition. Whereas Bi was incorporated into the core through solution doping technique, which was realized by dissolving Bi precursors (such as Bi-tris (2, 2, 6, 6- tetramethyl-3, 5-heptanedionate) and $BiCl_3$) in isopropanol alcohol or ethanol. Fabricated preforms and their core compositions are described in detail in

subsequent sections.

2.3 Fibre drawing process

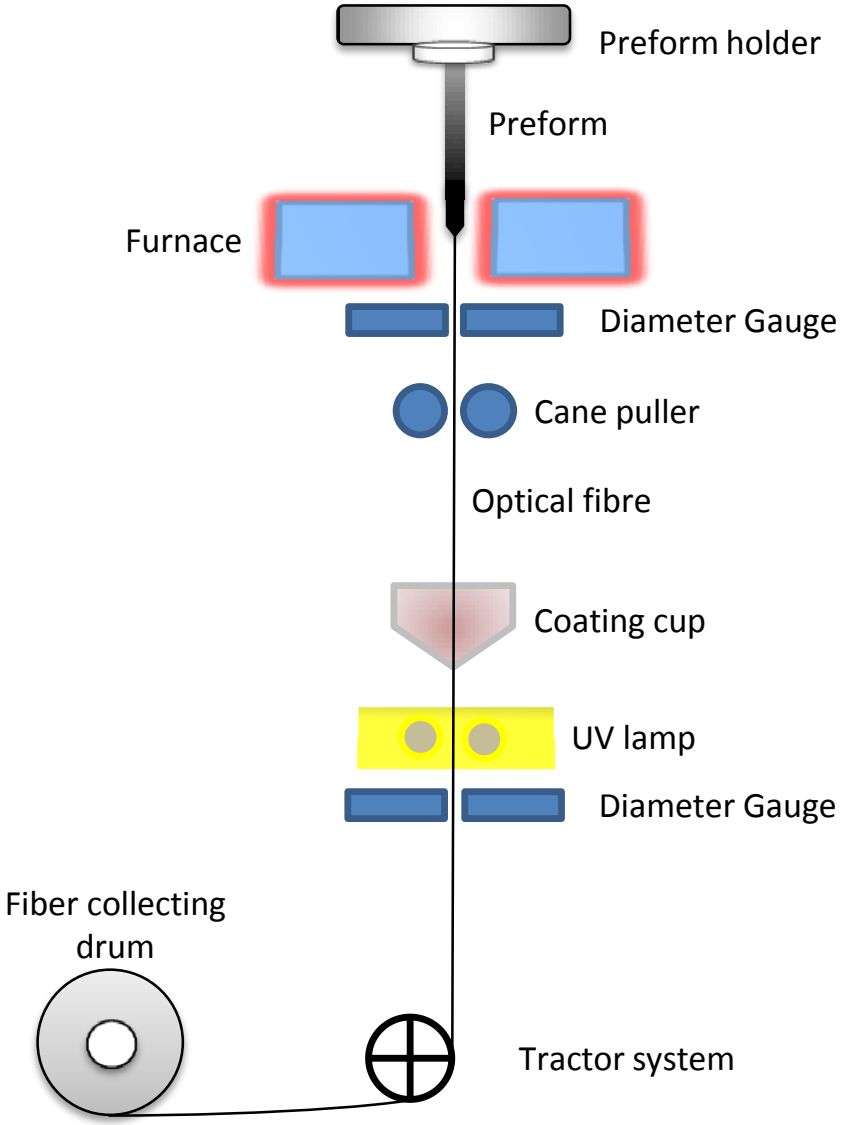

FIGURE 2.3: Fibre drawing process

Fabricated preforms were drawn into fibres by using optical fibre drawing process as shown in Fig 2.3. The process of drawing Bi-doped fibres was straightforward similar to drawing of conventional preforms. Before starting the drawing process the refractive index profile of the preform was measured by using PK2600 preform analyser. From the measured refractive index profile, one can find the preform core (P_{co}) and clad (P_{cl}) diameters. The draw speed (V_f) can be calculated from the known parameters such as

preform clad (P_{cl}) diameter, feed speed (V_p) and required fibre clad diameter (F_{cl}) from the following equation 2.1

$$V_f = V_p \frac{P_{cl}^2}{F_{cl}^2} \tag{2.1}$$

The draw process involves the following steps. Initially, the preform is loaded into the drawing tower and then adjusted at the centre of the furnace entrance. Then the preform is moved down to the heating region of the furnace. Once the preform is adjusted in the furnace centre, the furnace is switched on to heat up to the fibre drawing temperature. The preform inside the furnace is also heated up by heat transfer from the furnace element to preform rod. A drop is formed at the heated zone and this drop of preform falls down due to the gravity. When the drop followed by hair-thin fibre comes out of the furnace the drop is cut and then feed the fibre thread into the capstone (cane puller). One can start the feed of the preform and the feed speed is adjusted depending on the required fibre diameter. Once the required diameter was reached we will feed the fibre through the coating dies that are selected according to the fibre diameter. The fibre goes through the coating dies into the coating cup to apply coating. Depending on the application of the fibre, high or low index coating will be selected. Immediately after the fibre comes out of the coating cup, it passes through an ultraviolet (UV) curing lamp where the coating gets cured. Then the fibre is fed through the capstone and eventually collected by using a fibre bobbin. Presence of diameter gauges after the furnace and the UV curing lamp helps to monitor the diameter of fibre with and without coating, respectively. By monitoring the fibre diameter in a real-time and by adjusting the draw parameters the fibre with desired core and clad diameter can be fabricated.

2.4 Characterisation techniques

2.4.1 Cut-back technique

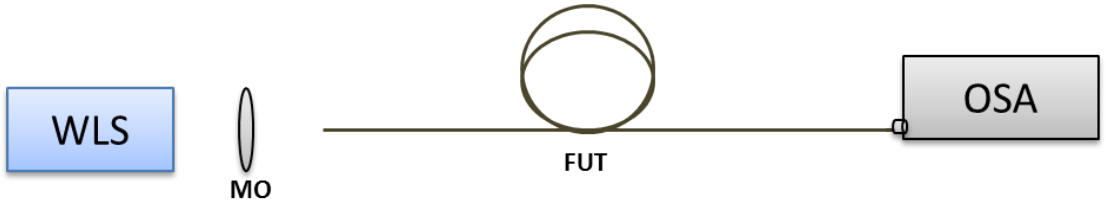

FIGURE 2.4: Schematic of cut-back technique

Schematic of cut-back technique to measure fibre absorption is as shown in Fig 2.4. A tungsten halogen lamp as white light source (WLS), microscopic objective (MO) and an

optical spectrum analyser (OSA) were used to build the experimental setup of cut-back technique. Initially the fibre under test (FUT) of length L_1 was placed in the setup as shown in Fig 2.4. The absorption of the FUT is measured then the fibre is cut back to length (L_2) and the absorption is measured again. By the two absorption measurements and by knowing the measured lengths (L_1, L_2) one can find the absorption per unit length of the fibre by using equation 2.2

$$\text{Absorption(dB/m)} = \frac{Abs_{\text{after}} - Abs_{\text{before}}}{L_1 - L_2} \tag{2.2}$$

Where L_1, L_2, and Abs_{before}, Abs_{after} are length of the fibre and the corresponding absorption before and after the cut-back.

2.4.2 Unsaturable loss measurement

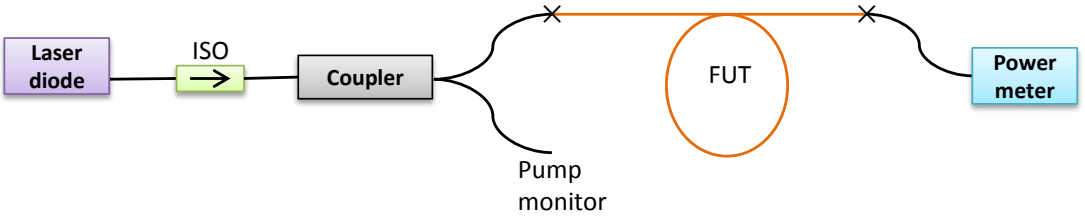

FIGURE 2.5: Schematic of unsaturable loss measurement

Schematic experimental setup to measure UL is shown in Fig 2.5. The setup consists of a laser diode, an isolator, a coupler and a power meter. The laser diode wavelength selection is based on the Bi-doped fibre host glass and the pump wavelength to develop laser or amplifier. Isolator is used to protect the pump from back reflections and a coupler is used to monitor the input pump power. Few precautions need to be considered when measuring the UL they are; 1. the end of the doped fibre should be angle cleaved to avoid back reflections and 2. it is also necessary to use short fibre lengths to prevent any amplified spontaneous emission (ASE) generation. The input pump power P_{in} is varied and the corresponding output power P_{out} is measured by using a power meter. Using measured input power P_{in} and output power P_{out} before and after the FUT, the UL of fibre can be calculated by using equation 2.3

$$\text{Unsaturable loss (dB/m)} = \frac{10}{L} \log_{10} \frac{P_{in}}{P_{out}} \tag{2.3}$$

2.4.3 Gain and noise figure measurement

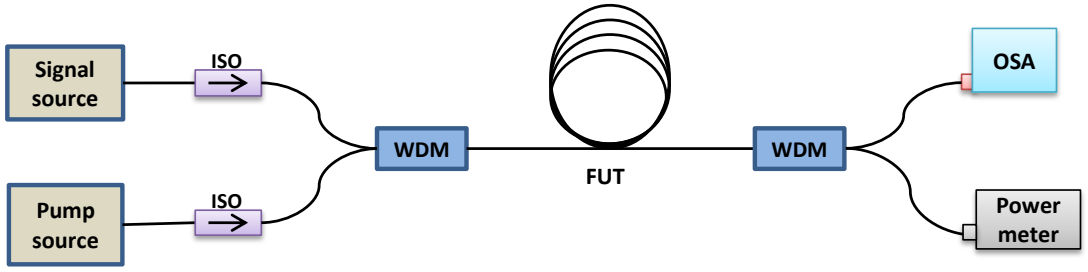

FIGURE 2.6: Experimental set up to measure gain and noise figure

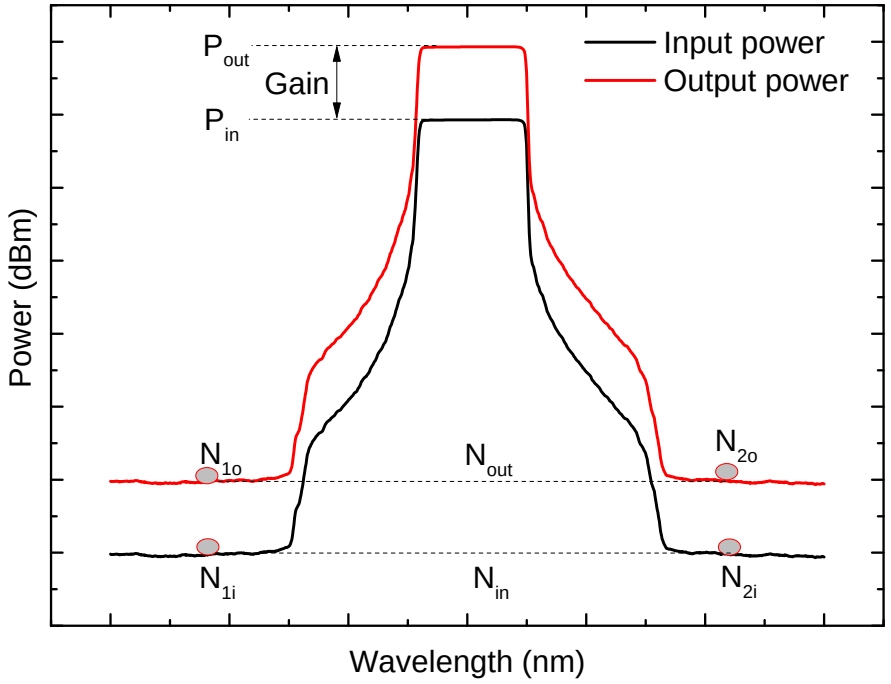

FIGURE 2.7: Spectral measurements to determine gain and noise figure

The experimental set up to measure gain and noise figure is shown in Fig 2.6. Here we need a signal source, pump source, wavelength division multiplexer (WDMs), isolators (ISO), fibre under test (FUT) and an optical spectrum analyser (OSA) and also a power meter. The signal source selection depends on the wavelength band (C-band, L-band and O-band) in which the gain and noise figure (NF) of the fibre need to be measured. Pump source selection depends on the fibre absorption band. WDMs and isolators are chosen based on the signal and pump sources. Gain and NF of fibre can be calculated by measuring the input and output signal powers before the FUT and after the output WDM by an OSA as shown in Fig 2.7.

Gain of the amplifier is defined as the difference between the output and input signals when the power levels are measured on a logarithmic scale.

$$\text{Gain(dB)} = P_{\text{out}} - P_{\text{in}} \tag{2.4}$$

Where P_{in}, P_{out} are the power levels for input and output signals, respectively as shown in Fig 2.7.

Amplification of an optical signal takes place by stimulated emission of ions from an upper energy level to the ground level. The ions in the upper energy level can also emit radiation by the process of spontaneous emission. This spontaneous emission appears over the entire fluorescent band and is completely incoherent with respect to the signal beam. Some of this spontaneously emitted radiation is coupled to the LP_{01} mode of the fibre and as it propagates through the gain medium in both forward and backward direction it gets amplified. The resultant optical radiation is referred as amplified spontaneous emission(ASE). This incoherent radiation also propagates with the signal and interfere with the signal when it is detected by the photo detector. This results in the generation of noise that ultimately limits the receiver sensitivity of an optical fibre transmission system. Hence it is important to measure the noise figure of an amplifier. In this thesis we used interpolation technique to measure the NF of an amplifier. It is so called because the ASE at the signal wavelength is determined by measuring ASE level at a wavelength just above and below the signal and interpolating to determine the level at signal wavelength as shown in Fig 2.7. Noise figure of the amplifier is then calculated by 2.5

$$\text{NF(dB)} = \frac{N_{\text{out}} - N_{\text{in}}G}{h\nu G(B.W)} + \frac{1}{G} \tag{2.5}$$

Where $N_{in} = \frac{N_{1i}+N_{2i}}{2}$ and $N_{out} = \frac{N_{1o}+N_{2o}}{2}$ are the noise power for input and output signals, respectively. B.W and ν are optical spectrum analyser (OSA) noise bandwidth and signal frequency. $h = 6.626 * 10^{-34}$ J.s is the Plank's constant and G is amplifier gain [108, 109]. To measure the input and output signal powers an optical spectrum analyser (YOKOGAWA AQ6370) with a resolution bandwidth of 0.5nm was used.

2.5 Fabrication of Bi-doped preforms

We fabricated Bi-doped preforms with different host glasses such as aluminosilicate and phosphosilicate to cover the wavelength band from 1150-1500nm. MCVD-solution doping technique was used to fabricate these preforms. In this section, a detailed fabrication procedure of Bi-doped preforms is presented (fabrication was done jointly with A. A. Umnikov).

2.5.1 Bi-doped aluminosilicate preforms

Bi-doped preforms with aluminium host glass were fabricated to develop lasers and amplifiers in the wavelength band from 1150-1250nm. MCVD-solution doping method as mentioned at the beginning of this chapter was used to fabricate these preforms. Initially, a soot layer of silica was deposited on the inner wall of F300 silica tube with outer and inner diameters of 16 and 13mm, respectively. The tube with deposited silica porous layer was withdrawn from the MCVD lathe and then the soot preform was soaked in an $AlCl_3$ methanol solution. After the porous layer infiltration with aluminium dopant source solution, the tube was again taken onto the MCVD lathe for drying. Subsequently, the solvent was removed from the porous layer by passing a dry oxygen (O_2), nitrogen (N_2) and helium (He) mixture flow through the tube, while rotating it. After that $AlCl_3$ was oxidized in an O_2 flow at a temperature about 1150^oC to form a silica porous layer deposited with Al_2O_3. The alumina concentration in the core was adjusted by $AlCl_3$ concentration in source solution to achieve desirable refractive index profile. In this step porous layer was remained un-sintered with maintained porous structure and used once again for solution doping process involving the solution of Bi precursor. This two-step process was implemented due to the solubility problem of precursors we used and to avoid sedimentation with the simultaneous dissolving of Al and Bi precursors in one source solution.

In the second step to obtain a Bi-doped core, we used $Bi(tmhd)_3$ in isopropanol solution as a precursor. Again solution doping process was used to impregnate the soot body with the solution of $Bi(tmhd)_3$ in isopropanol. Once the solution was impregnated uniformly along the length of the porous layer, the preform was taken onto the lathe and dried by passing N_2 and He mixture flow through the tube. The doping level of Bi was varied by changing the quantity of $Bi(tmhd)_3$ solved in alcoholic solution. In this way, we fabricated two (L30366, L30367) Bi-doped aluminosilicate preforms with core composition of SiO_2-Al_2O_3-Bi_2O_3. The preform L30366 was doped with a higher concentration of Bi compared to the preform L30367. The index difference between the core and clad was 0.008 in case of L30366 whereas in case of L30367 it was 0.009. These preforms had a transparent core with reddish colour when looking through preform tip. The preforms were drawn into fibres (A0621, A0647) with an outer diameter of 100μm and a core diameter of 8μm. In chapter 3, we will discuss the characteristics of these fibres in detail.

2.5.2 Bi-doped phosphosilicate preforms

Bi-doped preforms with phosphosilicate host were fabricated to develop lasers and amplifiers in the wavelength band from 1300-1500nm. In case of Bi-doped phosphosilicate preforms, a soot layer of phosphosilicate glass was deposited on the inner wall of F300 silica tube with an outer and inner diameters of 16 and 13mm, respectively. Then the tube with phosphosilicate porous layer was withdrawn from the MCVD lathe and was used for solution doping process with $Bi(tmhd)_3$ in isopropanol solution as a precursor.

Three Bi-doped phosphosilicate preforms L30368, L30369, L30370 with a core composition of SiO_2-P_2O_5-Bi_2O_3 were fabricated. All these preforms had a transparent core with yellow to brownish colour when looking through the preform tip. The three preforms were also solution doped with the same Bi concentration in source solution. In case of L30368 and L30369 sintering of porous layer and collapsing of preforms were done under mixed He and O_2 atmosphere with a ratio of 1:1 and 1:4, respectively. In case of the L30370 preform, complete O_2 atmosphere was used for sintering of the porous layer and collapsing of the preform. These preforms were drawn into fibres (A0623, A0622, A0625) with an outer diameter of 100μm and a core diameter of 13μm. The index difference between core and clad was measured to be 0.004 in all three fibres. The details of fibre characterisation are discussed and presented in chapter 4.

The Bi concentration of the fabricated preforms (L30368, L30369, and L30370) was low and required longer length for lasing and amplification. In order to reduce the length of required fibre for lasing and amplification, the concentration of the Bi-dopant needs to be increased. We used different solutions and optimised the MCVD-solution doping process parameters to increase the concentration of Bi in preform core. In the following section, the fabrication of high concentration Bi-doped preforms is presented.

2.5.3 High concentration Bi-doped phosphosilicate preforms

High concentration Bi-doped fibres are important specifically when designing pulsed fibre lasers and double clad fibre lasers. To investigate the possibility to achieve a higher concentration of Bi in fibres we used the same MCVD-solution doping fabrication technology but with different Bi solutions such as butyl acetate and n-octane instead of isopropanol solvent. The solubility of $Bi(tmhd)_3$ is higher in these solvents that make it easier to incorporate more Bi-dopant into the core by solution doping [110]. Here, source solutions were made with $Bi(tmhd)_3$ as Bi precursor and butyl acetate or n-octane as a solvent.

Two Bi-doped phosphosilicate preforms (L30439 and L30441) with a core composition of SiO_2-P_2O_5-Bi_2O_3 were fabricated. The preform L30439 was fabricated by using n-octane solution whereas L30441 was fabricated by using butyl acetate solution. The fabricated preforms were drawn into fibres (A0746, A0745) with core and clad diameters of 13 and 100μm respectively. The index difference between core and clad was measured to be 0.004. Absorption, unsaturable loss and lasing characteristics of these fibres were measured and are presented in Table 2.1. The characterisation techniques mentioned at the beginning of chapter 2 were used to measure the absorption and unsaturable loss. For lasing characterisation, a simple ring cavity as mentioned in chapter 4 with 80/20 coupler was used.

Preform No.	Fibre No.	Absorption@1267nm (dB/m)	%UL	Lasing
L30439	A0746	2	34	No
L30441	A0745	1.5	27	Yes

TABLE 2.1: Absorption, UL and laser performance in Bi-doped phosphosilicate fibres (A0746, A0745)

We noticed that fibre drawn from the preform L30441 (A0745) has low unsaturable loss compared to a fibre from the preform L30439 (A0746). Also, in case of fibre (A0745), lasing was obtained using 20m long fibre with an output power of 3mW whereas no lasing was observed using fibre A0746. It is observed that, fibres fabricated by using n-butyl acetate solvent has low UL and shown lasing action. From these observations, we selected n-butyl acetate solvent for further preform process optimisation. Preforms L30459, L30461, L30462 with the same core composition of SiO_2-P_2O_5-Bi_2O_3 were fabricated to optimise the process parameters such as temperature and flow of gases. The fabricated preforms were drawn into fibres (A0787, A0792, A0795) with core and clad diameters of 13 and 100μm respectively. The index difference between core and clad was measured to be 0.004 in all three fibres. Absorption, UL and lasing characteristics of these fibres were measured and shown in Table 2.2.

Preform No.	Fibre No.	Absorption@1267nm (dB/m)	%UL	Lasing
L30459	A0787	1.7	16	Yes
L30461	A0792	2.2	22	Yes
L30462	A0795	2	20	Yes

TABLE 2.2: Absorption, UL and laser performance in high concentration Bi-doped phosphosilicate fibres (A0787, A0792 and A0795)

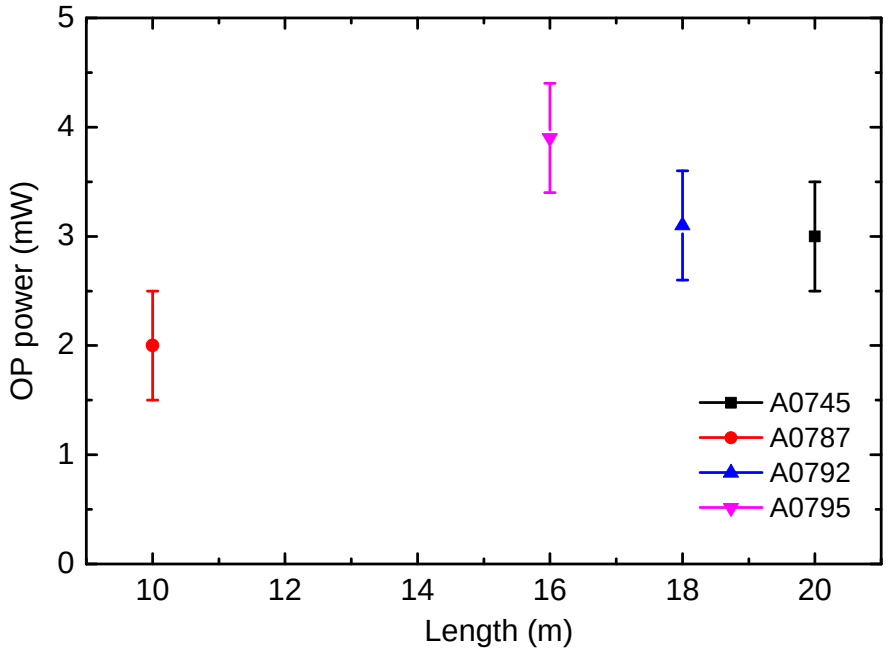

FIGURE 2.8: Laser performance in different length of high concentration fibres fabricated

Absorption and UL were measured in all the fibres by using characterisation techniques mentioned at the beginning of chapter 2. Absorption and UL were 1.7dB/m and 16%, respectively in case of A0787. In case of A0792 absorption and UL were 2.2dB/m and 22% whereas in A0795, absorption and UL were 2dB/m and 20%. These fibres were tested for lasing in a ring cavity with 80/20 coupler. Minimum fibre length required for lasing and the corresponding output power of fabricated Bi-doped fibres were shown in Fig 2.8. From these preform set, the fibre from L30459 has a low unsaturable loss and lasing is possible using only 10m long Bi-doped fibre with an output power of 2mW. This fibre was used to develop a mode-locked Bi-doped fibre laser and the details are discussed in chapter 5.

2.6 Electron probe microanalysis of Bi-doped fibres

Electron probe microanalysis (EPMA) is a non-destructive method to analysis elemental composition in micron-sized volumes like optical fibres, with sensitivity at the level of parts per million (ppm). EPMA of some of the fabricated Bi-doped fibres was performed and estimated the concentration of Bi and the co-dopants in the fibre. In the following section, we will discuss the results of EPMA

2.6.1 EPMA of Bi-doped aluminosilicate fibre

Preform No.	Fibre No.	Abs.@1120nm	%UL	Bi_2O_3 (Wt%)	Al_2O_3 (Wt%)
L30366	A0621	0.35 (dB/m)	35	0.02	7

TABLE 2.3: EPMA in Bi-doped aluminosilicate fibre

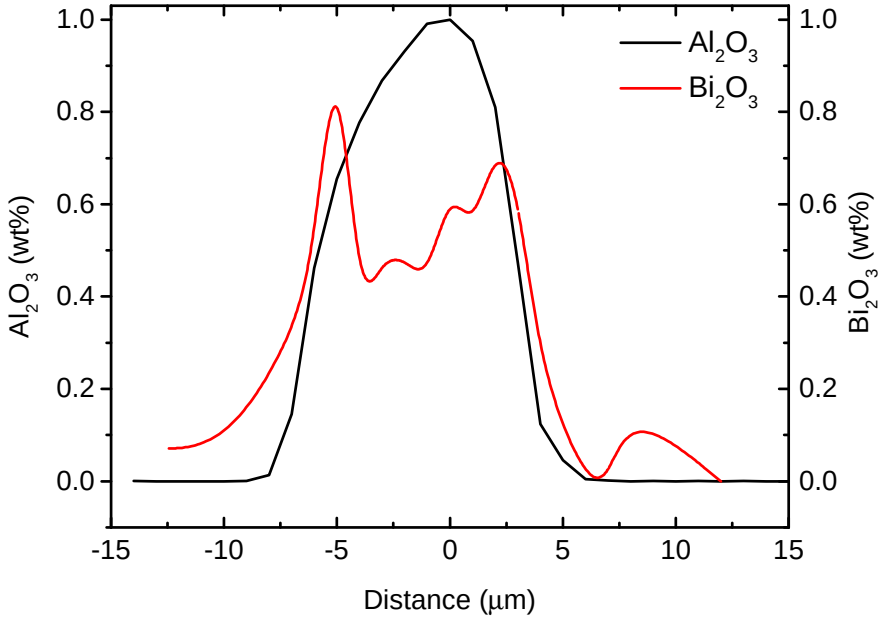

FIGURE 2.9: Normalized distribution of Al_2O_3 and Bi_2O_3 in fibre A0621

Among two Bi-doped aluminosilicate fibres fabricated, best performing fibre (A0621) with absorption and UL as shown in Table 2.3 is analysed for elemental composition by EPMA. This fibre contains SiO_2, Al_2O_3 and Bi_2O_3 within the core of the fibre. The concentration of Bi_2O_3 is relatively low. The EPMA showed that the concentration of Al_2O_3 was 7wt% whereas Bi_2O_3 was on average 0.02wt%. The normalized distribution of Al_2O_3 and Bi_2O_3 are shown in Fig 2.9. The concentration of Bi_2O_3 was very low as opposed to Al_2O_3. The distribution of Bi_2O_3 has followed Al_2O_3 profile with in the core region.

2.6.2 EPMA of Bi-doped phosphosilicate fibres

EPMA of fabricated Bi-doped phosphosilicate fibres as mentioned in Table 2.4 was also performed. These fibres contain SiO_2, P_2O_5 and Bi_2O_3 within the core of the fibre.

Preform No.	Fibre No.	Abs.@1267nm	%UL	Bi_2O_3 (Wt%)	P_2O_5 (Wt%)
L30368	A0623	2.8 (dB/m)	24	0.23	7.9
L30370	A0625	1 (dB/m)	7	0.11	8.8
L30459	A0787	1.7 (dB/m)	17	0.23	8

TABLE 2.4: EPMA in Bi-doped phosphosilicate fibres

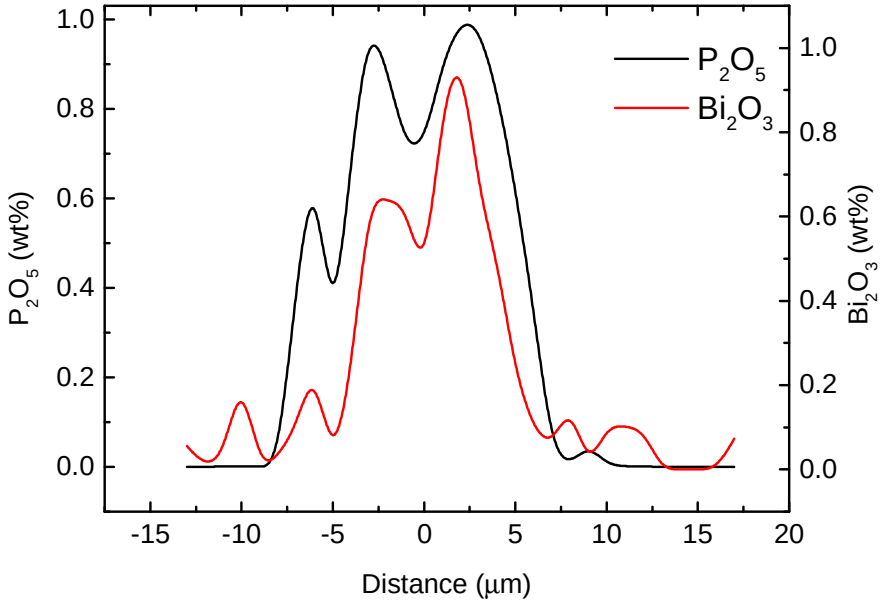

FIGURE 2.10: Normalized distribution of P_2O_5 and Bi_2O_3 in fibre A0623

In case of A0623, EPMA showed that, the concentration of P_2O_5 was 7.9wt% whereas Bi_2O_3 was 0.23wt%. The normalized distribution of P_2O_5 and Bi_2O_3 are shown in Fig 2.10. The distribution of Bi_2O_3 has followed the P_2O_5 profile within the core region.

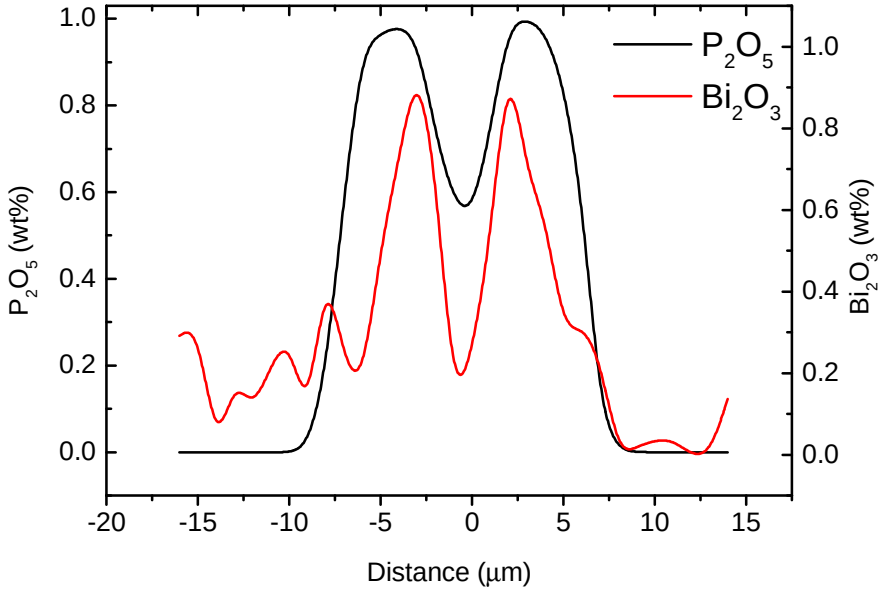

FIGURE 2.11: Normalized distribution of P_2O_5 and Bi_2O_3 in fibre A0625

In case of A0625, EPMA showed that, the concentration of P_2O_5 was 8.8 wt% whereas Bi_2O_3 was 0.11wt%. The normalized distribution of P_2O_5 and Bi_2O_3 are shown in Fig 2.11. Again the distribution of Bi_2O_3 follows the P_2O_5 profile within the core region.

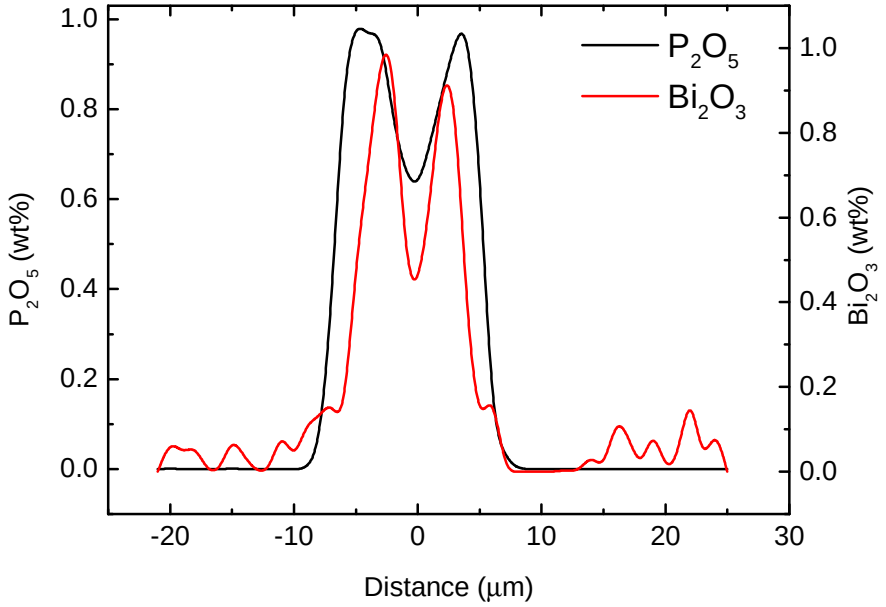

FIGURE 2.12: Normalized distribution of P_2O_5 and Bi_2O_3 in fibre A0787

In case of A0787, EPMA showed that, the concentration of P_2O_5 was 8wt% whereas Bi_2O_3 was 0.23wt%. The normalized distribution of P_2O_5 and Bi_2O_3 are shown in Fig 2.12. The distribution of Bi_2O_3 has followed the P_2O_5 within the core region. The dip at centre of the normalized distributions of P_2O_5 and Bi_2O_3 as in Fig 2.10, Fig 2.11 and

Fig 2.12 is due to the evaporation of P_2O_5 during sealing process of preform fabrication. Also, the ripples appeared in the cladding are measurement artefacts and are not real features of the fibre.

2.7 Conclusion

In this chapter 2, the conventional MCVD process and solution doping technique was discussed and then explained some modifications made in the conventional process to fabricate Bi-doped preforms with different co-dopants such as aluminosilicate and phosphosilicate. Other fabrication processes such as powder in tube or rod in tube methods can be used to develop Bi-doped fibres but these methods are not advanced enough such as MCVD process. They could increase the background losses in the fibre and also repeatable results may not be possible. The fibre drawing process was discussed in brief to give an idea on the fibre fabrication from the Bi-doped preforms. The characterisation techniques to measure absorption and unsaturable loss were discussed with experimental setups. Also gain and noise figure measurement procedure from the input and output signal was explained in detail. Efforts that we made to increase the Bi concentration by changing the solvent and by optimising the process parameters during the preform fabrication were discussed. Finally, the lasing performance of high concentration Bi-doped fibres also presented and showed the possibility of using a shorter length of Bi-doped fibres to develop lasers and amplifiers. Development of high concentration fibres were important to increase the absorption of the fibre and hence reduce the device length of lasers or amplifiers. Note here that the high concentration Bi-doped fibres induce higher UL due to various quenching effects. So it is important to increase the Bi-concentration as well as keep the unwanted losses at its minimum. Especially the high concentration Bi-doped fibres fabricated here are useful to develop mode-locked Bi-doped fibre lasers.

EPMA of selected Bi-doped fibres was discussed and presented the chemical composition of the core material in wt%. We observed that in case of Bi-doped aluminosilicate fibre (L30366-A0621) even with low Bi-concentration which is around 0.02Wt% the UL is 35%. The high UL in this fibre could be because of ESA present in Bi-doped aluminosilicate fibres. Whereas, in case of Bi-doped phosphosilicate fibres, L30368-A0623 and L30370-A0625 the UL was 24% and 7%, respectively. Even though these two preforms were made with similar Bi-content in isopropanal solution the atmospheric conditions during collapse and sealing are different. This could be the reason for different Bi-concentration in the final fibres and hence different UL. One can clearly notice that the UL is high in high concentration Bi-doped fibre L30368-A0623 compared to L30370-A0625. In case of L30459-A0787 even though the Bi-concentration in the final fibre is high, different

solution (n-butyl acetate) used here helped to reduce the UL. This clearly indicates that the fabrication conditions are very important in fabricating efficient Bi-doped fibres.

Chapter 3

Development of Bi-doped aluminosilicate fibre amplifier

3.1 Introduction

Bismuth (Bi) as an active dopant in glass host has been studied for the development of lasers and amplifiers in the wavelength region of 1150-1550nm [25, 26, 111]. Lasers and amplifiers in this region can find applications in medicine, spectroscopy, astronomy and optical fibre communication [65–67, 112–115]. The absorption and emission bands in Bi-doped fibres strongly depend on its co-dopants in glass matrix [11, 13]. Laser and amplifier operation around 1150, 1300 and 1450nm has been reported in Bi-doped fibres co-doped with aluminium (Al), phosphorous (P), and germanium (Ge), respectively [11, 50]. However, the Bi luminescence in the 1450nm wavelength band has attributed to pure silica matrix [50]. Recently, the laser and amplifier operation of Bi has been extended further to cover 1600-1800nm wavelength band by using germanosilicate fibres with high GeO_2 concentration [12]. There have been various demonstrations of Bi-doped fibre amplifiers in the 1280-1550nm wavelength band with the germanosilicate and phosphogermanosilicate host. These amplifiers have been shown to provide the maximum gain of greater than 20dB around 1427 and 1321nm, respectively [79, 116]. However, the gain in the 1150-1200nm wavelength band which uses aluminosilicate host has been comparatively less. Prior to this work, to the best of our knowledge, a maximum gain of about 5dB has been demonstrated in Bi-doped aluminosilicate fibre amplifier at room temperature at a wavelength of 1180nm. As a pump source, a high power Yb-doped fibre laser operating at 1060nm with a maximum output power of 6.5W was used [75]. The reason for the low efficiency of lasers and amplifiers made by Bi-doped fibres was explained by the unsaturable loss (UL) and excited state absorption (ESA) [56].

UL and ESA become significant in particular with Al co-dopant [117]. ESA has been shown to appear at both pump and signal wavelengths and increases towards the shorter wavelength side [118]. Pumping of Bi-doped aluminosilicate fibre from commercially available laser diodes (LDs) below 1000nm is not preferred despite strong Bi absorption at these wavelengths due to substantial pump induced ESA [58]. This makes the choice of the pump wavelength very critical. In this chapter, we will discuss the development of 1180nm Bi-doped fibre amplifier using Bi-doped aluminosilicate fibres. This particular wavelength has a specific application in astronomy as a laser guide star. In the following section, we will discuss briefly the laser guide star.

3.2 Laser guide star

FIGURE 3.1: Laser guide star [119]

Interest in space exploration has led to the development of telescopes with primary mirror sizes of 30m, these are called extra-large telescopes (ELT). These ELTs will help to increase the resolution and capable to see very fine details of the night sky. However, the resolutions of these telescopes that are placed on high latitudes of the earth are limited by the earth's atmosphere. The winds, varying temperature and pressure of the atmosphere lead to distortions of the wavefronts arrived from the objects being observed by the telescopes. One way to overcome this problem is to use space telescopes such as Hubble telescope but building a space telescope is very expensive and the mirror size used in these telescopes are limited by the maximum payload that a rocket can lift to transport it into space. Astronomers came up with the solution of using adaptive optics. This technique makes use of deformable mirrors in the telescope's beam path to introduce an additional and dynamic wavefront change to compensate the fluctuations introduced in the wavefront by an atmosphere. Actuators are placed on back of the mirrors which can

make adjustments at up to 1000 times per second, the result is a significant improvement in resolution offered by the earth-based telescopes. The appropriate reference object is required to use this adaptive optics technology to improve the resolution of the ground-based telescopes. Several years astronomers used natural star as a reference source and called it natural guide star. However, it is not always possible to find a natural guide star near the object that the astronomers want to observe or image. Even if there is a natural guide star close to a region that astronomers would like to observe, the brightness of the natural star might not be enough to use it as a natural guide star. To overcome these problems scientists came with a thought that what if we create our own star? This thought led to the invention of artificially generated guide star known as laser guide star (LGS) and is shown in Fig 3.1. In LGS, a laser beam of appropriate wavelength which is around 589nm is used to excite the sodium atoms in the mesosphere which is 90 to 100km away from earth and the resulting point-like beam spot emitted from the excited sodium atoms will act as a reference for adaptive optics of the telescope. The light emitted by the LGS is subjected to same deformations as that originating from the astronomical object. Adaptive optics reproduces the image of the LGS as a point object on the detector and in doing so simultaneously corrects the wavefront distortions for the light emitted from astronomical objects on the same line of observation.

In the past dye lasers or sum frequency mixing of solidstate lasers were used as LGS. However, these lasers are somewhat cumbersome to operate and require continuous or intensive maintenance. Especially the optomechanics involved in these lasers are not good for moving telescopes while imaging, due to this reason separate chambers are created to place these lasers to avoid the movement of optomechanics. The ideal source should be compact, robust and reliable under adverse conditions with less involvement of optical components. Recently, Toptica photonics developed a laser at 589nm involving a semiconductor diode laser, a Raman fibre amplifier and second harmonic generation technique. The laser produces more than 20W of output power with a line width of less than 5MHz. Raman fibre amplifier is opted to amplify the seed as there is no RE-doped fibre that can give amplification at this particular wavelength [119, 120]. Bismuth as a dopant in fibres is proved to be a prominent material capable of amplifying signals at 1180nm. The advantages of Bi-doped fibre amplifiers over Raman amplifiers are reduced fibre length and pump power. Thus the development of efficient Bi-doped fibre amplifiers can replace the Raman fibre amplifier in the current technology and can scale the power levels to more than 100W. Here we develop an amplifier around 1180nm specifically for laser guide star application using Bi-doped active fibre as a laser gain media.

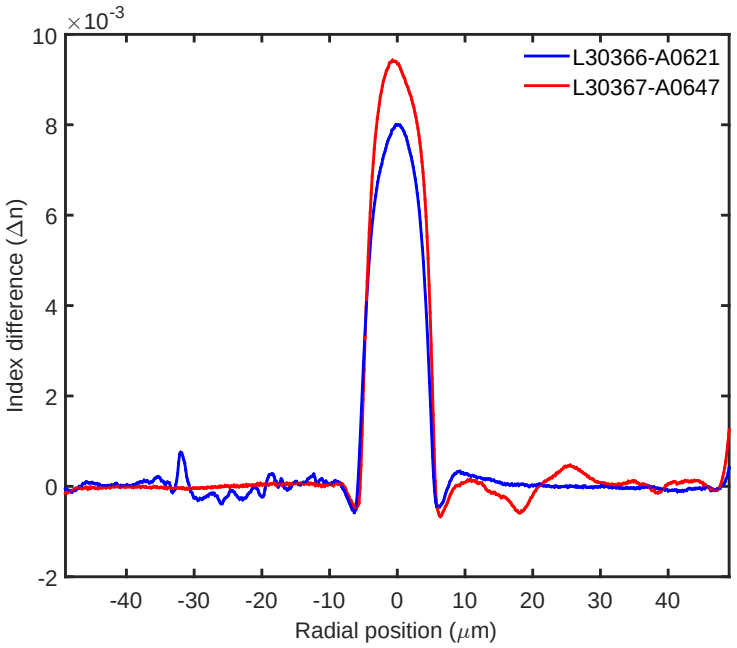

FIGURE 3.2: Refractive index profile of the fibres L30366-A0621 and L30367-A0647

3.3 Bi-doped aluminosilicate fibre amplifier

Two Bi-doped aluminosilicate fibres (L30366-A0621 and L30367-A0647) were fabricated as discussed in chapter 2. The resulting fibre drawn from the preform has the core and cladding diameter of 8 and 100μm, respectively. The refractive index profile of these fibres was measured and is shown in Fig 3.2. The ripples here are due to the cleaving of fibre involved in the measurement procedure. When the fibre cleaving is not flat this might lead to ripples in the measured profiles. The refractive index difference (Δn) between the core and cladding was found to be 0.008 in L30366-A0621 whereas in L30367-A0647 it is 0.009. The Al_2O_3 content in these fibres was around 3.5 mol% which is determined from the core-cladding index difference.

The absorption spectrum of these fibres was then measured by using cut-back method, with a white light source (WLS) and an optical spectrum analyser (OSA) and is shown in Fig 3.3. Both L30366-A0621 and L30367-A0647 fibres showed a broad absorption band around 1000nm which is a typical characteristic for Bi-doped aluminosilicate fibres. However, the pump band around 1000nm in case of L30366-A0621 is higher compared to L30367-A0647. This can be because of less incorporation of Bi dopant in case of L30367-A0647. Absorption in case of L30366-A0621 at 1047nm was 0.7dB/m and at 1120nm was 0.35dB/m whereas in case of L30367-A0647 it was 0.13dB/m at 1047nm and 0.07dB/m at 1120nm. The gain characteristics of L30367-A0647 were measured and found that it was not promising to develop an amplifier at 1180nm. The low concentration in case of L30367-A0647 which is almost seven times less (from the measured absorption

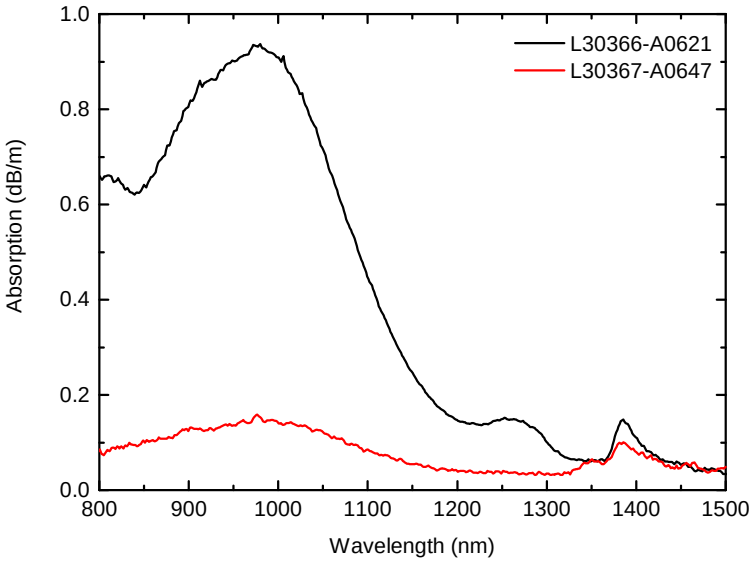

FIGURE 3.3: Absorption spectrum of Bi-doped aluminosilicate fibres

at 1047nm) compared to L30366-A0621 could be the possible reason for this. Hence, we chose L30366-A0621 for further detailed characterisation to develop an amplifier at 1180nm. From here onwards we will discuss only characterisation of fibre L30366-A0621.

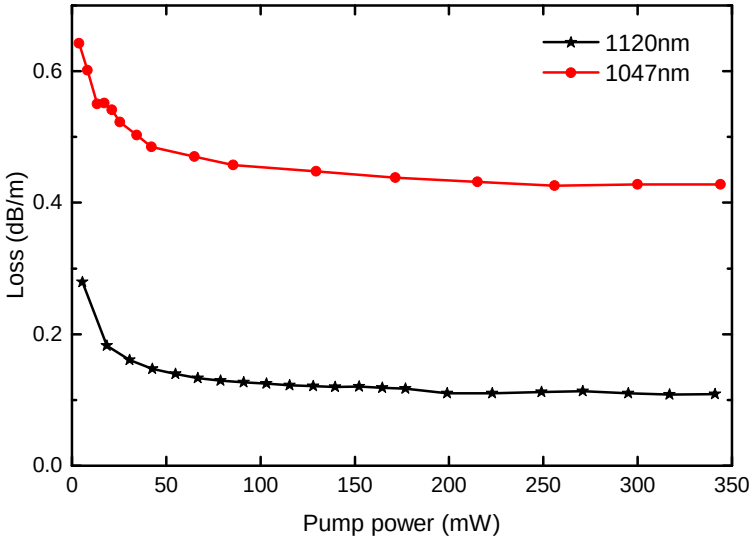

FIGURE 3.4: Loss variation with pump power for 1120 and 1047nm pump wavelengths

Bi-doped aluminosilicate fibres have a significant contribution from UL towards laser or amplifier performance. Reduction of UL is critical in enhancing the pump efficiency. The UL was measured to determine its contribution to the small signal loss. The UL measurement method explained in chapter 2 was used to measure the loss variation with pump power [56, 117]. The variation in loss with pump power was measured by laser sources operating at wavelengths of 1047 and 1120nm and is shown in Fig 3.4. The uncertainty in these measurements was around 3%. The 1047nm wavelength is

conventional pump choice for Bi-doped aluminosilicate fibres whereas 1120nm pump wavelength was chosen to test the performance of Bi-doped fibre in comparison with 1047nm.

Wavelength (nm)	Small signal loss (dB/m)	UL (dB/m)	UL%
1047	0.66	0.43	65
1120	0.28	0.1	35

TABLE 3.1: Small signal loss and UL at 1120 and 1047nm pumps

The contribution of UL to the small signal loss was 35% for 1120nm, whereas it was 65% for 1047nm pump wavelength as shown in Table 3.1.

3.3.1 Experimental setup

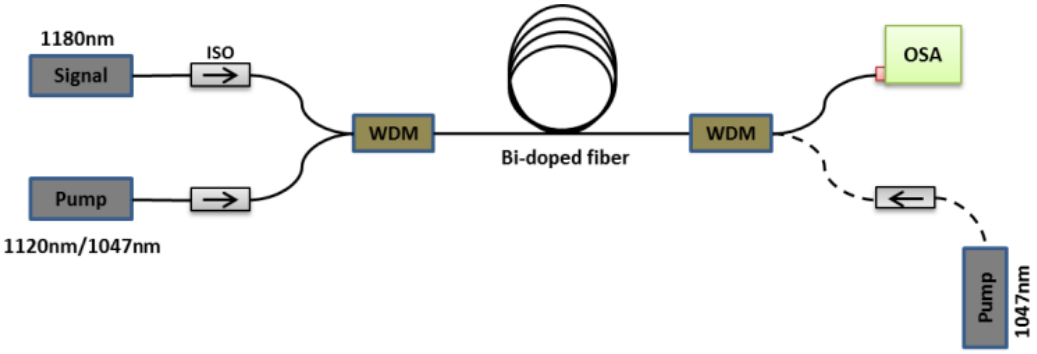

FIGURE 3.5: Schematic of the experimental setup to measure gain in Bi-doped fibre. (The 1047nm pump with dashed line was used for bi-directional pumping; otherwise, that port of the WDM was used to monitor the excess pump).

Fig 3.5 shows the schematic experimental setup used for the measurement of gain in Bi-doped fibre. The setup comprised of a 1180nm laser diode as an input signal source and a fibre pigtailed 1120nm laser diode and/or 1047nm Nd-YLF laser as the pump source. Isolators (ISO) were used to avoid back reflections and wavelength division multiplexers (WDMs) to combine signal and pump sources. The input and output signal spectra were taken using an OSA. The input signal was measured just before the fibre under test (FUT), whereas the output signal was calculated by taking into account the WDM loss that was used to separate pump from the signal. The gain was then measured by using the obtained input signal and the output signal just before and after the FUT. The following standard equation 3.1 was used to calculate the gain [10].

$$\text{Gain(dB)} = 10\log_{10}\frac{P_{\text{out}}}{P_{\text{in}}} \tag{3.1}$$

Where P_{in}, P_{out} are the signal power levels at input and output of FUT, respectively.

3.3.2 Results

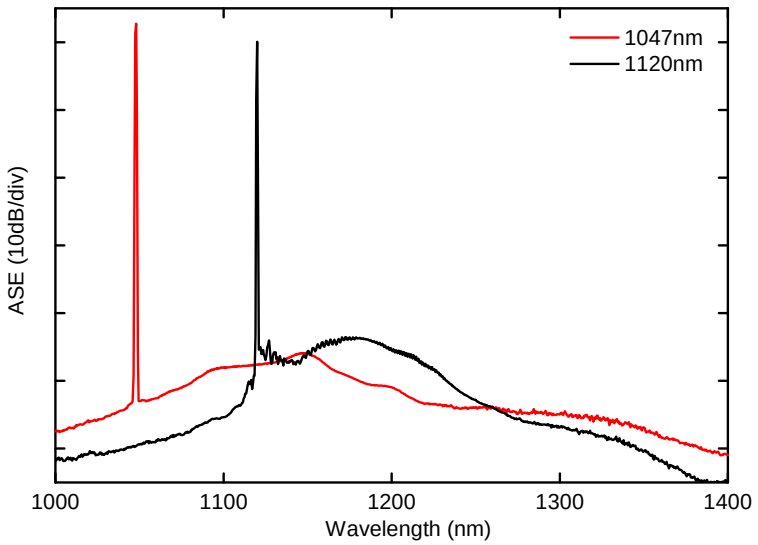

FIGURE 3.6: ASE spectra for 1047 and 1120nm pump wavelengths for 20 and 100m length of the fibre, respectively (Pump power: 350mW).

Amplified spontaneous emission (ASE) spectra were measured by individually pumping the fibre at wavelengths, 1120 and 1047nm, for fibre lengths of 100m and 20m, respectively. The maximum pump power used in both cases was 350mW. Fig 3.6 shows the ASE spectra for the case of individual pumping. The ASE peak with 1047nm pump appeared around 1150nm, whereas 1120nm pumping helps to push the ASE to slightly longer wavelength with a peak at 1180nm. This indicates that higher gain can be extracted at longer wavelengths by pumping with a 1120nm laser diode. This particular region is vital in order to obtain a source for laser guide star application in adaptive optics which was explained in more detail at the beginning of chapter 3 [67]. The laser developed at 1178nm can be frequency doubled using second-harmonic generation to obtain a source at 589nm [69]. It should be noted that the 1180nm input signal was used instead of 1178nm due to limited availability of the source, and results are expected to be similar for 1178nm.

In order to determine the optimum fibre length, the gain was measured with different fibre lengths for 1047 and 1120nm pumps, respectively. Fig 3.7 shows the gain variation with fibre length for the individual pumping. By using 1120nm pump, a maximum gain of about 8 and 7.5dB were obtained for the optimum fibre length of 100m with an input signal power of -4 and -1dBm, respectively. On the other hand, with 1047nm pump, a maximum gain of about 4.4dB was achieved for a length of 20m and for a signal power of -1dBm. The gain per unit length was very less in case of 1047nm pumping hence it

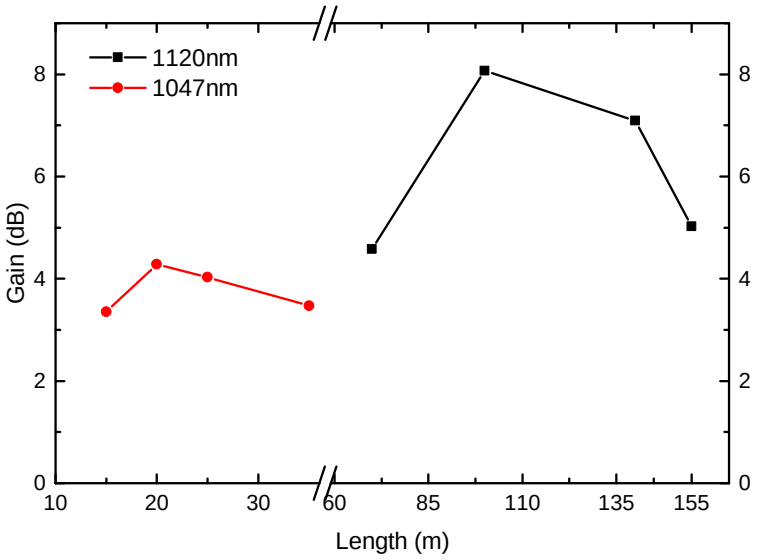

FIGURE 3.7: Gain variation with fibre length at 1180nm for two different pump wavelengths (Pump power: 350mW).

is hard to conclude the optimum length but we consider it is around 20m.About 70% gain enhancement was achieved for the 1120nm pump as compared to 1047nm pump. It can be suggested that the reduction in UL with 1120nm pumping allows higher gain to be extracted with a given pump power. However, the total length requirement for a maximum gain with 1120nm pumping increases as the Bi absorption decreases at this wavelength as compared to 1047nm.

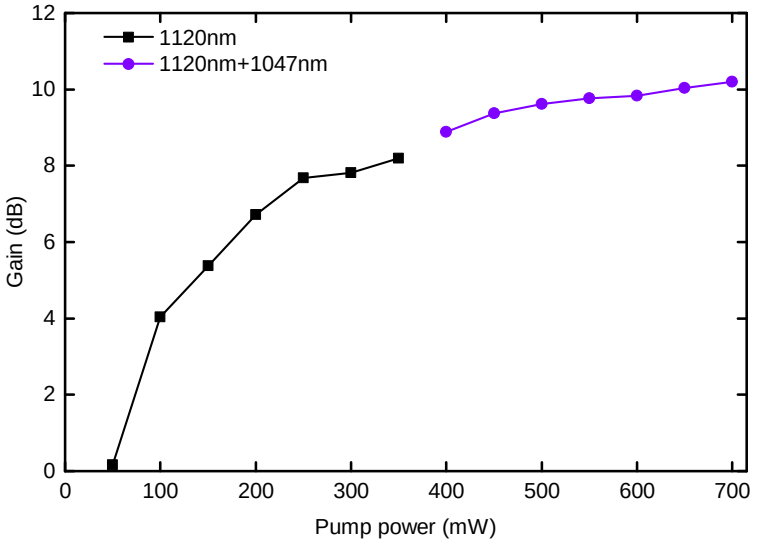

FIGURE 3.8: Gain variation with pump power at 1180nm for a 100m long fibre with a signal power of -4dBm

Fig 3.8 shows the gain variation with pump power for an input signal power of −4dBm and for a 100m long fibre. Initially, the gain was about 8dB for 350mW pump power with 1120nm pumping. To further enhance the gain of the amplifier, the pump power was

increased to a total pump power of 700mW by bi-directionally pumping the fibre with both 1120 and 1047nm pumps due to limited power available at 1120nm. The dashed line in Fig 3.5 shows the 1047nm pump used in the setup for bi-directional pumping. The gain was further increased by 2dB to a total of 10dB with 100m long fibre for bi-directional pumping as shown in Fig 3.8 [121].

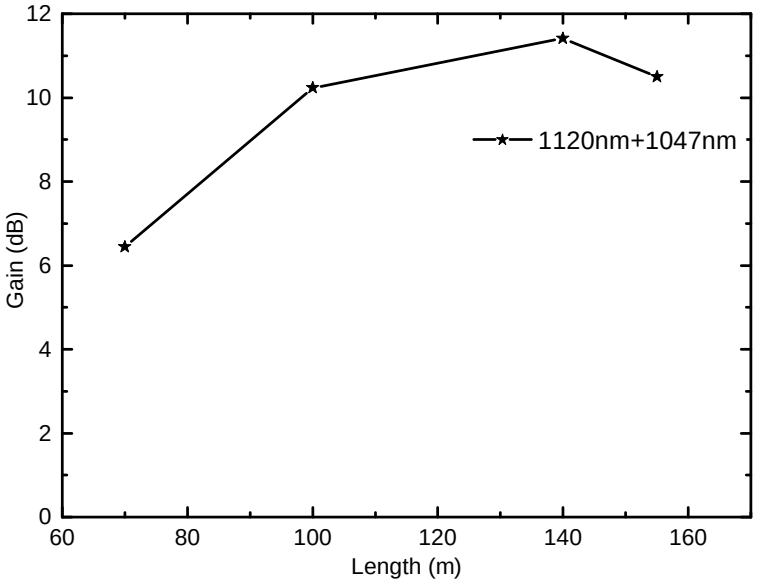

FIGURE 3.9: Gain variation with fibre length at 1180nm for bi-directional pumping (total pump power: 700mW) and for an input signal power of -4dBm.

To find the optimum fibre length for bi-directional pumping, the gain was measured in different lengths of the fibre as shown in Fig 3.9. The optimum fibre length for bi-directional pumping was increased to 140m with a maximum gain of about 11.5dB. Gain performance of more than 155m was not measured due to the limited available length of Bi-doped fibre.

To understand the effect of dual pumping, the unsaturable loss was measured and is shown in Fig 3.10. Co-directional pumping was used to measure the loss variation with pump power. WDM was used to combine the pump wavelengths 1120 and 1047nm. At first, 1120nm pump was switched on, and then its power was increased to a maximum value of 350mW (black line). After that, 1047nm pump was switched on and gradually taken to its maximum available power, while keeping the 1120nm pump power at its maximum value of 350mW. The total pump power from both laser diodes amounted to 700mW. It can be observed that by adding 1047nm pump to 1120 nm pump, the overall loss in fibre increased considerably (violet line). We believe that pumping at 1047nm is impeded by the ESA of the pump light, resulting in reduction of pump efficiency and roll over in gain at 1180nm when both the pump wavelengths were used in conjunction. It can be concluded that the total pump power increment would be preferred by increasing the power of 1120nm laser diode as opposed to using an additional 1047nm pump.

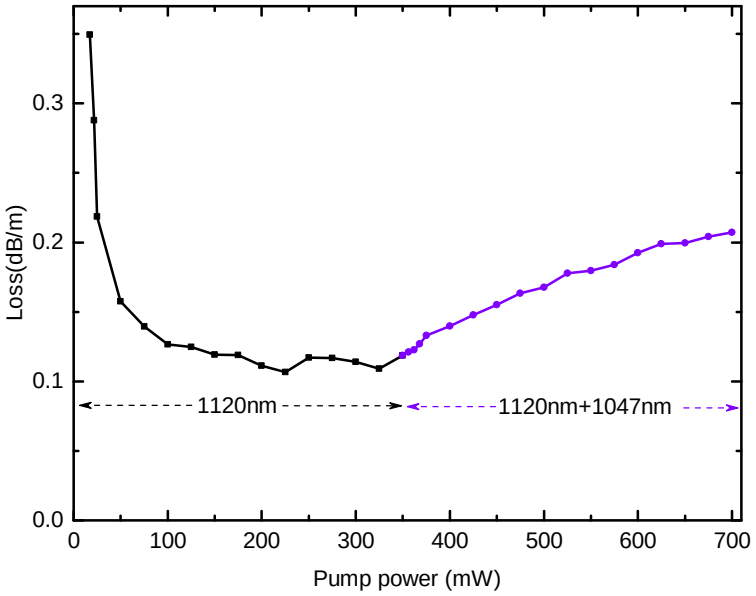

FIGURE 3.10: Loss variation in Bi-doped fibre for single 1120nm pumping (black line) and for dual pumping (1120nm + 1047nm) by varying the power of 1047nm pump while operating the 1120nm pump at its maximum power of 350mW (violet line)

3.4 Conclusion

In conclusion, Bi-doped aluminosilicate fibres were fabricated by MCVD-solution doping method. The fibre with high concentration among the two fabricated Bi-doped aluminosilicate fibres was selected to develop a fibre amplifier. A commercially available laser diode operating at 1120nm was used as a pump source to demonstrate the gain at 1180nm. The performance of the fibre for 1120nm pump was compared with the conventional pumping region around 1047nm. About 70% increase in gain was observed for 1120nm pumping as compared to 1047nm pump. The UL was 35% and 65% for 1120 and 1047nm pump wavelengths, respectively, indicating the likely reason for higher gain in the case of 1120nm pump. A maximum gain of 8dB was obtained for 100m long fibre. The gain of the amplifier was further increased by about 2dB using bi-directional pumping with 1120 and 1047nm pumps. The slow increment of gain with the addition of 1047nm pump was a result of higher unsaturable loss incurred in Bi-doped fibre at this pump wavelength as compared to 1120nm pump. It is understood that the bi-directional pumping will be efficient if we can use two 1120nm pump laser diodes instead of 1120 and 1047nm.

The 1180nm amplifiers are important in developing 590nm sources by frequency doubling. One of the important application of 590nm source is a laser guide star. In a laser guide star developed by Toptica photonics a Raman fibre amplifier was used to amplify the seed source of 1178nm and then frequency double the amplified signal through nonlinear process to develop a laser source at 589nm for laser guide star application. The

draw backs of Raman fibre amplifier are the required fibre length and high pump power to have efficient gain. This can be overcome by developing Bi-doped fibre amplifiers. Even though Bi-doped fibre amplifiers are not yet compete with Raman fibre amplifiers in terms of gain especially at 1180nm wavelength band the progress in Bi-doped fibre fabrication can lead to develop efficient Bi-doped fibre amplifiers. The advantage of Bi-doped fibre amplifiers is that one can use short length of doped fibre and low pump powers as compared to Raman fibre amplifiers. Here we made an initial demonstration of Bi-doped fibre amplifier that operates at 1180nm. We expect that better understanding of the nature of Bi active centres can lead to fabricate preforms with optimum conditions and will allow a further improvement in the amplifier performance.

Chapter 4

Bi-doped fibre laser and amplifier in the second telecommunication wavelength band

In this chapter, we report the fabrication of Bi-doped phosphosilicate preforms using modified chemical vapour deposition (MCVD)-solution doping technique under different atmospheric conditions. The preforms were drawn into fibres and are characterised for absorption and unsaturable loss (UL). An all-fibre Bi-doped laser in a ring cavity is demonstrated by direct diode pumping at 1267nm with a laser output power of 110mW operating at a wavelength of 1360nm. We also presented an all-fibre Bi-doped fibre amplifier operating in the O-band from 1300-1360nm with a maximum gain of 29dB at 1340nm.

4.1 Fibre fabrication and characterization

Fibre	L30368-A0623	L30369-A0622	L30370-A0625
He /O_2 flow ratio	1	0.25	only O_2
Abs.(dB/m)@1210nm	2	1.6	0.9
Abs.(dB/m)@1267nm	2.8	1.95	1
UL%@1210nm	46	17	14
UL%@1267nm	25	11	7

Table 4.1: Absorption and UL of BPSFs at two different pump wavelengths

As mentioned in chapter 2, three Bi-doped phosphosilicate preforms (L30368-A0623, L30369-A0622, L30370-A0625) were fabricated (from here onwards named as BPSF-1, BPSF-2 and BPSF-3) by depositing phosphosilicate soot under similar fabrication conditions. The soot body was impregnated by the same Bi solution for all the preforms. The only difference between fabricated preforms was the variation of oxygen (O_2) and helium (He) flow ratio during the porous layer sintering and the preform collapse stages, while maintaining the total gas flow as constant. The variation of O_2 and He flow ratio were mentioned in Table 4.1. The preforms were drawn into fibres with a core and cladding diameter of 13 and 100μm, respectively.

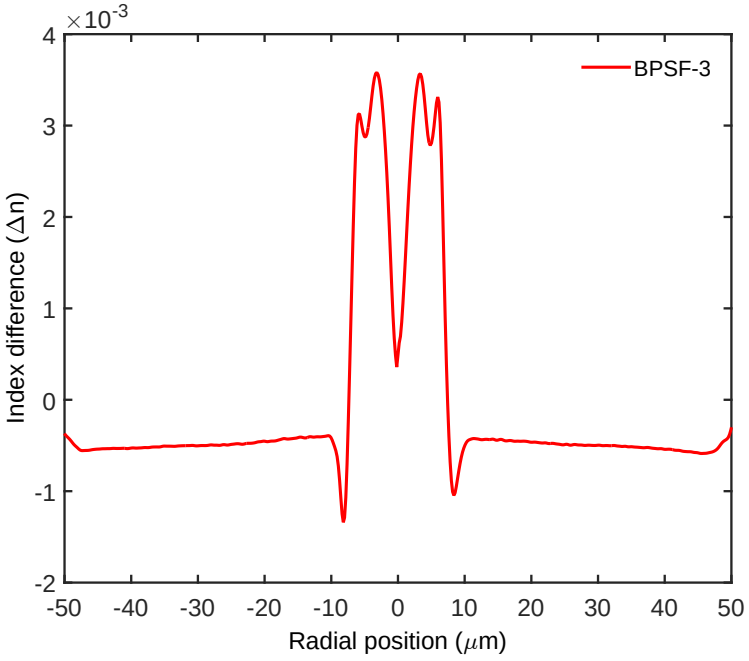

FIGURE 4.1: Refractive index profile of fibre (BPSF-3) measured by Inter Fibre Analyser (IFA)

The refractive index profile of one of the fibres (BPSF-3) was measured and is shown in Fig 4.1. The dip at the centre of the index profile is due to the evaporation of P_2O_5 during sealing process of preform fabrication. The index difference (Δn) between the core and clad was found to be around 0.004.

The absorption spectra of all BPSFs were measured by cut-back method using a white light source (WLS) and an optical spectrum analyser (OSA) and are shown in Fig 4.2. The influence of fabrication conditions on absorption characteristics can be seen from Fig 4.2. BPSF-1 which was fabricated with 1:1 of O_2 to He ratio has shown an absorption peak around 1255nm accompanying a small water peak at 1380nm. Whereas in BPSF-2, fabricated under excess O_2 (4: 1 ratio of O_2 to He), the 1255nm peak shifted to around 1335nm and it was less pronounced. In BPSF-3, that was fabricated under complete

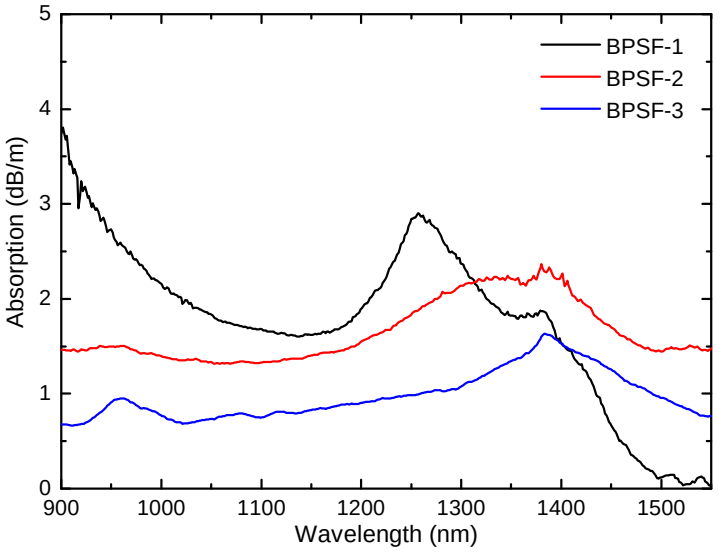

FIGURE 4.2: Absorption spectra of Bi-doped phosphosilicate fibres

O_2 atmosphere the 1255nm peak disappeared. Also, the absorption in BPSF-3 reduced compared to BPSF-1 and BPSF-2. The UL was measured for all three BPSFs at two wavelengths 1210 and 1267nm using the measurement technique discussed in chapter 2. The UL was around 25% (46%), 11% (17%) and 7% (14%) at pump wavelength 1267nm (1210nm) in BPSF-1, BPSF-2 and BPSF-3, respectively and is mentioned in Table 4.1 .

4.2 Bi-doped fibre laser

4.2.1 Introduction

Exploring fibre lasers and amplifiers in new wavelength bands have been the research interest for decades. The 1150-1500nm wavelength region is one of such bands with demanding applications such as wideband optical fibre communication, medicine, spectroscopy, and astronomy. Bismuth (Bi) doped fibres have paved the way to develop lasers and amplifiers in this wavelength band, thanks to its broad luminescence characteristics. Bi-doped aluminosilicate, phosphosilicate and germanosilicate fibres have shown luminescence around 1150nm, 1300nm and 1450nm, respectively [50]. In particular, Bi-doped fibres which exhibit luminescence around 1300nm has specific importance as their operating wavelength region coincides with the second telecommunication window. Bi-doped phosphogermanosilicate fibres have been used to demonstrate lasers from 1280-1360nm with a 30W Raman fibre laser operating at 1230nm as a pump [79]. Among these, the reported efficiency of laser operating at 1360nm was 9.5% and 18% at low and high pump powers, respectively. Moreover, a 100m long Bi-doped fibre was used for laser demonstration. Here we develop an all-fibre Bi-doped laser in a ring cavity by

direct diode pumping at 1267nm. The laser operates at 1360nm with an output power of 110mW.

4.2.2 Experimental setup

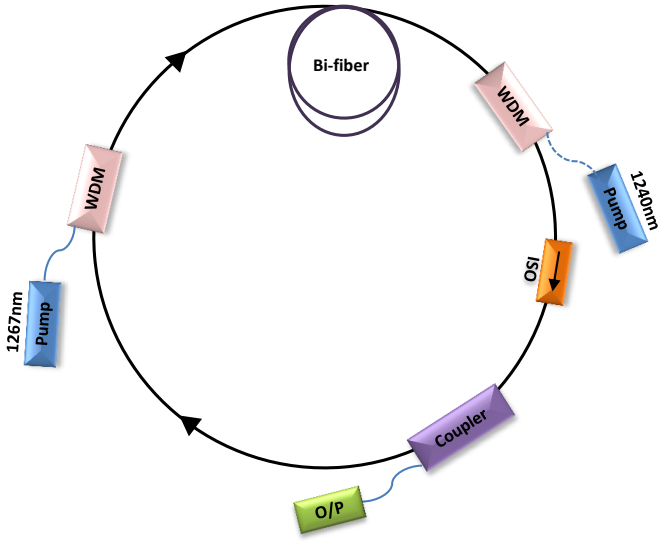

FIGURE 4.3: Schematic experimental setup of Bi-doped fibre laser

The experimental setup of Bi-doped fibre laser in a ring cavity is shown in Fig 4.3. It consists of a fibre pigtailed pump laser diode operating at 1267nm, two wavelength division multiplexer (WDM) to combine and separate pump and signal wavelengths at input and output of FUT, an isolator (ISO) for unidirectional operation of the cavity, and an optical coupler of which one port is used for cavity feedback and other port is used to take the output from the ring cavity. The maximum available pump power from the 1267nm laser diode was 390mW. The 1267nm pumping wavelength was chosen due to lower UL in BPSF among the available pump laser diodes. The absorption values at 1267nm pump wavelength measured by WLS were found to be 2.8dB/m,1.95dB/m and 1dB/m in BPSF-1, BPSF-2 and BPSF-3, respectively.

4.2.3 Results

At first, a laser diode operating at 1267nm, BPSF-1 and a coupler with an input/output coupling ratio of 70/30 was used to construct the ring cavity. No lasing action was obtained in this fibre at any fibre length despite being highest absorption at the pump wavelength. Next, BPSF-2 was tested using the same coupling ratio and it shows lasing at a wavelength of 1360nm. The length of the fibre was optimized to achieve maximum laser efficiency. The optimum fibre length was found to be 50m with a maximum output

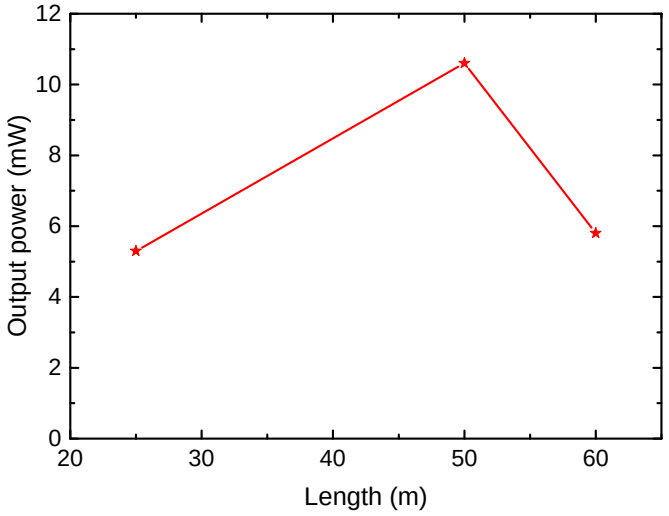

FIGURE 4.4: Optimum length of BPSF-2 for 390mW of pump power

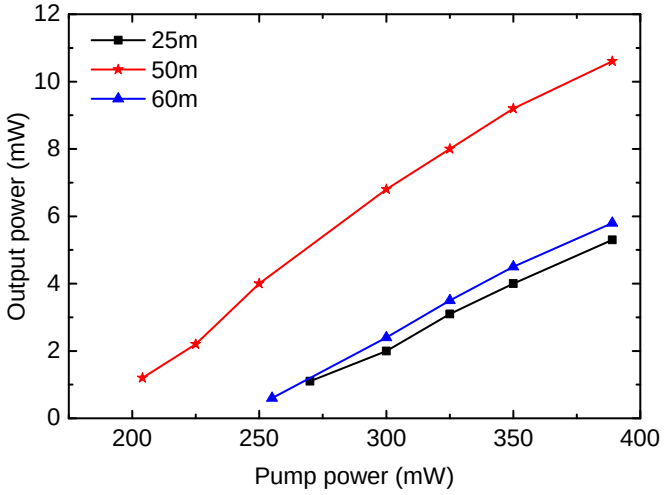

FIGURE 4.5: Pump power vs. output power of BPSF-2

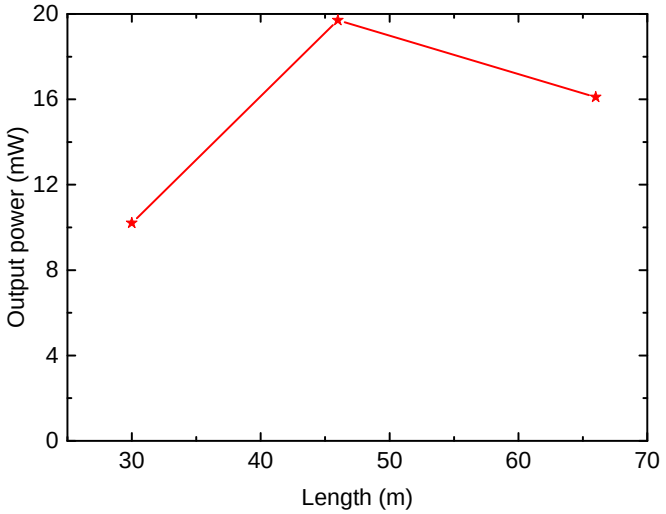

FIGURE 4.6: Optimum length of BPSF-3 for 390mW of pump power

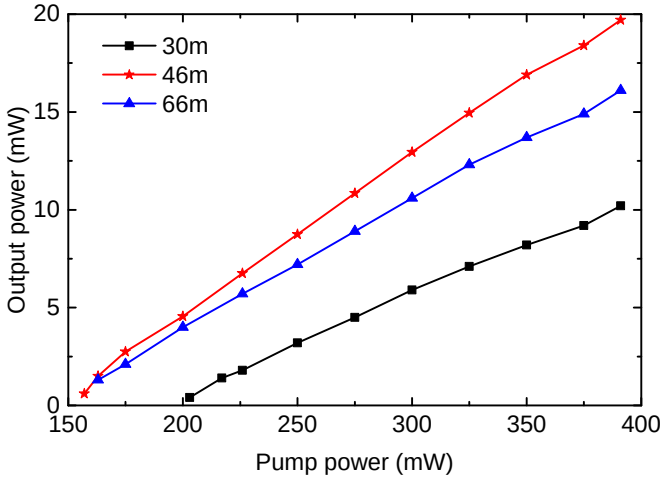

FIGURE 4.7: Pump power vs. output power of BPSF-3

power of 10mW as shown in Fig 4.4. The laser efficiency was measured in different length of fibre and a maximum efficiency of 5% was obtained as shown in Fig 4.5. Subsequently, BPSF-3 was tested in the same experimental setup and optimized the length to obtain maximum output power as shown in Fig 4.6. The laser developed with BPSF-3 has a laser efficiency of 8% with an output power of 20mW for an optimum fibre length of 46m as shown in Fig 4.7. The threshold pump power was 157mW.

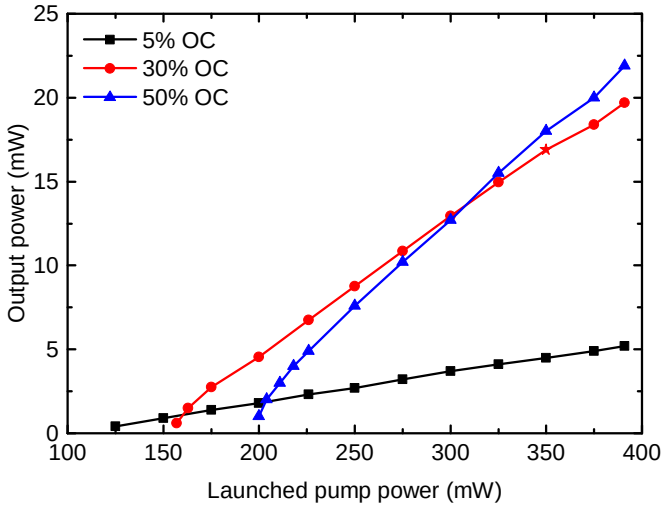

FIGURE 4.8: Output power vs launched pump power with different output coupling (OC) for 46m long BPSF-3

To find out the optimum coupling ratio we then varied the output coupling ratio in the ring cavity. The laser efficiency in BPSF-3 was increased to 11% with an output power of 22mW for the 50/50 coupling ratio as shown in Fig 4.8. The laser spectrum of BPSF-3 taken by an OSA is shown in Fig 4.9.

Among all three fibres, BPSF-3 was found to be the most efficient fibre with high efficiency [122]. This can be explained by the lower UL measured in BPSF-3 compared

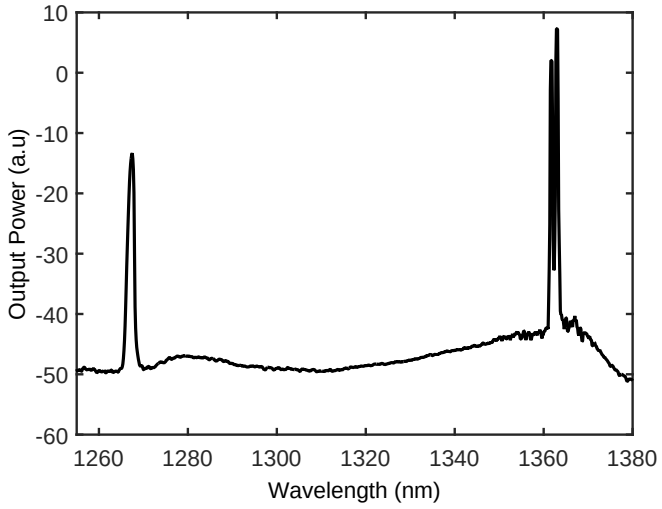

FIGURE 4.9: Optical spectrum of the Bi-doped fibre laser

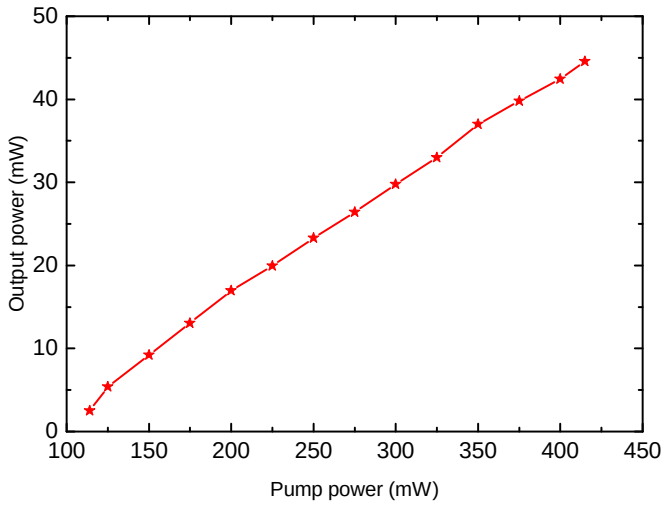

FIGURE 4.10: Slope efficiency of 50m fibre with 50/50 coupling ratio

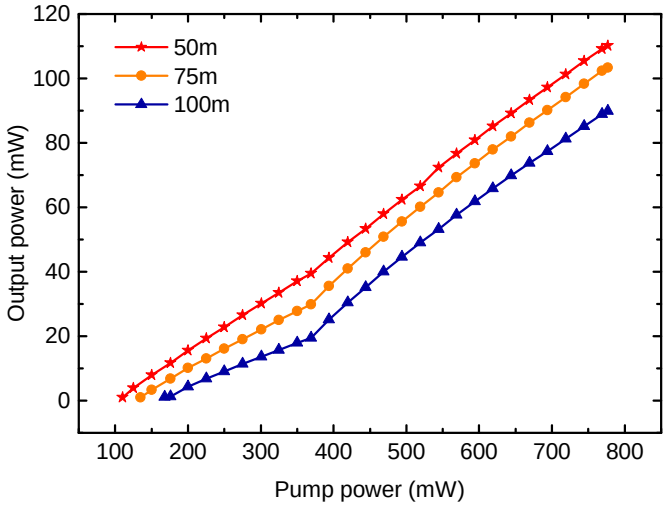

FIGURE 4.11: Optimum length for bi-directional pumping

to BPSF-1 and BPSF-2. Further, the Bi-doped preform of BPSF-3 was over jacketed and redrawn into a single mode fibre with a core and clad diameter of 11 and 150μm. The cut-off wavelength of the fibre was measured and found to be 1100nm. This single mode BPSF-3 was replaced in the cavity as shown in Fig 4.3 and measured the laser efficiency again for a fibre length of 50m. The laser efficiency was increased to 13.6% with an output power of 45mW as shown in Fig 4.10. To further increase the pump power a laser diode operating at 1240nm was added to the same cavity in a bi-directional pumping configuration (dashed line) as shown in Fig 4.3. The total pump power was increased to 770mW. The slope efficiency of the Bi-doped single mode fibre was measured with different length of the fibre and further improvement in laser efficiency was observed. For an optimum length of 50m, the laser efficiency was amounted to be 18% with an output power of 110mW as shown in Fig 4.11. The output power levels of the Bi-doped fibre laser was limited by the available pump power of laser diodes.

4.3 Bi-doped fibre amplifier with a flat gain of 25dB, operating in the wavelength band 1320-1360nm

4.3.1 Introduction

The demand for optical fibre communication is persistent over the last decade because of the increased accessibility of the internet, cloud computing, and machine-to-machine communication arising from the internet of things (IOTs), etc. Continuous research efforts are being made to develop various technologies to cope with the capacity requirements in optical fibre communication. One of them is the introduction of space-division multiplexing (SDM) in the C-band using multi-core fibres (MCF), multi-mode fibres (MMF), and multi-element fibres (MEF) [6, 105, 123]. Another approach is to develop efficient amplifiers in the second telecommunication window. The latter one would be the immediate solution to increase the capacity of optical fibre communication. Advances in fibre fabrication techniques have reduced the losses of silica fibres to <0.4dB/km in the O-band [124, 125]. However, lack of efficient amplifiers has rendered this window, currently, non-ideal for optical fibre communication. Recent developments in bismuth (Bi)-doped fibre amplifiers covering the low loss window of silica fibres have shown great potential to enable a wideband transmission, thanks to its broad luminescence characteristics [11, 14, 25, 115, 126, 127]. Bi-doped aluminosilicate, phosphosilicate, and germanosilicate fibres have shown luminescence peaks around 1150, 1300, and 1450nm, respectively [11, 50, 128]. Also, it has been shown that the luminescence window can be extended up to 1800nm in a high germania (GeO_2)-doped Bi fibres [12, 80]. In particular, Bi-doped phosphosilicate fibres (BPSF) have a specific importance as their

emission wavelength region coincides with the O-band. A maximum gain of 24.5dB has been reported at 1321nm with a corresponding noise figure (NF) of 4-6dB in a Bi-doped phosphogermanosilicate fibre amplifier. The amplifier used 200m of fibre length and a Raman fibre laser operating at 1230nm as a pump source with a pump power of 460mW [79, 129]. Here, we use Ge-free BPSF to develop a flat and wideband amplifier in the O-band by careful selection of pump wavelengths. Also, commercially available laser diodes (LDs) were used as pump sources.

4.3.2 Experimental setup

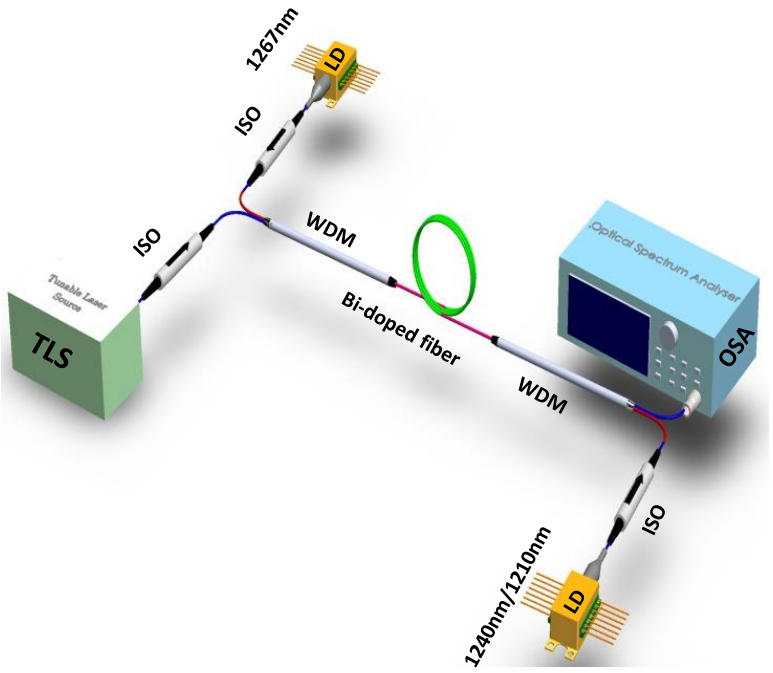

FIGURE 4.12: Schematic experimental setup of Bi-doped fibre amplifier

The preform corresponding to fibre with relatively good efficiency among BPSF-1, BPSF-2, BPSF-3 was selected and over jacketed. This preform (L30370-A0625) is then redrawn into a single mode fibre with a core and clad diameter of 11 and 150μm. The cut-off wavelength of the fibre was measured to be around 1100nm [122]. This single mode BPSF-3 was then used to study the pump wavelength dependent Bi gain and demonstrated an all-fibre, laser diode pumped, Bi-doped fibre amplifier operating in the spectral region 1300-1360nm.

The experimental setup of the Bi-doped fibre amplifier is shown in Fig 4.12. It is comprised of a tunable laser source (TLS) with an operating wavelength region of 1260-1360nm. The Bi-doped fibre was pumped at 1267 or 1240nm and also at 1267nm in combination with 1240/1210nm as shown in Fig 4.12. The maximum available power

of 1267 and 1240nm laser diodes was 360 and 400mW, respectively. Whereas, the maximum power of the 1210nm laser diode was limited to 300mW. Isolators (ISO) were used to avoid back reflections and wavelength division multiplexers (WDMs) to combine/separate signal and pump wavelengths. The input and output signal spectra were taken using an OSA. The input signal was measured just before the Bi-doped fibre under test, whereas, the output signal was calculated by taking into account the WDM loss that was used to separate the pump from the signal. The gain and NF were then calculated by using the following standard equations 4.1 and 4.2 and from the measured input and output signals [10].

$$\text{Gain(dB)} = 10\log_{10}\frac{P_{\text{out}}}{P_{\text{in}}} \tag{4.1}$$

$$\text{NF(dB)} = \frac{N_{\text{out}} - N_{\text{in}}G}{h\nu G(B.W)} + \frac{1}{G} \tag{4.2}$$

Where P_{in}, P_{out}, N_{in} and N_{out} are the signal power and noise power for input and output signals, respectively. B.W and ν are optical spectrum analyser (OSA) noise bandwidth and signal frequency.

4.3.3 Results

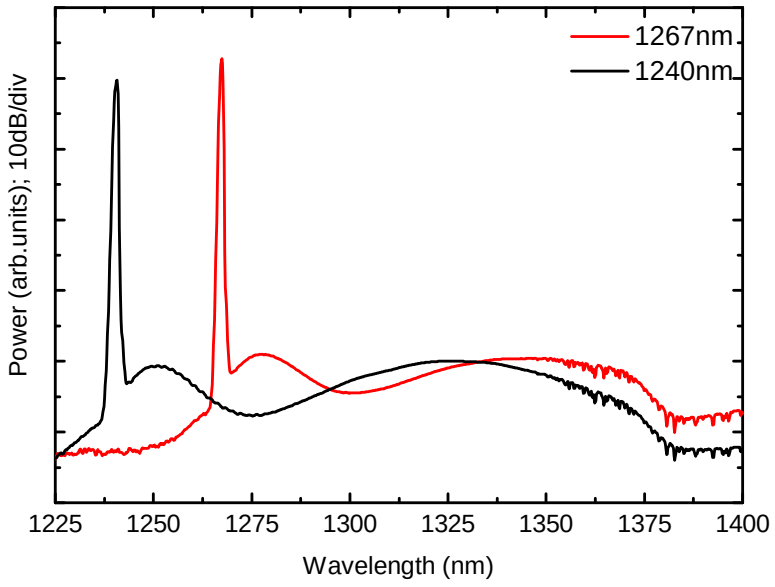

FIGURE 4.13: ASE spectra for 1267nm or 1240nm pump wavelengths for a 100m long Bi-doped fibre when pumped with a maximum available power of laser diodes

Initially, the fibre was individually pumped with 1267 or 1240nm laser diodes at their maximum available pump power. The amplified spontaneous emission (ASE) spectra were measured just after the 100m long Bi-doped fibre and are shown in Fig 4.13. The ASE spectrum corresponding to the 1240nm pump has a peak at 1325nm, whereas the 1267nm pump has a peak around 1350nm, thereby, indicating that the gain can be pushed toward the longer wavelength using a 1267nm pump.

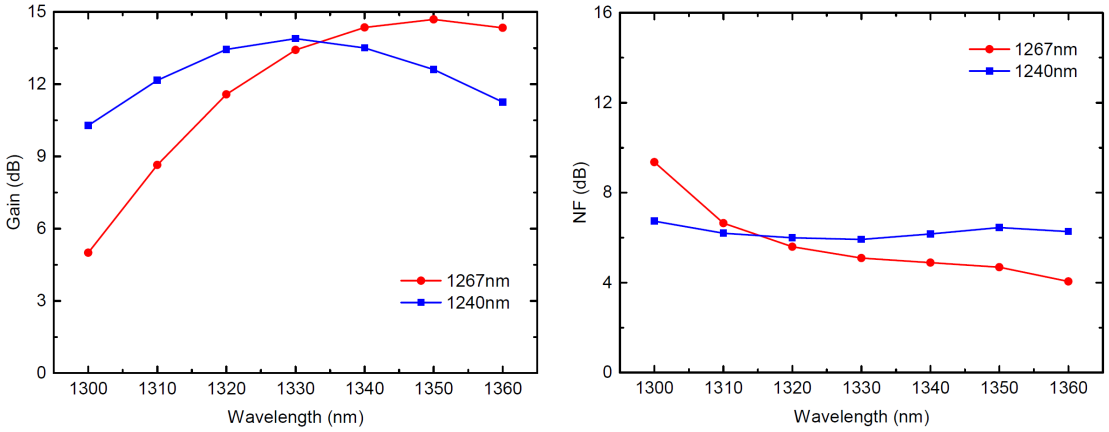

FIGURE 4.14: Gain and NF characteristics for the maximum available power of 360mW (1267nm) or 400mW (1240nm) with optimum fibre lengths of 100m and 75m, respectively (Signal power: -10dBm)

Subsequently, to develop an amplifier, the length of the fibre was optimized for a maximum gain using the experimental set up shown in Fig 4.12. It was found that the 100m long fibre was optimum with the 1267nm pump for a pump power of 360mW and 75m was the optimum fibre length with the 1240nm pump for a pump power of 400mW. The gain and NF characteristics of optimum Bi-doped fibre corresponding to 1267 and 1240nm pumps are shown in Fig 4.14. The input signal power was -10dBm. The 1267nm pumping provided a maximum gain of 15dB and a NF of 5dB at a wavelength of 1350nm. The gain at 1300nm was only 5dB. In the case of the 1240nm pump, a maximum gain of 14dB and a NF of 6dB were obtained at 1330nm. It should be noted that the gain at 1300nm was 10dB, which is double the gain of the 1267nm pumping. It can be concluded that the 1267nm pump can push the gain toward the longer wavelength, whereas the 1240nm pump allows the gain to operate at a shorter wavelength. Thus, by pumping the fibre using both the 1267 and 1240nm pumps, we could maximize the gain over a broad wavelength band.

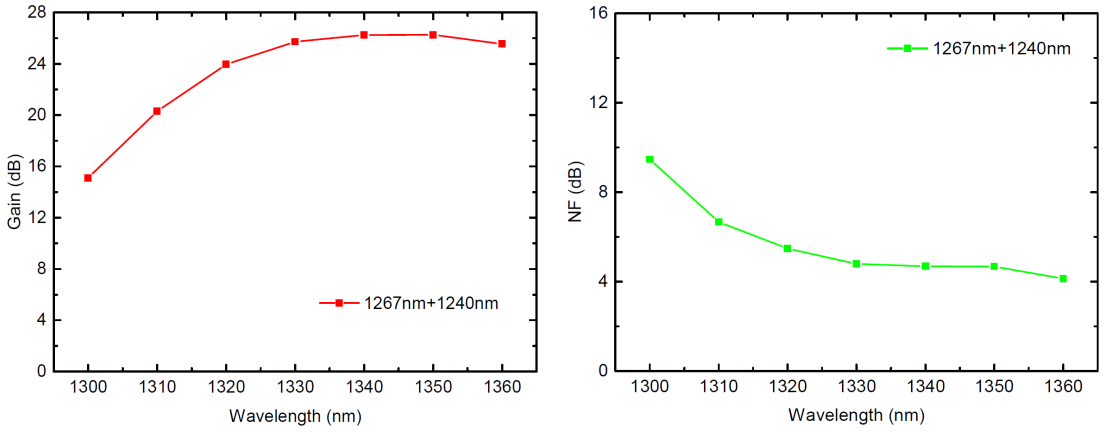

FIGURE 4.15: Amplifier performance with bi-directional pumping by 1267nm (360mW) and 1240nm (400mW) LDs for a signal power of -10dBm

In order to realize this, the Bi-doped fibre was simultaneously pumped using both the pumps (1267 and 1240nm) operating at their maximum output power, as shown in Fig 4.12. The total pump power of the laser diodes amounted to 760mW. The gain and NF characteristics of the amplifier with simultaneous pumping for an input signal power of -10dBm is shown in Fig 4.15. The optimum length of the fibre for bi-directional pumping with 760mW of pump power was found to be 150m. A maximum gain of 26dB with a NF of about 5dB was obtained at 1340nm. The gain in the wavelength band of 1310-1360nm was more than 20dB.

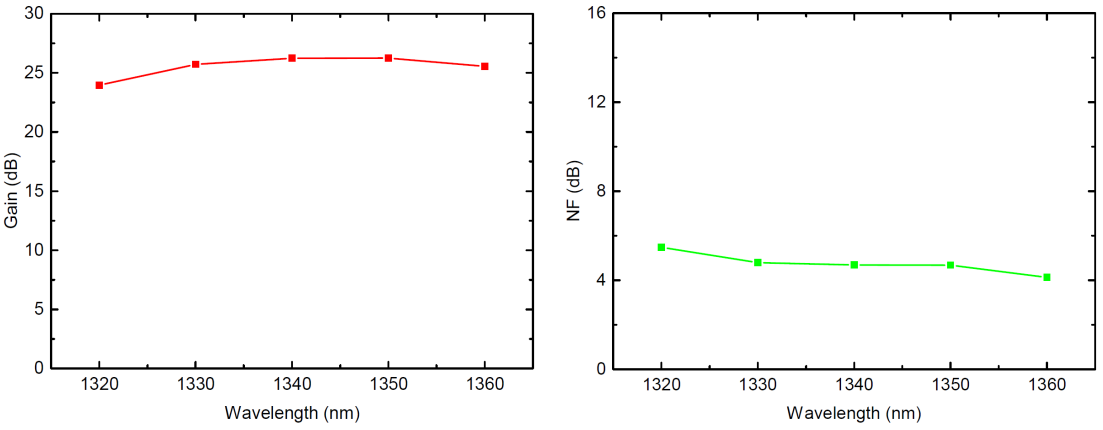

FIGURE 4.16: The flat gain characteristics of the amplifier from 1320-1360nm

Moreover, a flat gain of 25±1dB with a NF of <6dB was achieved over a 40nm bandwidth (1320-1360nm), as shown in Fig 4.16. The optical signal to noise ratio (OSNR) was more than 30dB. It can be noted that this amplifier could potentially operate even at wavelengths longer than 1360nm, which we are currently unable to measure due to the limitations of available signal source (TLS) operating wavelength range.

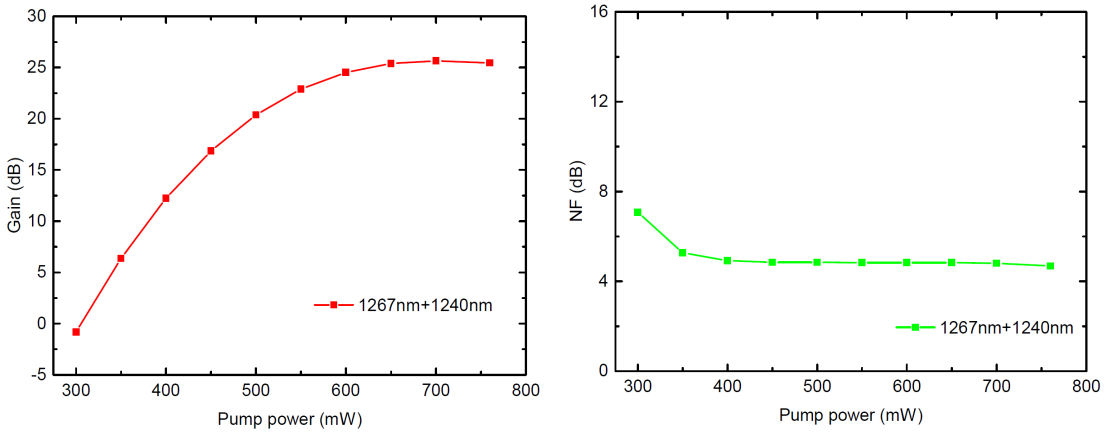

FIGURE 4.17: Variation of gain and NF with pump power for bi-directional pumping at 1267nm and 1240nm for an input signal power of -10dBm and operating at a wavelength of 1340nm)

Fig 4.17 shows the gain and NF variation with the pump power for the 150m long fibre in the bi-directional pumping configuration measured at a wavelength of 1340nm. A maximum gain of 26dB with a NF of 5dB for a pump power of 760mW was obtained for an input signal power of -10dBm.

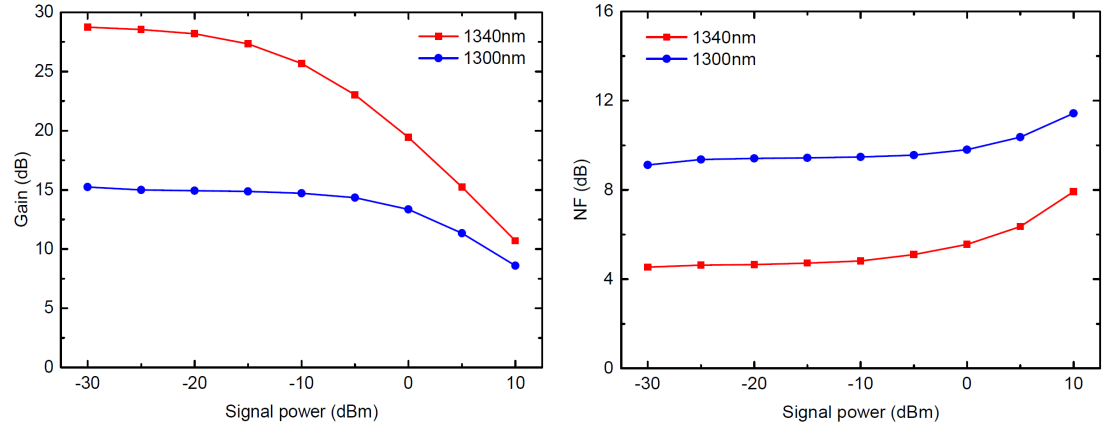

FIGURE 4.18: Characteristics of the amplifier with input signal power at wavelengths of 1300nm and 1340nm, when dual pumping with 1267nm and 1240nm laser diodes operating at their maximum power

The gain variation with input signal power is also shown in Fig 4.18 at two signal wavelengths 1300 and 1340nm. The small signal gain for an input signal power of -30dBm, at a 1300nm wavelength was about 15dB whereas it was 29dB at 1340nm. Moreover, a NF of 5dB at 1340nm has been achieved for a broad range of input signal power.

We also investigated the amplifier performance for a pump wavelength shorter than 1240nm in combination with the 1267nm pump. A bi-directional pumping scheme was explored again, in which the 1267nm pump with an output power of 360mW was fixed

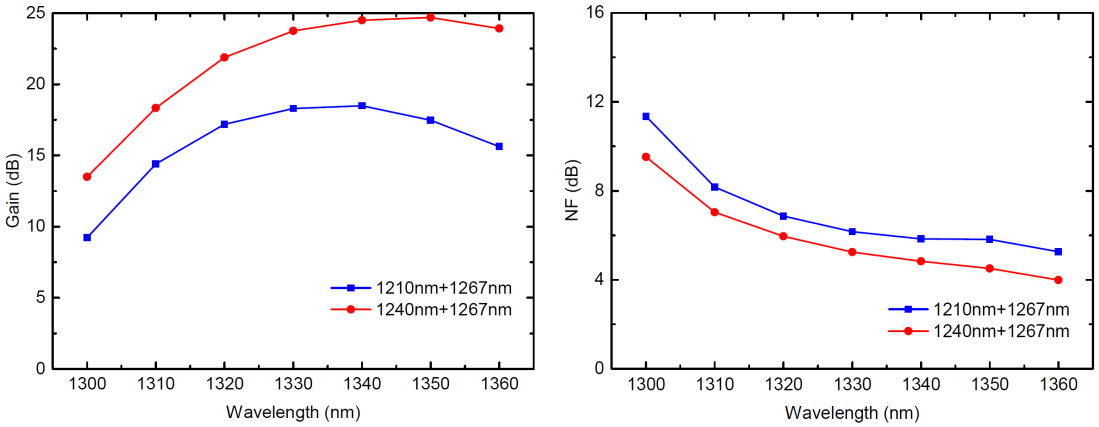

FIGURE 4.19: Gain and NF characteristics of the amplifier by dual pumping at 1210nm or 1240nm pump in conjunction with 1267nm pump [pump powers: 1210nm or 1240nm @ 300W; 1267nm @ 360mW, signal power: -10dBm]

at the signal input end of the amplifier. A second pump operating at a wavelength of 1210nm (or 1240nm) was used at the signal output end with a maximum power of 300mW. The total pump power amounted to 660mW in both cases for a fair comparison. A fibre length of 150m and an input signal power of -10dBm were used. A gain of 21±1dB with a NF of <5dB has been obtained in the wavelength region 1330-1360nm for 1210+1267nm pumping. When using 1240+1267nm pump the gain was increased to 24±1dB as shown in Fig 4.19. This can be attributed to the higher unsaturable loss of fibre at 1210nm compared to a 1240nm pump. Thus the optimum pumping wavelengths for our dual pumped BPSF amplifier with a broad gain spectrum were found to be around 1240 and 1267nm.

4.4 Conclusion

In conclusion, BPSFs were fabricated under different oxidation conditions by standard MCVD-solution doping technique. Absorption, UL and laser efficiency have been measured in all BPSFs and found to be strongly correlated with the fabrication conditions. The UL was found to be low at 1267nm in comparison with 1210nm pump wavelength. A Bi-doped fibre laser operating at 1360nm has been demonstrated with a laser efficiency of 11% by direct diode pumping at 1267nm. The same fibre was made single mode and the slope efficiency was further increased to 13.6%. Finally, an efficiency of 18% with an output power of 110mW was demonstrated using bi-directional pumping with a total pump power of 770mW.

In another experiment, the BPSF with lowest UL and best performance in terms of lasing was used to develop an all fibre Bi-doped fibre amplifier. The gain profile dependence

of the amplifier on pump wavelengths was demonstrated. It has been shown that with a 1267nm pump, the amplifier gain is pushed toward the longer wavelength with a gain peak appeared close to 1350nm, whereas with a 1240nm pump the gain is shifted to shorter wavelength side with a maximum gain obtained at around 1330nm. The amplifier was also bi-directionally pumped using two pumps in order to flatten the gain spectrum of the amplifier. A flat gain of 25±1dB was demonstrated over a 40nm bandwidth covering the wavelength region of 1320-1360nm (which is limited by the input signal source) by bi-directional pumping the fibre at wavelengths 1267 and 1240nm. Furthermore, a small signal gain of about 29dB was obtained for an input signal power of -30dBm. Also, the fibre used here was drawn several times from different sections of the preform and tested for amplifier configuration and the results were found to be similar.

This Bi-doped fibre amplifier can be very useful to open up the O-band for optical fibre communication. For example the loss of Corning SMF 28e fibre is around 0.32dB/km in the wavelength band 1300-1360nm. If we consider an input signal power of 10dBm, after travelling through the SMF 28 e over a distance of 62.5km the output signal will be -10dBm with an induced loss of 20dB. If we use a Bi-doped fibre amplifier that we developed after the 62.5km SMF 28e we can amplify the -10dBm signal to approximately 25dB for an output signal of 15dBm. The 15dBm signal can be transmitted further to a distance of 31km to achieve an output signal of 5dBm. This way one can establish a communication link in the O-band. The other advantage of our amplifier is, it has flat gain within 40nm bandwidth which is important when it is required to send the signals over CWDM or DWDM along the transmission link.

Chapter 5

Bismuth-doped all fibre mode-locked laser operating at 1340nm

5.1 Introduction

Mode-locked fibre lasers have proved to be an important tool in many different applications including telecommunication, spectroscopy, medicine, materials processing, and imaging. The advantages of passive mode-locked fibre lasers are that they are compact, low-cost, flexible and simple in design. The maturity of rare earth (RE) fibre fabrication technology to develop ytterbium (Yb), erbium (Er) and thulium(Tm) or holmium (Ho) doped fibres made them an obvious choice to explore 1, 1.5 and 2μm pulsed fibre lasers, respectively [130, 131]. However, the wavelength band from 1.15 to 1.45μm remains relatively unexplored due to the unavailability of efficient RE gain media despite several important applications [131]. The specific applications of lasers and amplifiers in this wavelength window include sources for second telecommunication band as well as the development of visible lasers through the second-harmonic generation [14, 132]. Bismuth (Bi)-doped fibres have shown prominent progress in developing amplifiers and lasers covering the wavelength band from 1.15 to 1.8μm in different glass hosts (i.e., aluminosilicate, phosphosilicate and germanosilicate). Bi-doped fibre amplifiers and lasers have seen extensive progress in the last few years reaching gain and efficiency values close to 30dB and 50%, respectively [50, 80, 128, 133]. In addition, the broad luminescence of Bi-doped fibres is an added leverage to develop sub-picosecond pulsed lasers. Although, Bi-doped fibres are a promising active medium to develop efficient pulsed fibre lasers in the wavelength band inaccessible by RE-doped materials, a comparatively

low gain per unit length is the current challenge to develop mode-locked fibre lasers with a short length active fibre gain medium. The first Bi-doped pulsed fibre laser was demonstrated in 2007 with 50ps pulses at 1161nm using a semiconductor saturable absorber mirror (SESAM) [82]. Since then a number of studies have reported on Bi-doped pulsed fibre lasers based on saturable absorbers, such as SESAM and carbon nanotube (CNT) [84, 86, 87, 91]. However, the pulse dynamics in Bi-doped fibres are not yet well understood due to the quenching effects such as unsaturable loss (UL) and excited state absorption in these fibres [56]. In recent years pulse bunching was observed in Bi-doped germanosilicate fibres [94, 95]. A phenomenon that occurs due to an interaction between the solitons generated in mode-locked fibre lasers with a total cavity in anomalous dispersion regime [134, 135]. Here, we used a relatively high concentration Bi-doped phosphosilicate fibre (L30459-A0787), fabricated by modified chemical vapour deposition (MCVD) process in conjunction with standard solution doping technique as mentioned in chapter 2, was used to design a ring cavity mode-locked fibre laser and to study the pulsing phenomena at 1340nm without any saturable absorber such as SESAM or CNT within the cavity. The effect of pump power on pulse width was studied with results showing that the pulse width variation from 1.5 to 3ns with a maximum pump power of 335mW. Further, the output of mode-locked Bi-doped fibre laser (ML-BDFL) was amplified in a master oscillator power amplifier (MOPA) configuration wherein a 100m long Bi-doped fibre was used to achieve a maximum average power of 18mW. Soliton bunching was confirmed and a true pulse width of 1.2ps was reported with the measured autocorrelation.

5.1.1 Dispersion

Dispersion in an optical fibre is an important parameter, especially when dealing with ultrashort pulses with a broad spectrum. The zero dispersion wavelength of conventional optical fibre is around 1310nm. The dispersion regime below zero dispersion wavelength is called normal dispersion regime (negative dispersion, D<0 and β_2 >0). The dispersion regime above zero dispersion wavelength is called anomalous dispersion regime (positive dispersion, D>0 and β_2 <0). In the normal dispersion regime, longer wavelengths (a red component of the pulse) travel faster compared to shorter wavelengths that leads to positive chirp. In case of anomalous dispersion regime, shorter wavelengths (a blue component of the pulse) travel faster compared to longer wavelengths that leads to negative chirp. In a fibre, if both anomalous dispersion and self-phase modulation present at the same time then the negative chirp generated by the anomalous dispersion is compensated by the positive chirp introduced by SPM and leads to a soliton generation as

shown in Fig 5.1 [9]. Dispersion in an optical fibre can be calculated from β_2 by using equation 5.1 as mentioned below

$$D = -\frac{2\pi c}{\lambda^2}\beta_2 \tag{5.1}$$

Where c is the speed of light and λ is the wavelength of operation and β_2 is the group velocity dispersion.

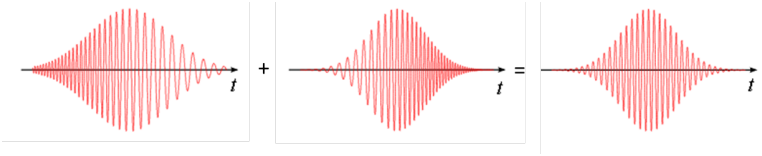

FIGURE 5.1: Pulse evolution in presence of anomalous dispersion and SPM [136]

5.1.2 Spectral sidebands

When a soliton propagates in a fibre laser,it encounters various periodic perturbations such as gain, filtering, and loss due to splices or output couplers. The perturbed soliton sheds dispersive radiation as it is reshaped back into a soliton. These linear dispersive waves are generated over the broad spectrum of the soliton and have a dispersion relation

$$k_{lin} = -\frac{|k^{"}|}{2}\Delta w^2 \tag{5.2}$$

Where Δw is the frequency offset from the peak of the soliton spectrum. Each frequency component then propagates at its own phase velocity. The dispersive waves generated each period Z_p will interfere distructively except at frequencies that are phase matched. This phase-matching condition is expressed by $Z_p(k_s - k_{lin}) = 2\pi m$ where $k_s = -\frac{|k^{"}|}{2\tau^2}$ is the propagation constant of the soliton, m is an integer, Z_p is the perturbation length (length of the laser). By using equation 5.2 in the above relation, we can solve for frequeny offset Δw where phase matching occurs (or position of Kelly side bands) and is given by

$$\Delta w = \pm\frac{1}{\tau}\sqrt{m\frac{8Z_o}{Z_p} - 1} \tag{5.3}$$

The chromatic dispersion of the fibre can be retrieved from the position of the Kelly side-bands in an optical spectrum. For long pulses $8Z_0 = 4\pi\frac{\tau^2}{|k^{"}|}$ is large, so the sidebands are located far from the peak of the soliton. If the average dispersion and laser length

are kept constant as the pulse width decreases, then Z_0 will decrease and the sidebands will be located closer to the peak of the soliton [137].

5.1.3 Autocorrelation

An optical autocorrelator is a device to measure the duration of ultrashort pulses with picosecond or femtosecond pulse width, where an electronic photo-detector would be slow. The basic principle of optical autocorrelator is to split an incoming beam into two copies and to superimpose those with a variable temporal delay. A non-linear interaction is used for obtaining a signal that depends on the pulse overlap, and the pulse duration [138]. Here we used an FR-103XL autocorrelator to measure the autocorrelation of the mode-locked Bi-doped fibre laser. The experimental setup of the commercially available FR-103XL autocorrelator is shown in Fig 5.2.

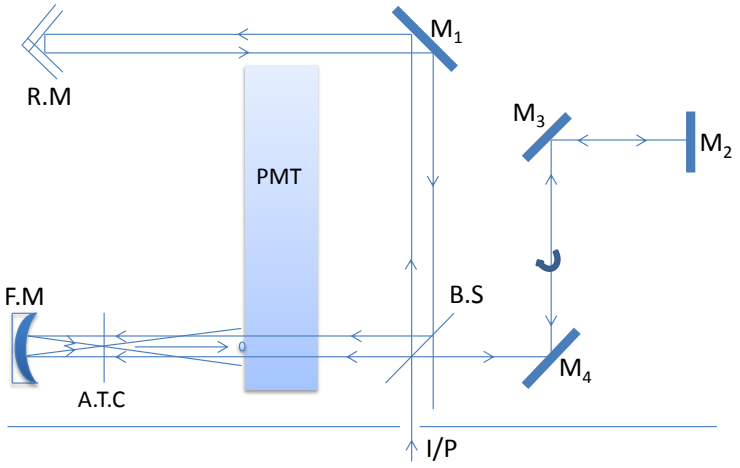

FIGURE 5.2: Experimental setup of the commercially available FR-103XL autocorrelator [139]

Initially, the input beam is directed into the autocorrelator by using a fibre coupled input. The beam falls on an infrared (IR) pellicle beam splitter (B.S) and is split into two identical beams. One of the two beams is directed towards the fixed arm and the other beam is directed towards the delay arm of the Michelson interferometer. The beam in the fixed arm reflected back towards the pellicle beam splitter by using a retroreflector mirror (R. M) after passing through the mirror (M_1). The beam in the delay arm is reflected back towards the pellicle beam splitter (B. S) by a mirror (M_2) after passing through a pair of parallel mirrors (M_3 and M_4). The pair of parallel mirrors centred about a rotating axis in the delay arm introduces repetitive linear delay generation. The two beams from the beam splitter are focused on S.H.G angle tuned crystal (A.T.C) ($LiIO_3$ crystal) by means of a focusing mirror (F.M). The generated S.H.G beam then falls on the photomultiplier tube (PMT) and produces an output at the oscilloscope to

measure the autocorrelation pulse width. Dispersion is entirely minimised in the FR-103XL by the use of metallic high reflecting coatings and focusing the beam into the NL crystal by means of a curved mirror. Also, the beams lie in the horizontal plane through the centres of M_1 and input aperture [139].

The conversion factor from the FWHM autocorrelation trace width (T_{FWHM}) to the actual pulse width (t_p) is a function of the pulse shape assumed. Table 5.1 shows the relation between T_{FWHM} and t_p for commonly used pulse shapes.

Pulse shape.	t_p/T_{FWHM}
Hyperbolic Secant	0.647
Gaussian	0.707
Rectangular	1
Triangular	0.692

TABLE 5.1: Relation between T_{FWHM} and t_p for commonly used pulse shapes [138]

5.2 Mode-locked Bi-doped fibre laser

5.2.1 Experimental setup

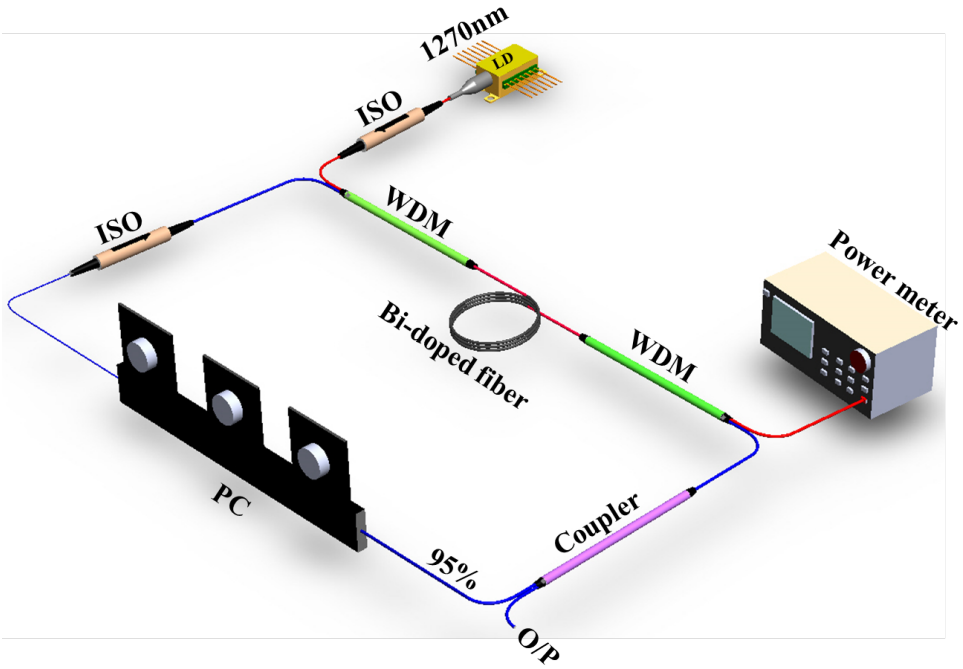

FIGURE 5.3: Schematic experimental setup of mode-locked Bi-doped fibre laser

The ML-BDFL was constructed with a ring cavity architecture as shown in Fig 5.3. Initially, a laser diode (LD) operating at 1270nm with a total pump power of 335mW was used to pump the Bi-doped fibre. An isolator was placed to ensure unidirectional operation; while a 95:5 coupler was used to extract a 5% signal out of the ring cavity. A polarization controller (PC) was employed to control the polarization in the cavity for stable pulsing. An optical spectrum analyser (OSA), RF spectrum analyser (400MHz), InGaAs photodetector (5GHz) and an oscilloscope (2.5GHz) were used to study the ML-BDFL characteristics. The active fibre was characterised for absorption and UL using a white light source (WLS) and a laser diode (LD) prior to its use in the ring cavity. The measured small signal absorption and the UL at 1270nm pump wavelength were 1.7dB/m and 17%, respectively.

5.2.2 Results

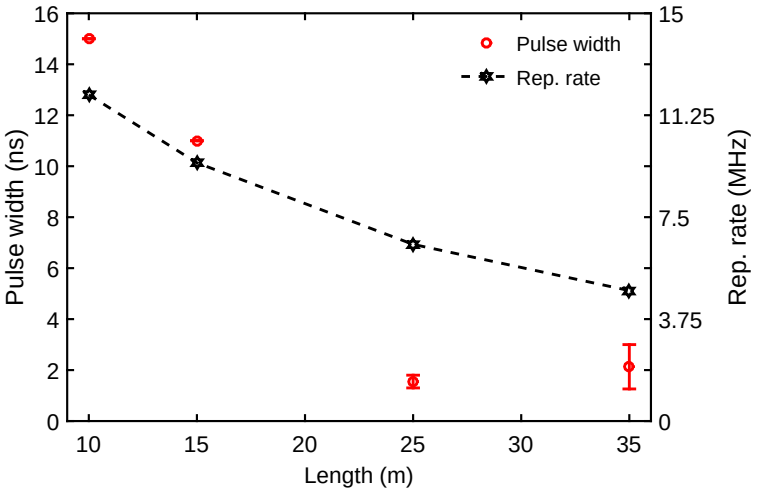

FIGURE 5.4: Pulse width and Rep.rate variation with different length of Bi-doped fibre for a single 1270nm laser diode pumping

Initial measurements of the effect of fibre length on ML-BDFL performance showed a pulse width of 3ns with a maximum output power of 3mW at a fibre length of 25m as shown in Fig 5.4. For this length, the ML-BDFL generated pulses with a repetition rate of 6.3MHz at 1340nm that agrees with the cavity round trip time. Here we observed that the polarization adjustments are necessary to make the ML-BDFL stable.

We also observed that the pulse width increased slowly with pump power from 1.5 to 3ns as shown in Fig 5.5. Note that here the pulse width increased with pump power, clearly indicating that the pulsing behaviour is not due to q-switching in which the pulse width would be expected to decrease with increasing pump power. Throughout this experiment the pulse repetition rate remained fixed at the cavity round-trip time, further indicating that the BDFL was operating in the mode-locked regime instead of

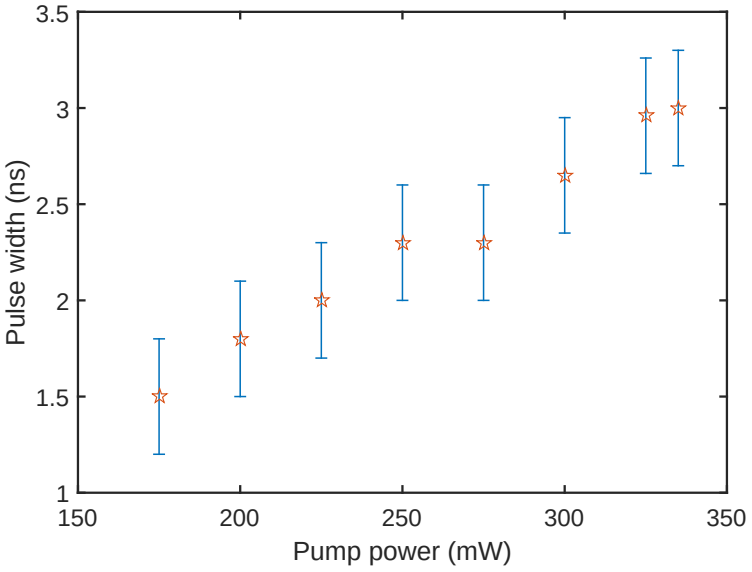

FIGURE 5.5: Pulse width variation with pump power of 25m long Bi-doped fibre for a 1270nm laser diode pumping

the q-switched regime. The cavity contains approximately 7.8m of passive fibre due to the WDMs, isolators, couplers and a polarization controller in addition to 25m of Bi-doped fibre.

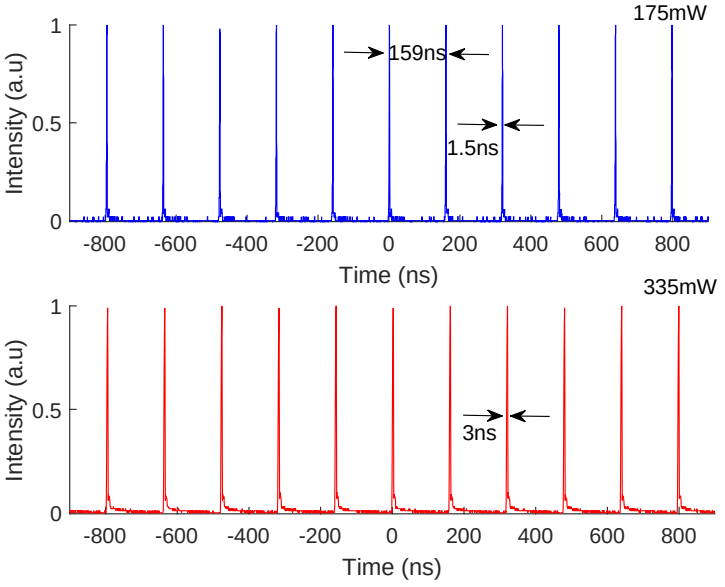

FIGURE 5.6: Pulse train of the ML-BDFL at minimum and maximum pump power of 175 and 335mW, respectively with pulse widths of 1.5 and 3ns

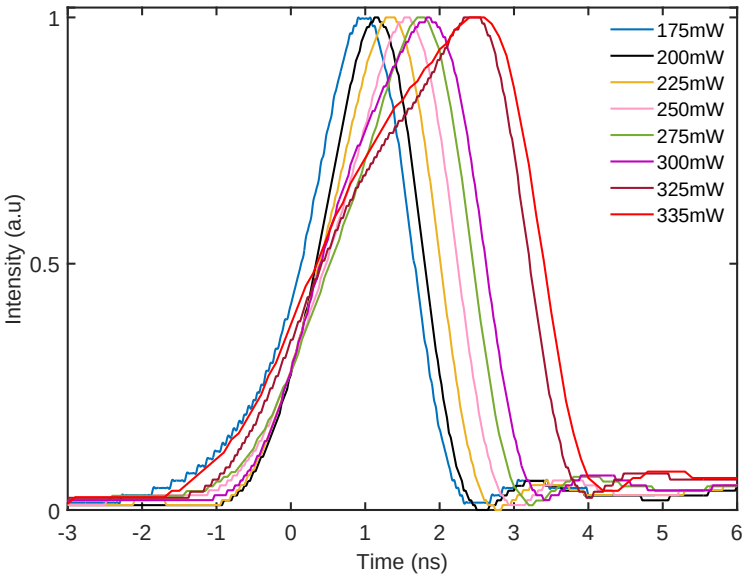

FIGURE 5.7: Single pulse width variation with pump power

Pulse trains with a pulse width of 1.5 and 3ns were measured by an oscilloscope at a pump power of 175mW and 335mW, respectively and is presented in Fig 5.6. A pulse period at both pump powers remained constant at 159ns. Further, the single pulse width variation with pump power is shown in Fig 5.7.

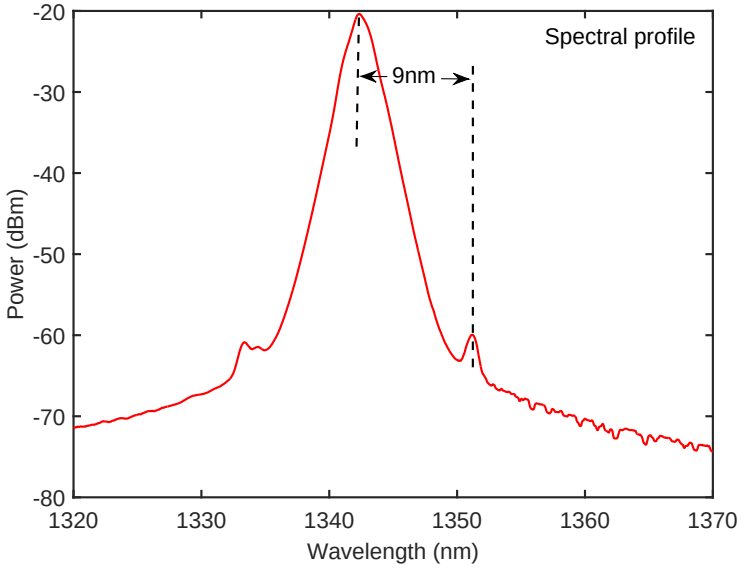

FIGURE 5.8: Optical spectrum of the ML-BDFL at a pump power of 335mW for a 25m long Bi-doped fibre

The optical spectrum shows a central wavelength at 1342nm and a 3dB bandwidth of 1.6nm at the maximum pump power of 335mW as shown in Fig 5.8. The appearance of Kelly sidebands in the optical spectrum indicates that the ML-BDFL operates in the

anomalous dispersion regime. From the optical spectrum, and assuming that the pulses were transform limited, the output pulse width was expected to be ∼1ps. The measured larger pulse width can be attributed to soliton bunching while the increase in pulse width with pump power is expected due to the increase of soliton number [135, 140]. However, the existence of sub-picosecond pulses within the pulse envelope could not be directly confirmed because of the limitations imposed by the bandwidth of detector and oscilloscope. The measured sideband shift from the central wavelength was around 9nm to the first order sideband as shown in Fig 5.8. From the measured optical spectrum, the total dispersion of the cavity was calculated by the following equations [141, 142]

$$\Delta\lambda = \pm\frac{\lambda^2}{2\pi c t_0}\sqrt{-1+\frac{8nZ_0}{Z_a}} \tag{5.4}$$

$$\text{where } Z_0 = \frac{\pi t_0^2}{2\,|\beta_2|} \tag{5.5}$$

Where c, n are the speed of light in vacuum and order of the sideband, respectively. Z_a is the cavity length, Z_0 is soliton period and T_{FWHM}=1.763 t_0 is pulse duration at FWHM.

The calculated dispersion was 4.5pskm^{-1}nm^{-1} at 1343nm confirming that the cavity operates in the anomalous dispersion regime and the laser operates in the soliton pulse regime.

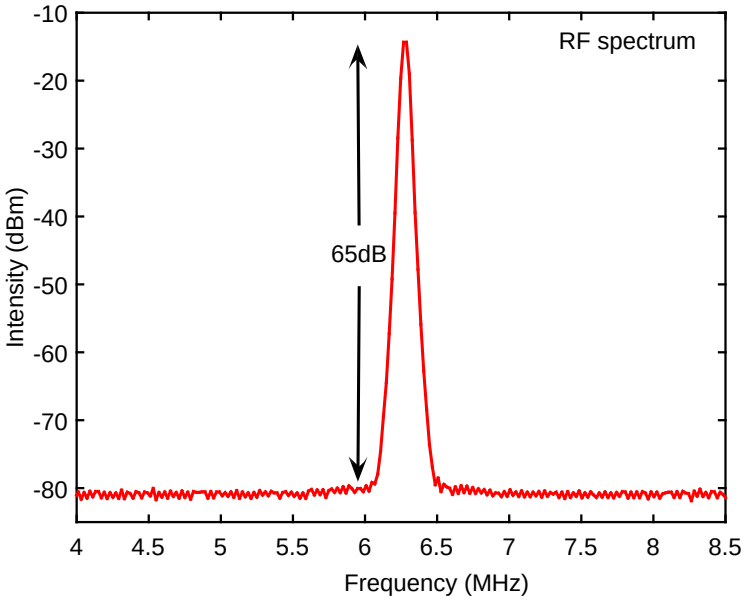

FIGURE 5.9: RF spectrum of the ML-BDFL at a pump power of 335mW for a 25m long Bi-doped fibre

The RF spectrum of the ML-BDFL is presented in Fig 5.9. The measured RF spectrum shows good harmonic purity with a signal to noise ratio (SNR) of 65dB at a fundamental repetition rate of 6.3MHz, thereby indicating a stable pulsing.

5.3 Master oscillator power amplifier

5.3.1 Experimental setup

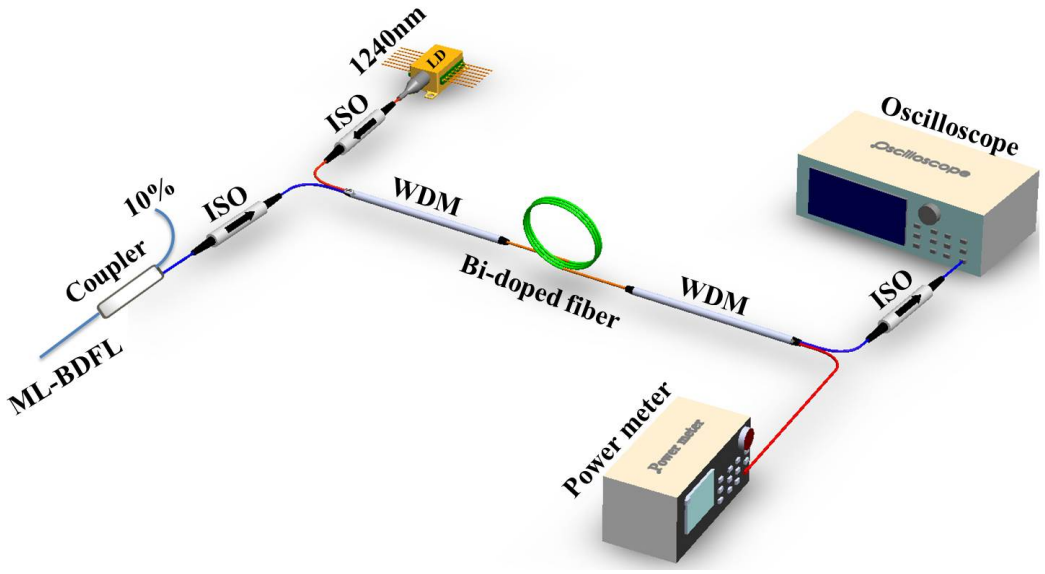

FIGURE 5.10: Experimental setup of master oscillator power amplifier (MOPA)

In order to amplify the signal power of the ML-BDFL, the MOPA as shown in 5.10 was constructed. A 90/10 coupler was inserted between the ML-BDFL and the amplifier. The 10% port was used to monitor the output of ML-BDFL while the 90% port was used as input to the amplifier. A 1240nm pump laser diode having a maximum pump power of 420mW was used to pump Bi-doped fibre. Two WDMs were used to combine and separate pump and signal at the input and output, respectively. Isolators were used to avoid back reflections into the cavity of the ML-BDFL and to protect the 1240nm pump. The active Bi-doped fibre used in the MOPA was different from the fibre used for ML-BDFL. This Bi-doped fibre (L30370-A0625) had a core and cladding diameter of 11 and 150μm, respectively. The UL in this Bi-doped fibre was 7% [133].

5.3.2 Results

Fig 5.11 shows the dependence of MOPA output signal power on pump power for a fixed seed power of 2.5mW (3.95dBm). At this fixed seed power, the MOPA signal

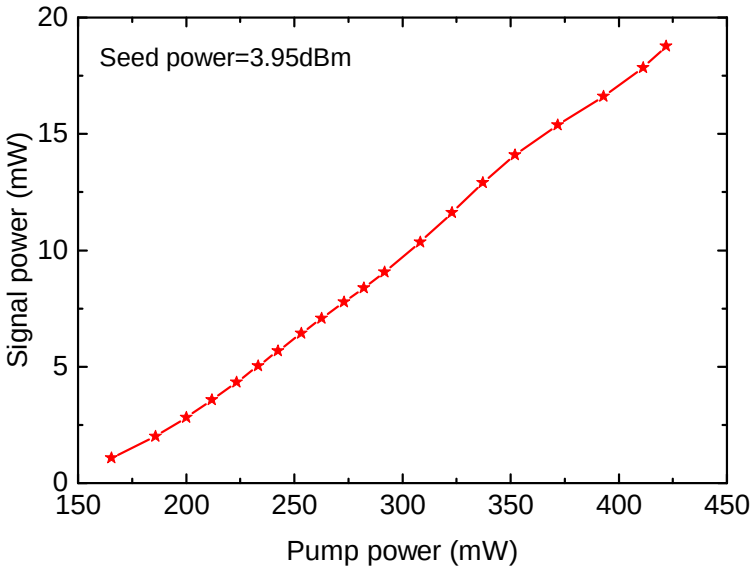

FIGURE 5.11: Variation of signal power with pump power of MOPA for a fixed input seed power of 2.5mW (3.95dBm)

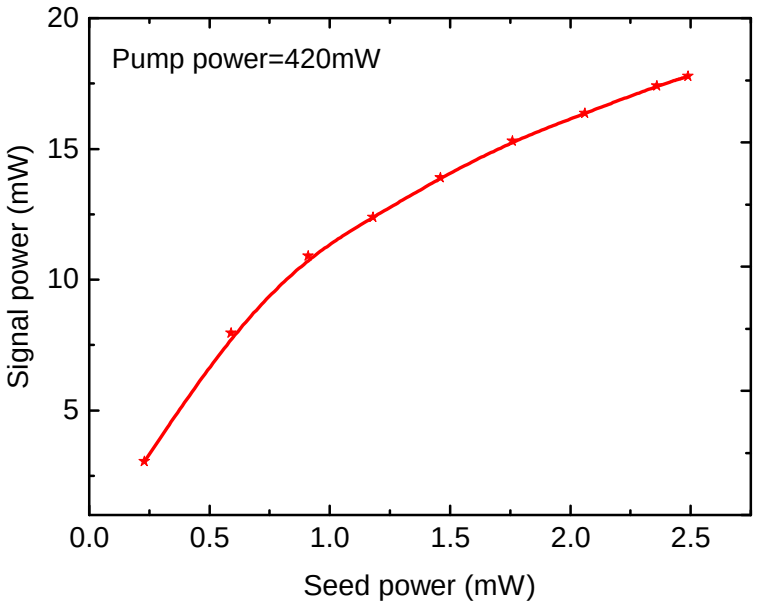

FIGURE 5.12: Signal power variation of MOPA with seed power for fixed pump power of 420mW

power increased with a slope efficiency of 7.25% up to a maximum of 18mW and is limited by the maximum available pump power of 420mW. In a second experiment, the MOPA pump power was fixed at 420mW while the seed power was increased as shown in Fig 5.12. Here the MOPA output power increased with ML-BDFL seed power, again reaching a maximum of 18mW. The laser spectrum and pulse profile measured at the output of the MOPA shows that no significant distortions were introduced by the 100m long Bi-doped fibre used in MOPA. A maximum average power of 18mW was achieved with a pulse width of 2.5ns. Corresponding peak power and the energy were 1.15W and

2.9nJ.

5.4 Autocorrelation

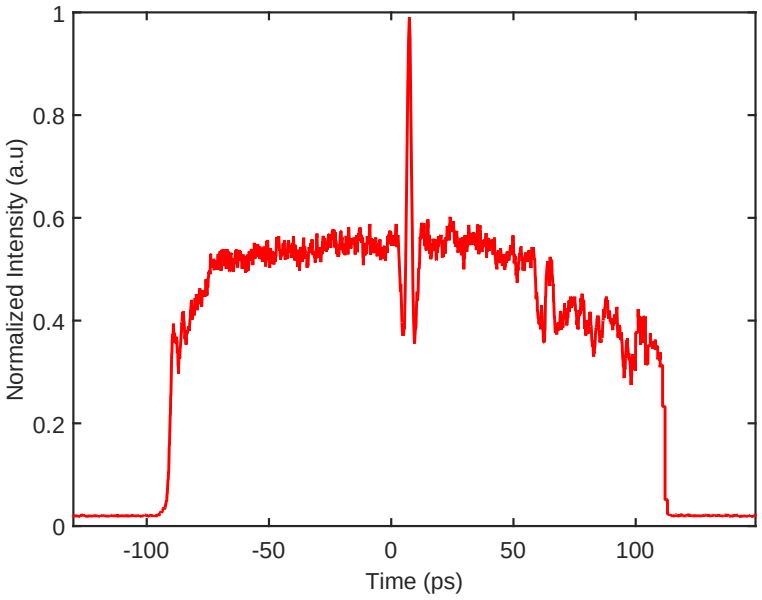

FIGURE 5.13: Autocorrelation trace of the mode-locked Bi-doped fibre laser

The true pulse width of the mode-locked Bi-doped fibre laser was measured by an autocorrelator (Femtochrome, FR-103XL) in conjunction with an oscilloscope and is shown in Fig 5.13. The measured autocorrelation trace has a large pedestal which is a signature of soliton bunching in mode-locked fibre laser systems [95, 134, 135, 140–142].

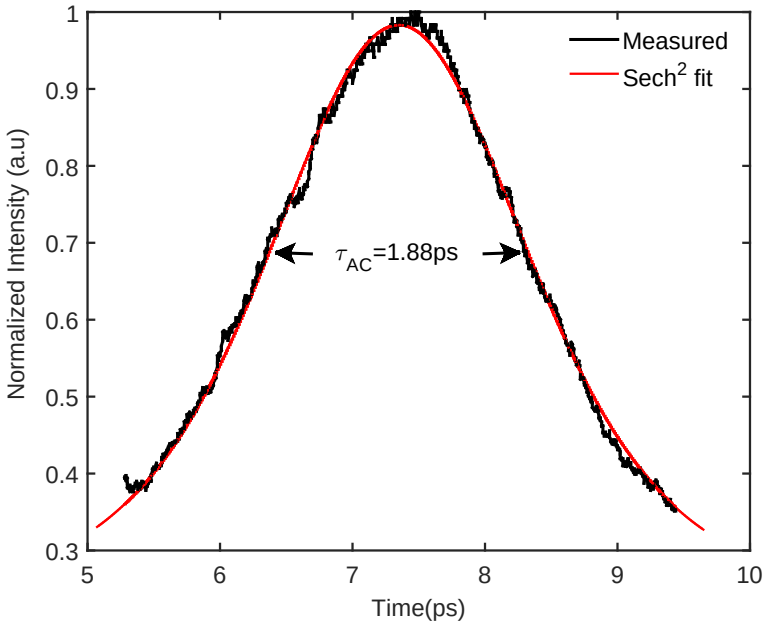

FIGURE 5.14: The sech^2 fitting of the autocorrelation trace

Fig 5.14 shows the autocorrelation trace excluding the pedestal fitted to a hyperbolic-secant function. The FWHM of autocorrelation (τ_{AC}) was found to be 1.88ps. Assuming a hyperbolic-secant pulse shape, the pulse width at FWHM of ML-BDFL was 1.2ps.

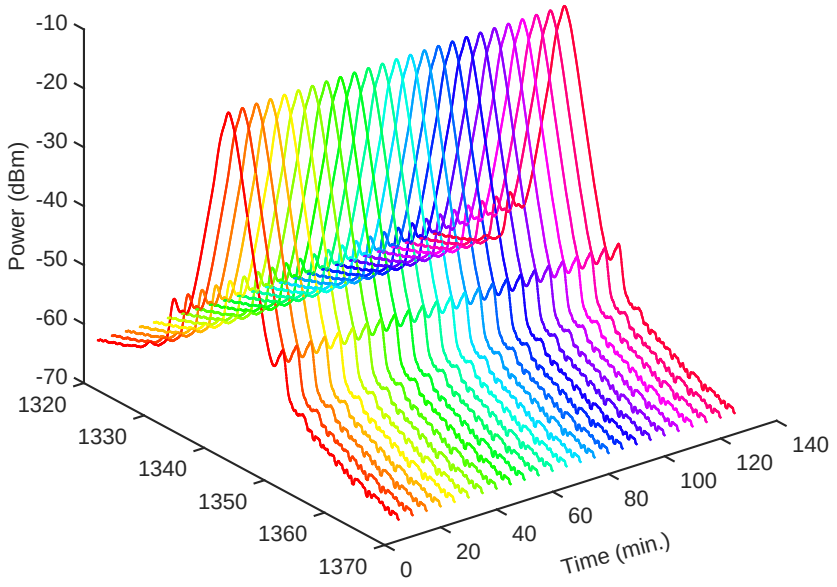

FIGURE 5.15: Optical spectrum of the ML-BDFL observed over 2hrs of time

To analyse the stability of the ML-BDFL the spectrum was monitored for 2hrs at a maximum output power of 18mW in an OSA as shown in Fig 5.15. During this period the ML-BDFL was undisturbed by external perturbations. The stability of the acquired

spectra over time indicates that the operation of the mode-locked Bi-doped fibre laser was stable.

5.5 Conclusion

In conclusion, a Bi-doped phosphosilicate fibre fabricated by the MCVD-solution doping technique was used to study the pulsing phenomenon in an all-fibre Bi-doped mode-locked laser operating at 1340nm without any saturable absorber. The impact of pump power on pulse width was examined and a pulse width variation from 1.5 to 3ns was reported. The maximum average output power of the ML-BDFL was 3mW with a 3ns pulse width. The average output power was further increased to 18mW using a MOPA and a corresponding peak power of 1.15W and a pulse energy of 2.9nJ were achieved. The measured autocorrelation of the ML-BDFL confirms the soliton bunching phenomenon with a true pulse width of 1.2ps. Here one can prevent the pulse bunching phenomena by changing the total cavity dispersion to normal regime because anomalous dispersion leads to soliton formation in the cavity and induce soliton interaction to generate pulse bunching. A stable operation of the ML-BDFL was verified by the RF spectrum with an SNR of 65dB at a fundamental repetition rate of 6.3MHz. To the best of our knowledge, for the first time, we observed picosecond pulses from a Bi-doped mode-locked fibre laser without any saturable absorber such as SESAM or CNT in the cavity. Further study is required to understand the mechanism of such pulsing phenomenon in Bi-doped fibres.

At present, no RE-doped material in silica host can produce gain in the 1330nm wavelength band. Bi-doped fibres is the only way to develop mode-locked fibre lasers in the O-band. The broad gain bandwidth of Bi-doped fibres is an added advantage to develop ultrashort pulsed fibre lasers. One can also develop tunable pulsed fibre lasers by using broad gain Bi-doped fibres. However, there are some challenges involved to develop efficient Bi-doped pulsed fibre lasers. One is the lowest gain per unit length which necessitates one to use longer length of fibres in the mode-locked laser cavity. This can be overcome by developing high concentration Bi-doped fibres but these high concentration Bi-doped fibres always induce unwanted losses such as UL and ESA. Hence it is not only important to develop high concentration Bi-doped fibres but also reduce the unwanted losses to its minimum.

Chapter 6

Core and cladding pumped wideband multi-element Er-doped fibre amplifiers in C+L bands

6.1 Core pumped wideband multi-element Er-doped fibre amplifier

6.1.1 Introduction

Surges in cloud computing, mobile user numbers and social media, are challenging the optical communication industry to keep up with demand for higher data capacity without increasing the cost per bit. This has motivated research groups to continue their efforts in finding new ways to increase the capacity of optical fibres. The capacity of single mode optical fibres, however, is currently approaching the non-linear Shannon limit [143]. As a result, space division multiplexing (SDM) has recently been proposed. There have been several demonstrations of high data rate SDM transmission employing multi-core fibres (MCF), multi-mode fibres (MMF) and multi-element fibres (MEF) [6, 105]. However, there is still a need for further development and refinement of the above approaches for its commercialization. Concurrently, increasing the optical bandwidth for dense wavelength division multiplexing (DWDM) has been a subject of significant interest. Extending the bandwidth of the amplifiers can enable the low-loss window of silica fibres (1480-1620nm) for DWDM transmission. Erbium (Er) can provide broadband amplification covering the wavelength band of 1500-1620nm [144–148]. A double-pass parallel wideband amplifier was demonstrated by using Er-doped fibres (EDFs) from 1530 to 1605nm but the reported noise figure (NF) varies from 5.6 to 8.2dB [149]. Raman

amplification is another way to realize wideband amplifiers, but the number of pump sources and power requirements are high [150–152]. In this chapter, we demonstrate the flexibility offered by multi-element fibre geometry in tuning the gain profile of the amplifier. To develop wideband amplifiers we used MEF comprised of three, five and seven fibre elements (3-MEF, 5-MEF and 7-MEF). Note here that the 5-MEF was used in cladding-pumped configuration. Schematic cross-sectional view of 3-MEF, consisting three Er-doped fibre elements drawn under a common high-index polymer coating is shown in the inset of Fig 6.1. Er-doped preforms, fabricated by modified chemical vapour deposition (MCVD)-solution doping technique were stretched, cut and stacked together to obtain 3-MEF and 7-MEF preforms. The preform cores were doped with Al and Er ions, producing a measured refractive index step (Δn) of 0.005 (fabricated by S. Jain and T. C. May-Smith). The fibres were drawn to a clad diameter of 125μm, resulting in a core diameter of 11μm with an overall coated diameter of 310 and 460μm for 3-MEF and 7-MEF, respectively [102]. The absorption in each element of 3-MEF and 7-MEF at 980nm was 10dB/m. In the following sections, we will study the gain and NF of 3-MEF and 7-MEF to develop core pumped multi-element Er-doped fibre amplifier.

6.1.2 Experimental setup for 3-MEF characterisation

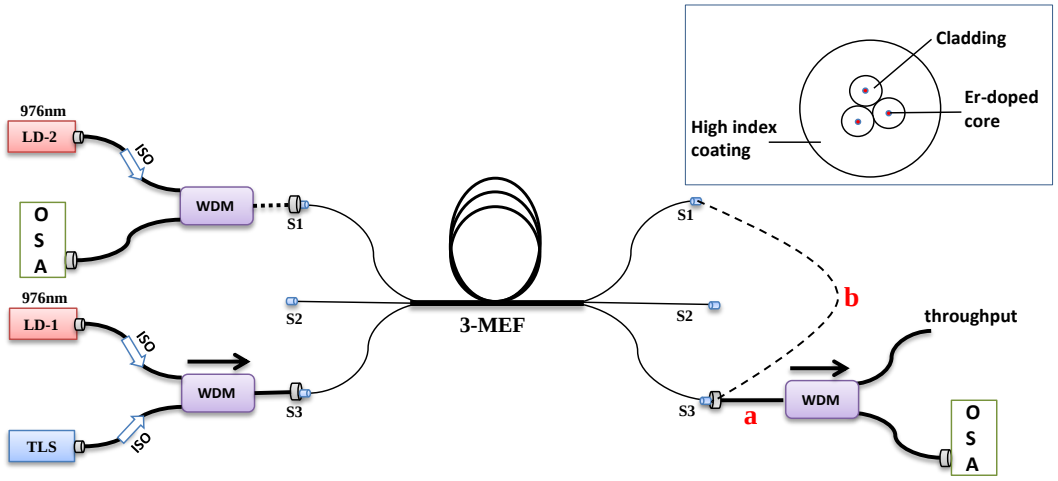

FIGURE 6.1: 3-MEEDFA schematic experimental setup to measure gain and NF of ;a-single fibre element, b-cascaded fibre elements (Inset: cross-sectional view of Er-doped 3-MEF)

Fig 6.1 shows the schematic diagram of the experimental setup used to measure the gain and NF of Er-doped 3-MEF. The setup comprised of a tunable laser source (TLS) as an input signal, 976nm pump laser diodes (LD-1, LD-2), isolators (ISO), and 980/1550nm wavelength division multiplexers (WDM) at the input/output to combine/separate the

signal and the pump. The input and output signals of different wavelengths were measured by the optical spectrum analyser (OSA). The spectra obtained were then used to calculate the gain and NF of each fibre element of the 3-MEF. A 3m length of 3-MEF was used for gain and NF measurements. The fibre elements were indexed as S1, S2, and S3 for identification at both ends of the MEF as shown in Fig 6.1.

6.1.3 Results

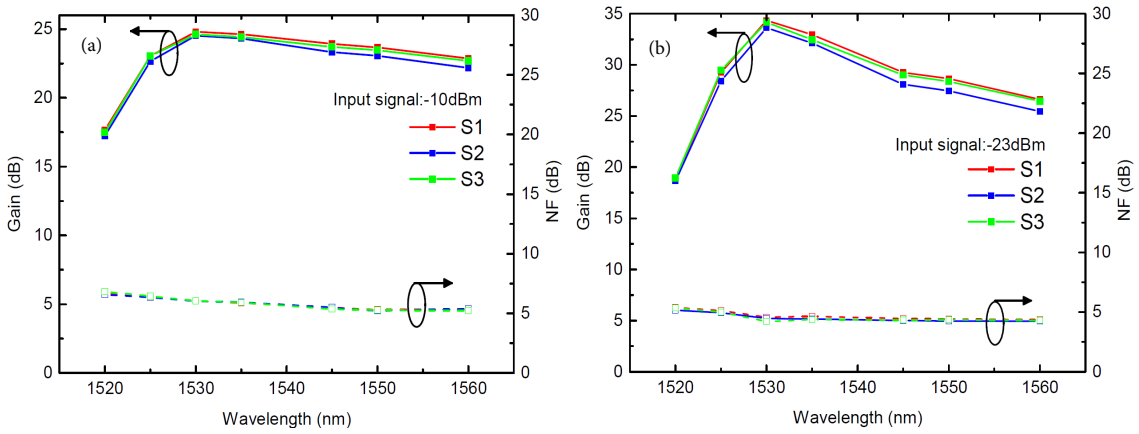

FIGURE 6.2: Gain and NF of fibre elements S1, S2 and S3 for a pump power of 208mW for an input signal power of (a) -10dBm (b) -23dBm

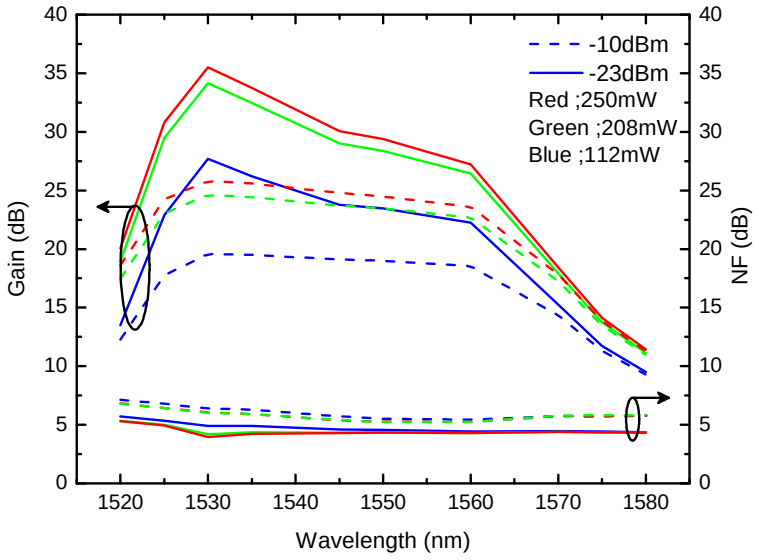

FIGURE 6.3: Gain and NF variation in fibre element S3 of MEF for different input signal and pump powers

Input signals of -10dBm, and -23dBm were used for the characterisation. The characteristics of all three fibre elements were found to be similar as shown in Fig 6.2. Fig 6.3 shows the gain and NF characteristics of S3 with pump powers of 112mW, 208mW and

250mW. A maximum gain of 36dB was observed at 1530nm in the C-band for an input signal power of -23dBm and for a pump power of 250mW. Also, the NF was <4.5dB in the 1520-1570nm wavelength region.

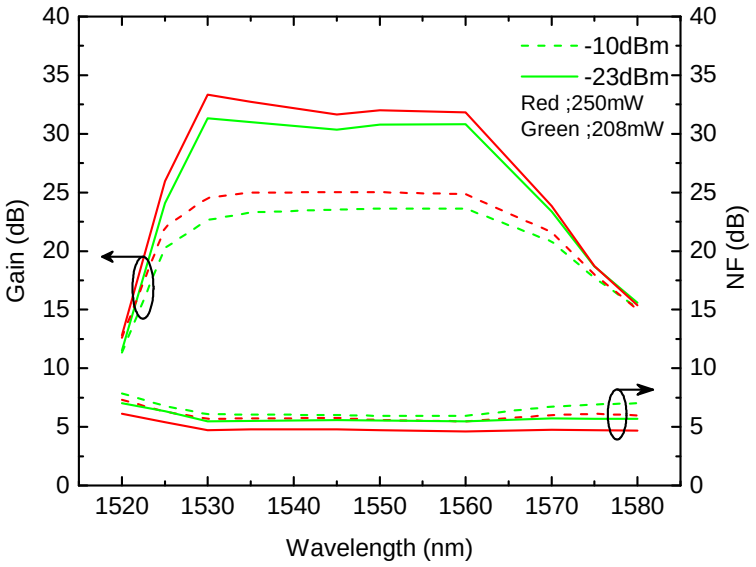

FIGURE 6.4: Gain and NF variation of 2-cascaded fibre elements for different input signal and pump powers

The fibre elements were then cascaded one-by-one by splicing the output of one fibre element to the input of another fibre element to observe the effect on gain profile. It can be seen from Fig 6.4 that the gain at short wavelengths decreased, whereas the gain at longer wavelengths increased after cascading of two fibre elements. The cascaded amplifier provided a flat gain of 33±1dB in the wavelength region of 1530-1560nm for an input signal of -23dBm. A split-band amplifier can be designed in which one of the fibre elements (S1) is used for short wavelength amplification and the other two fibre elements are cascaded (S2 + S3) for long wavelength amplification. This would provide >20 dB gain in the wavelength range of 1520-1570nm (50nm).

The pump power requirement in a cascaded amplifier can be further reduced by bi-directional pumping. To demonstrate this effect, the two cascaded fibre elements were bi-directionally pumped from two 976nm laser diodes. The pump power of one of the laser diode (backward) was varied while the other laser diode (forward) was maintained at a fixed power of 60mW to tune the gain profile of the amplifier. The amplifier gain characteristics in bi-directional configuration for -10dBm and -23dBm input signal powers are shown in Fig 6.5 and Fig 6.6. For a total pump power of 140mW, the gain is >30dB in the wavelength region of 1530-1560nm and ≥20dB in the wavelength region of 1525 to 1570nm for input signals of -23dBm and -10dBm, respectively. To further enhance the gain at longer wavelength side we studied the gain and NF characteristics of 7-MEF in the following section.

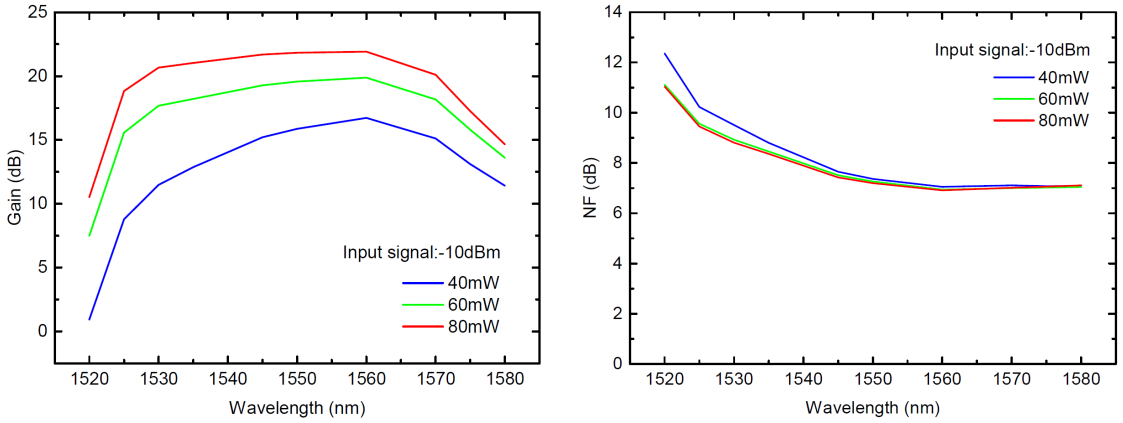

FIGURE 6.5: Gain and NF for cascaded two fibre elements with bi-directional pumping for an input signal of -10dBm, The pump power of one of the laser diodes was varied while the other laser diode was maintained at a fixed power of 60mW

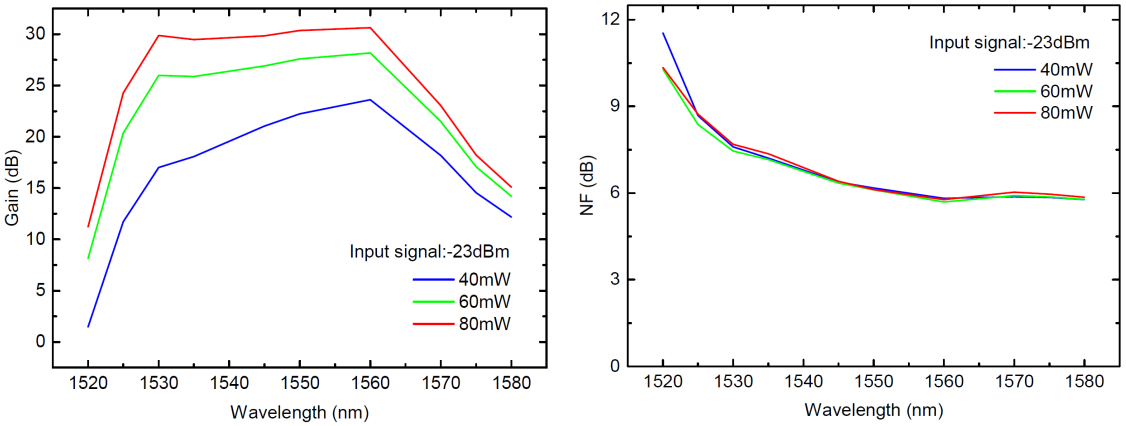

FIGURE 6.6: Gain and NF for cascaded two fibre elements with bi-directional pumping for an input signal of -23dBm, The pump power of one of the laser diode was varied while the other laser diode was maintained at a fixed power of 60mW

6.1.4 Experimental setup for 7-MEF characterisation

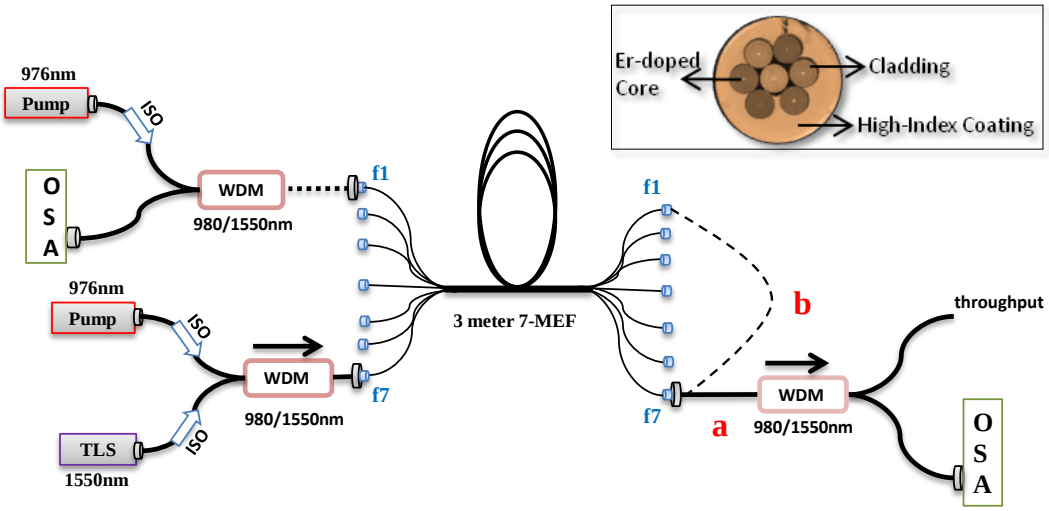

FIGURE 6.7: 7-MEEDFA schematic experimental setup to measure gain and NF of ;a-single fibre element, b-cascaded fibre elements (Inset: cross-sectional view of Er-doped 7-MEF)

Fig 6.7 shows the schematic diagram of the experimental setup used for the characterisation of Er-doped 7-MEF. The setup comprised of a tunable laser source (TLS), 976nm pump laser diodes (LD), isolators (ISO), 980/1550nm wavelength division multiplexer (WDM), and an optical spectrum analyser (OSA). A 3m length of 7-MEF was used for the gain and NF measurements. The fibre elements were indexed as f1 to f7 for identification as shown in Fig 6.7. Input signal powers of -10dBm and -23dBm were used for characterisation of gain and NF.

6.1.5 Results

Initially, individual elements of the 7-MEF were co-pumped with pump powers of 112mW, 208mW and 250mW. It was found that all the fibre elements of 7-MEF were similar gain and NF characteristics. The gain and NF of all fibre elements of 7-MEF were shown in Fig 6.8 for an signal power of -10dBm and -23dBm with a pump power of 250mW. The wavelength dependent characteristic of a single element (f4) with different pump powers is also shown in Fig 6.9. A maximum of 37dB gain and <4.5dB NF was achieved for the input signal power of -23dBm and for a pump power of 250mW. Also, the gain at 1520nm was greater than 20dB.

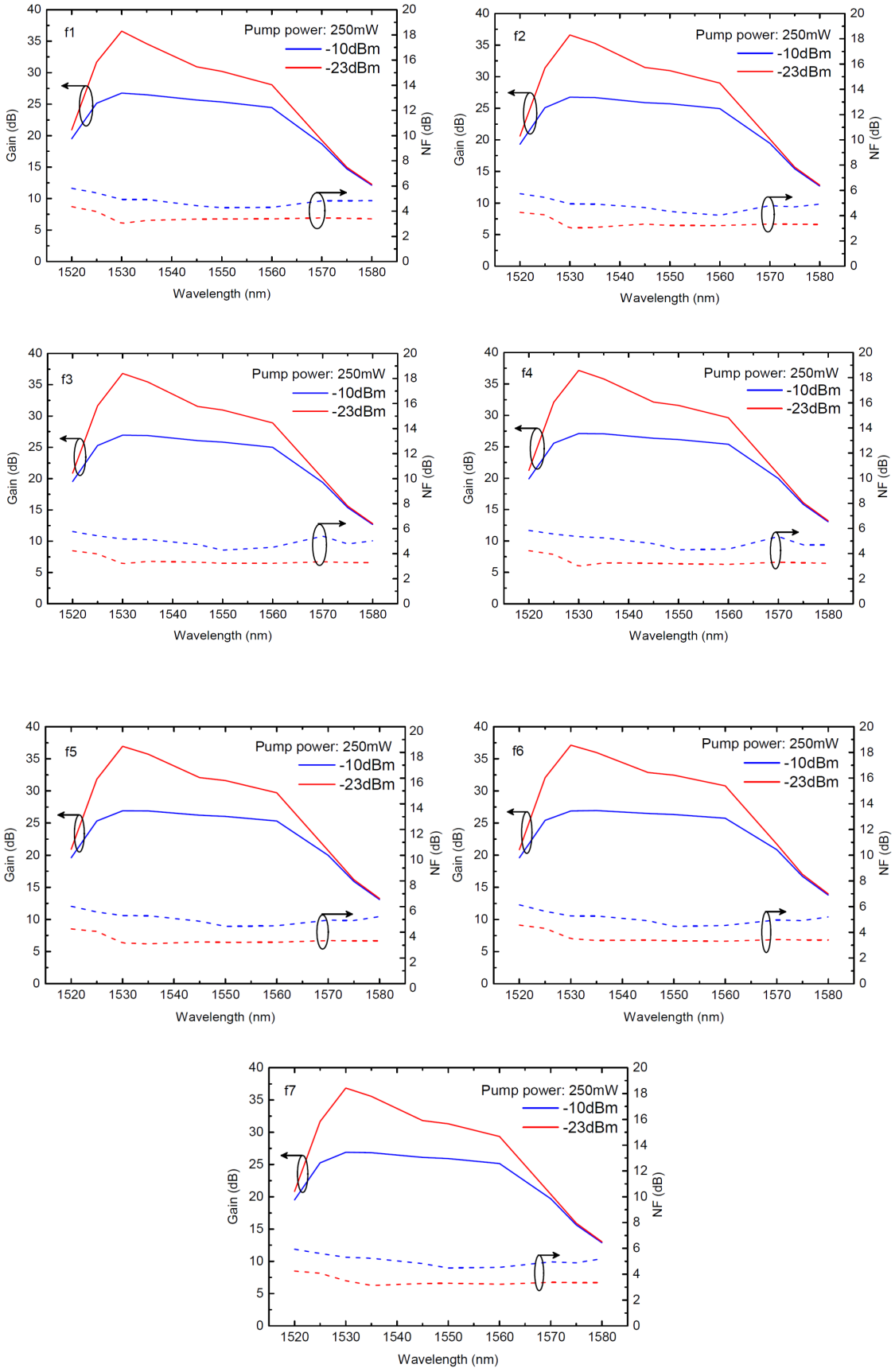

FIGURE 6.8: Gain and NF with wavelength for Er-doped 7-MEF at a pump powers of 250mW for elements f1, f2, f3, f4, f5, f6 and f7

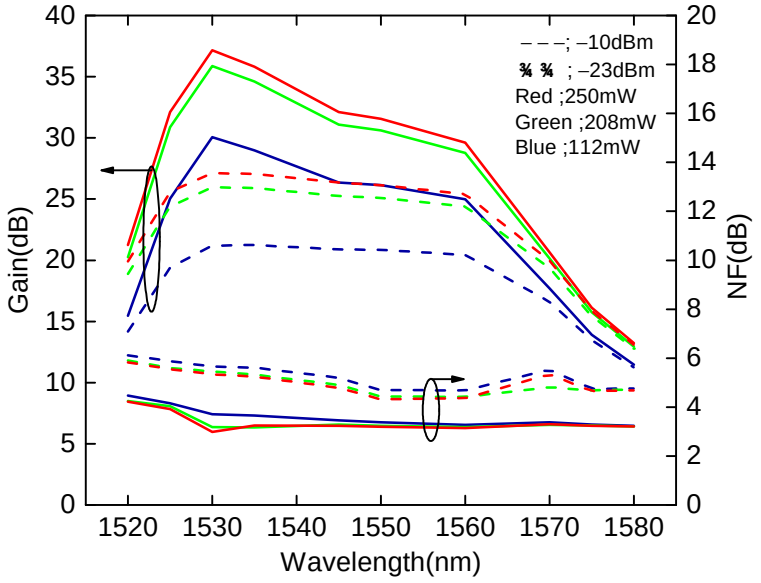

FIGURE 6.9: Variation of gain and NF with wavelength for single element of Er-doped 7-MEF at different pump powers

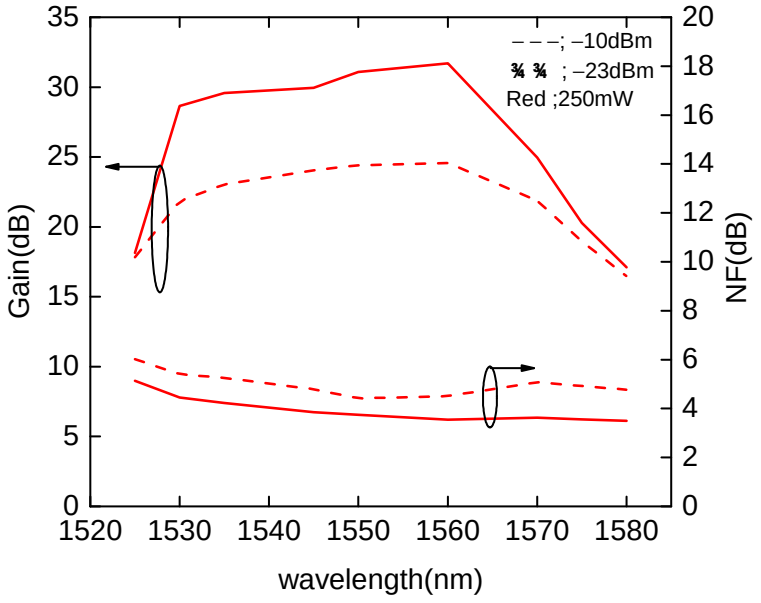

FIGURE 6.10: Gain and NF characteristics of 2-element cascade at a maximum pump power of 250mW

The fibre elements were then cascaded in series by connecting the output of one element to the input of the next, and the variation in the gain profile was observed. The gain and NF spectra for the 2-element cascade was shown in Fig 6.10 at a maximum pump power of 250mW. For an input signal power of -23dBm, the average gain in the C-band was 30dB with a gain variation of $\pm$1.5dB. Moreover, the NF was less than 4.5dB for the entire C-band. As expected, the gain in the 2-element cascade shifted towards longer wavelength compared to the single element, while reducing the gain at 1530nm.

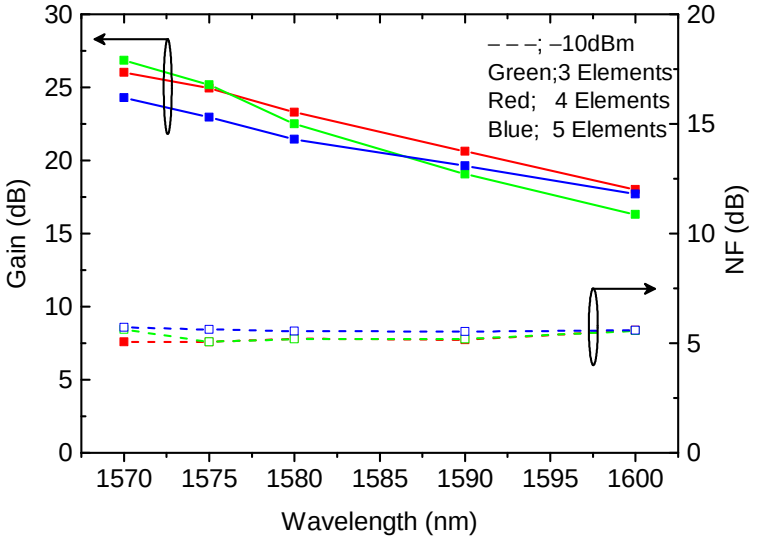

FIGURE 6.11: Gain and NF characteristics of different cascade configurations for bi-directional pumping with a total pump power of 320mW, input signal power: -10dBm

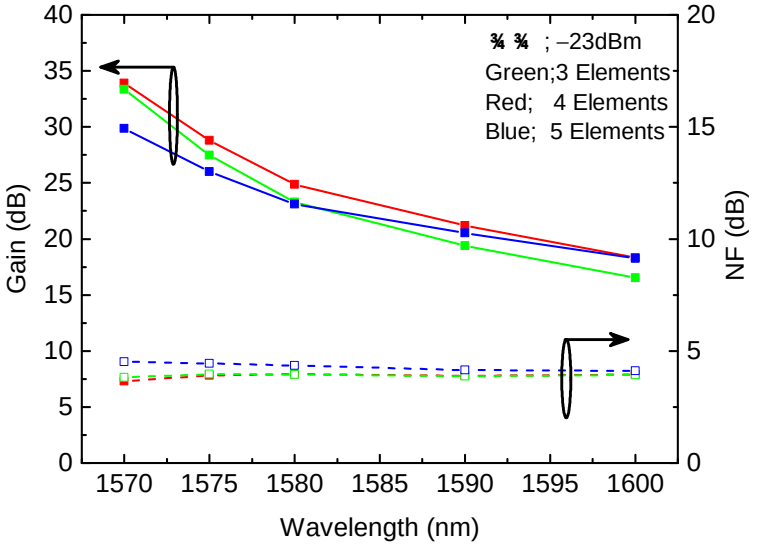

FIGURE 6.12: Gain and NF characteristics of different cascade configurations for bi-directional pumping with a total pump power of 320mW, input signal power: -23dBm

Similarly, the gain in the L-band was enhanced by cascading more fibre elements as shown in Fig 6.11 and Fig 6.12. It was observed that the available pump power was not sufficient to provide efficient gain for a cascade containing more than 2 fibre elements. The gain and NF characteristics of 4-element cascade of 7-MEF for the bi-directional pumping scheme with a total pump power of 320mW (forward pump power: 170mW, backward pump power: 150mW) were studied. A minimum gain of 20dB and NF less than 4dB were observed from 1580 to 1595nm with the input signal power of -23dBm as shown in Fig 6.12. It should be noted that a further increase in either forward or backward pump power did not improve the performance of the amplifier.

From Fig 6.11 and Fig 6.12 it can be observed that the gain was higher in the 4-element compared to the 3-element cascade at longer wavelengths. However, noticeable gain depreciation was observed when further cascading the fibre elements. For a 6-element cascade, the gain is 16±1dB in the wavelength range of 1580 to 1600nm. It was found that the 4-element cascade was optimal for efficient L-band amplification with a total pump power of 320mW.

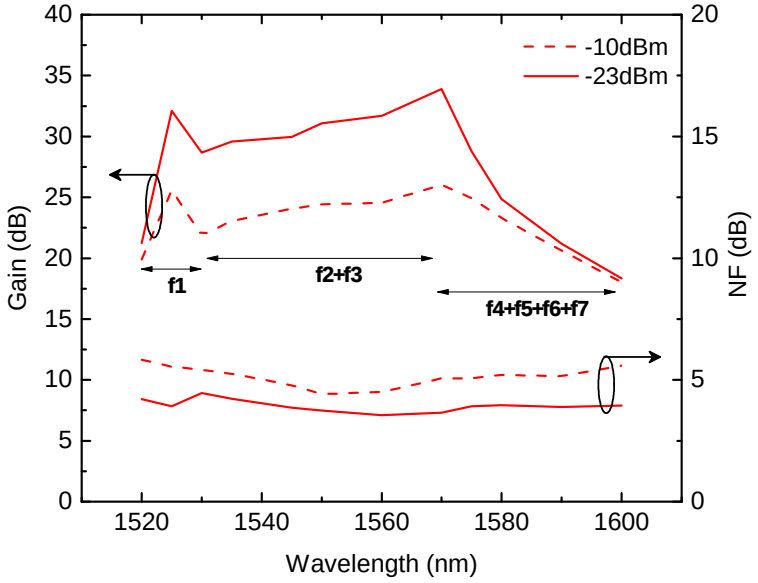

FIGURE 6.13: Performance of a split-band MEEDFA in the wavelength region of 1520 to 1600nm (Pump powers used: f1-250mW, f2+f3-250mW, f4+f5+f6+f7-320mW)

Our results indicate that a split-band multi-element Er-doped fibre amplifier (MEEDFA) can be configured by utilizing all the fibre elements. A single fibre element (f1) and a 2-element cascade (f2+f3) can be pumped single ended to cover the 1520-1530nm and 1530-1560nm wavelength regions, respectively. At the same time remaining 4-elements (f4+f5+f6+f7) can be cascaded and pumped bi-directionally for L-band amplification. The performance of the proposed amplifier is shown in Fig 6.13 for an input signal power of -10 and -23dBm. Such an amplifier provides at least 20dB gain starting from 1520 to 1595nm with a NF less than 6dB and 4.5dB for an input signal power of -10 and -23dBm, respectively.

6.2 Cladding-pumped Er/Yb-doped multi-element fibre amplifier for wideband applications

6.2.1 Introduction

We also followed another approach to demonstrate broadband amplifiers covering both C and L bands from a single amplifier using MEF in the cladding pumping configuration as shown in Fig 6.14. The fabrication of MEF for cladding pumping is briefly mentioned here. At first, a preform with Er/Yb-doped core was stretched and cut into 4 equal pieces. The four Er/Yb-doped rods were then stacked along with a coreless suprasil F-300 rod. The fibre was then drawn from the preform assembly which comprised a central coreless pump fibre element surrounded by four Er/Yb signal fibre elements. The MEF was coated with low-index polymer coating suitable for cladding pumping [153]. Each fibre element had a cladding diameter of 80μm, whereas the core diameter in signal fibre-elements was about 8μm (fabricated by S. Jain and T. C. May-Smith). The cladding absorption at a wavelength of 975nm was measured and found that it has variation between 2.2-4.1dB/m. The core absorption at wavelengths of 1536nm was measured and an element-to-element variation between 36-61dB/m was noticed. The microscope image of the 5-MEF cross-section is shown in the inset of Fig 6.14. The signal fibre elements were arbitrarily coded as F1, F2, F3 and F4, respectively, and the pump fibre element was coded as P. In cladding pumped MEFA, a single central multimode pump is shared by multiple Er/Yb-doped signal fibre elements which allow the amplifier to operate in a multiport configuration [153–155]. Moreover, the MEF based wideband amplifier can be developed either by using signal fibre elements with different Er/Yb-doping concentrations or by cascading the signal fibre elements. In cladding-pumped MEFA, the fibre length can be varied by cascading the signal fibre-elements, which allows better control on the amplifier performance. The cladding-pumped MEFA provides an advantage over conventional C+L split band EDFA through its potential for component sharing and thereby reduces the overall cost of the amplifier. A single high power, low brightness LD is enough to pump the cladding-pumped MEF and extract gain from all the four fibre elements instead of four separate LDs in core pumped configuration. Also no WDMs are required in case of cladding pumping configuration as the pump and signal are launched into different fibre elements. Here, we present a very brief study of the gain and noise figure (NF) characteristics of cladding-pumped MEFA [103].

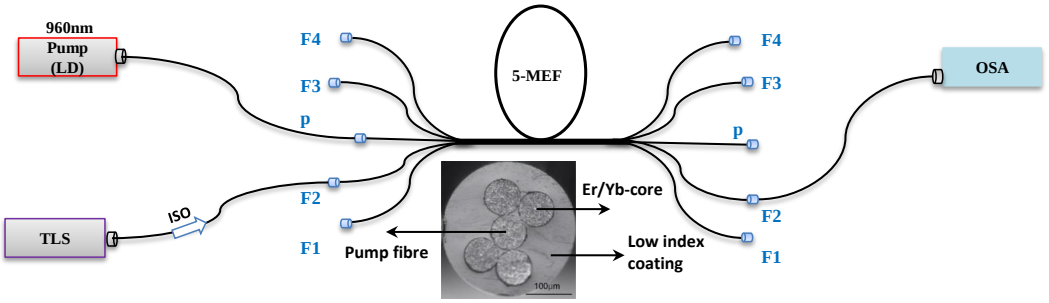

FIGURE 6.14: Schematic of experimental setup for gain and noise figure measurement (Inset shows the microscope image of the 5-MEF)

6.2.2 Experimental setup

The experimental setup to measure gain and NF in the signal fibre elements is shown in Fig 6.14. It comprised of a multi-mode pump laser diode (LD) operating at a wavelength of 960nm, a tunable laser source (TLS) operating in both C and L bands and an optical spectrum analyser (OSA). The signal fibre elements, in which cores are doped with Er/Yb, were separated at each end by simply removing the coating and then standard single mode fibres were spliced at the input/output of each of the fibre elements for efficient launch/extraction of the signal light. Also, a pump delivery fibre (105μm core and 125 μm cladding) was tapered to 80μm and spliced to the pump fibre element for efficient launching of the pump from the laser diode (characterization was done jointly with Saurabh Jain).

6.2.3 Results

Fibre No.	Gain/NF (dB) @ 1536nm	Gain/NF (dB) @ 1545nm	Gain/NF (dB) @ 1555nm
F1	35/11	36/10	29/8
F2	31/13	38/11	33/8
F3	34/11	35/9	28/8
F4	37/7	36/7	28/6

TABLE 6.1: Gain of different fibre elements in 6m 5-MEF at different wavelengths for a pump power of 6.4W, Input signal power;-23dBm

Initially, the gain and NF in different fibre elements of 5-MEF were measured. The gain characteristics of each fibre element were not similar due to element-to-element variation in core and clad absorption. A maximum gain of 37dB and corresponding NF of 7dB was achieved at 1536nm in F4 with an input signal power of -23dBm and for a

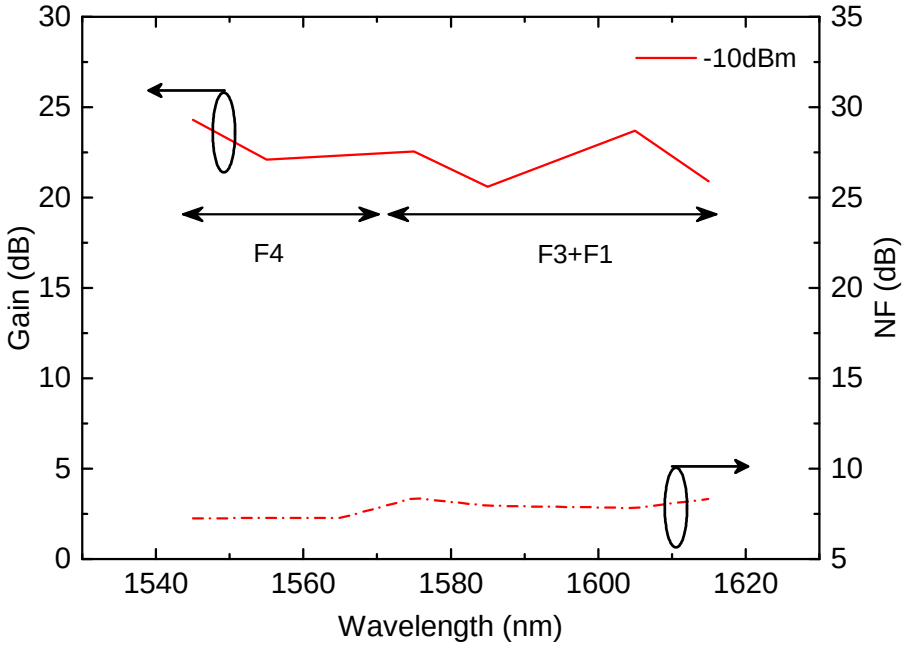

FIGURE 6.15: Performance of a split band MEFA with gain >20dB (1545-1615nm) using 12m MEF at 10W of pump power (-10dBm input signal)

pump power of 6.4W. Further, the gain was measured in 6m, 9m and 12m lengths of 5-MEF by 6.4W pump power for -10dBm of signal power, to shift the gain towards longer wavelength side. It was found that 6.4W of pump power is not enough to have gain values >10dB in the L-band using 12m length of 5-MEF. A maximum gain of >20dB was obtained from 1545-1565m with increased pump power of 10W using -10dBm of input signal power but the gain above 1570nm was <15dB. The fibre elements of 12m 5-MEF were then cascaded (F3+F1, F3+F1+F2) and measured the gain for -10dBm of input signal with a pump power of 10W. A gain of more than 20dB was achieved from 1570-1615nm [103]. A split-band cladding pumped MEFA has been proposed covering both C and L bands in which one of the fibre elements (F4) is operating in the C-band and other two elements (F3+F1) are cascaded to provide sufficient gain in the L-band. The performance of such an amplifiers is shown in Fig 6.15. A relatively flat gain of (22±1.5 dB) was achieved for -10dBm of input signal in 12m MEF with 10W of pump power from 1545-1615nm.

6.2.4 Conclusion

In conclusion, we considered MEF novel geometry to develop wideband amplifiers around 1550nm wavelength band. The feasibility of MEF geometry was proved by developing wideband amplifiers using 3-MEF and 7-MEFs. A gain of >20dB and NF ≤4.5dB in the wavelength region of 1520-1570nm was demonstrated using Er-doped 3-MEF amplifier.

It was also shown that, in case of cascaded configuration of the amplifier, the overall pump power required was significantly reduced through bi-directional pumping as compared to co-pumping while maintaining the similar gain characteristics. To further extend the bandwidth into L-band, gain and NF of 7-MEF are studied and a wideband MEEDFA was demonstrated, in which each fibre element provided a maximum gain of 37dB and a NF less than 4.5dB, with the pump power of 250mW and for an input signal power of -23dBm. A split-band MEEDFA configuration was proposed, which enabled the MEEDFA to provide wideband amplification covering a 75nm bandwidth (1520-1595nm) with gain of $\geq$20dB.

Further, taking the advantage of novel MEF geometry and cladding pumping configuration to reduce the cost of the amplifier by sharing the components a MEF based Er/Yb-doped cladding pumped amplifier has been demonstrated for a wideband operation covering both C and L band. A maximum gain of 37dB and corresponding NF of 7.3dB in the C-band has been obtained in one of the fibre elements for the MEF length of 6m at 6.4W of pump power and -23dBm of the input signal. We have also investigated the cladding pumped MEFA performance for different fibre length, pump power, and cascading configuration. A relatively flat gain of 22$\pm$1.5dB has been achieved across the wavelength band of 1545-1615nm. The performance of the broadband amplifiers can be further improved by tailoring the doping concentration and fibre design of MEF elements hence further extend the bandwidth of MEEDFA both into S and L bands.

Chapter 7

Conclusions and future scope

7.1 Bi-doped fibres for lasers and amplifiers

7.1.1 Introduction

In this chapter, I will give a brief overview of the work we were discussing in this thesis and present my thoughts towards extending it further. Here, we fabricated Bi-doped fibres with aluminosilicate and phosphosilicate hosts to develop amplifiers and lasers in the wavelength band from 1150-1500nm. Effect of unsaturable loss was considered as a critical factor for the poor performance of Bi-doped fibres and efforts were made to reduce it by optimising the fabrication conditions and pump wavelengths to improve the performance of amplifiers and lasers. Also, the experimental setups were designed to be compact using commercially available laser diodes as pump sources.

Fabricated Bi-doped aluminosilicate fibres were used to demonstrate amplifier at 1180nm. Both 1047 and 1120nm pump wavelengths were considered to study the performance of the amplifier. A 70% improvement in gain was reported with 1120nm pumping compared to 1047nm. Further bi-directional pumping scheme was implemented employing 1120 and 1047nm lasers to increase the gain. A 12dB maximum gain at 1180nm with bi-directional pumping was reported. The less improved gain with bi-directional pumping was attributed to the high unsaturable loss measured at 1047nm pump wavelength. A conclusive suggestion was made based on the results that instead of 1047nm in combination with 1120nm in a bi-directional scheme, a 1120nm pump can improve the gain performance of the amplifier further.

To develop amplifiers and lasers in the O-band, Bi-doped phospshosilicate fibres were fabricated. The effect of fabrication conditions on absorption and unsaturable loss were

studied. Fibre with low UL was selected to develop efficient amplifiers and lasers around 1330nm, suitable for use in optical fibre communication. Initially, the laser efficiency of fabricated fibres was studied in a ring cavity configuration. The performance of the efficient fibre was optimised by measuring the efficiency with different length of the Bi-doped fibre and for different output coupling ratio. A 22mW fibre laser operating at 1360nm with a slope efficiency of 11% was reported with 1267nm pumping using an optimum 50-50 coupling ratio in a 50m long Bi-doped fibre [122]. The efficiency of the laser was further improved by optimising the fibre parameters and also using bi-directional pumping configuration. A laser with an output power of 110mW with a slope efficiency of 18% was reported.

The Bi-doped fibre with an optimum laser performance was also used to develop an amplifier from 1300-1360nm. Gain performance of the amplifier with 1210, 1240, and 1267nm pump wavelengths was studied and showed that the combination of 1240 and 1267nm pumping can flatten the gain from 1320-1360nm. A flat gain amplifier with a 25dB gain with a gain variation of $\pm$1dB was reported for a signal power of -10dBm. The gain of the amplifier was further increased to 29dB for -30dBm of input signal power.

Later, we optimised the fabrication process to increase the concentration of Bi in the fibre so that the lasing and amplification can be achieved in a short length of the Bi-doped fibre. These high concentration Bi-doped fibres are required to develop pulsed fibre lasers and also for cladding-pumped fibre lasers. One of the fabricated fibres with low unsaturable loss, and efficient lasing performance in a minimum 10m length of Bi-doped fibre was used to develop a mode-locked fibre laser operating at 1340nm.

A simple ring cavity was used to construct the laser and a polarisation controller was used to enable the mode-locking. Effect of fibre length and pump power on pulse width was studied. A 25m length of the fibre was found to be an optimum length to have a minimum pulse width of 1.5ns at the lasing threshold. A pulse width variation from 1.5ns to 3ns was observed with the increase of pump power. Kelly sidebands in the optical spectrum were noticed and it was concluded that the cavity dispersion was in the anomalous regime and the mode-locking operation is in soliton regime. The Fourier transform limited pulse width was calculated from the measured optical spectrum and found to be 1ps. The observed larger pulse width of 1.5ns was attributed to the soliton bunching. Due to the low average output power of ML-BDFL which is of 3mW, we developed a master oscillator power amplifier (MOPA) to increase the output power levels and to study the autocorrelation spectra of the mode-locked laser. A different fibre with high gain was used to develop the amplifier. An input power of 2.5mW with a pulse width of 3ns was injected into the amplifier. The performance of the MOPA with pump power and input signal power was reported. An output signal power of

the ML-BDFL was increased to 18mW after passing through the amplifier without any distortions in the optical spectrum. A pedestal in the measured autocorrelation spectra was noticed which is a signature of soliton bunching. The measured autocorrelation spectra indicated a true pulse width of 1ps.

We also worked towards the development of broadband Er-doped fibre amplifiers in the 1550nm wavelength band using novel multi-element fibre geometry which is developed at ORC, University of Southampton, UK. MEF consists of multiple fibre elements under a common coating. The fibre elements can be accessed by removing the coating of MEF. A conventional amplifier setup was used to develop the broadband amplifier using Er-doped 3 and 7-MEF (3, 7-fibre elements under common coating) as an active media. The fibre elements were cascaded to shift the amplifier gain towards longer wavelength, therefore, improving the gain at long wavelength region. A minimum gain of 20dB was demonstrated from 1520-1595nm in a split band configuration [156].

Further, we also shown a broadband cladding pumped MEF amplifier. The MEF for cladding pumping configuration consists of 5-elements in which one of the elements being a pump guiding passive fibre whereas remaining four elements were doped with Er/Yb. The pump light which is guided in the passive element will couple to the signal elements as it passes along the length of the fibre and leads to amplification of the signal. A conventional amplifier setup was used to study the gain and NF characteristics of the amplifier. The advantage of cladding pump configuration is component sharing and hence reduced the cost of the developed amplifier. A gain of more than 20dB was demonstrated from 1545 to 1615nm by optimising the length and pump power [103].

7.1.2 Future scope

The field of Bi-doped fibres for lasers and amplifiers come a long way in terms of fabricating these fibres and also to demonstrate lasers and amplifiers using the fabricated Bi-doped fibres. The MCVD-solution doping technique which is used to fabricate Bi-doped fibres is well known over the years to incorporate RE-dopant into the fibre core. The same method is also used to introduce Bi-dopant in different host materials such as aluminosilicate, phosphosilicate and germanosilicate to access the wavelength band from 1150-1800nm for lasers and amplifiers. Even though it is easy to introduce Bi-dopant in the core by using MVCD-solution doping technique the reaction process in forming Bi active centres is completely depends on the process parameters such as temperature and atmospheric conditions and the amount of Bi introduced in the fibre core. The reason for this is the complicated chemistry involved with Bi. So far the Bi concentration used in fibre is relatively low for laser and amplifier demonstrations. The low Bi-concentration

leads to longer device length (10's of meters). The increased amount of Bi in the core introduces unwanted losses such as unsaturable loss (UL) and excited state absorption (ESA) which are detrimental to laser and amplifier performance. Fabrication of high concentration Bi-doped fibres with low UL and ESA will lead to construct lasers and amplifiers with short length. In this thesis, we made significant efforts to optimize the fabrication conditions and to develop high concentration fibres while not compromising with the UL and ESA. One of the developed fibres has 16% UL and lasing in 10m length of an active Bi-doped fibre. These fibres were important to develop pulsed fibre lasers and cladding-pumped fibre lasers. One can further optimise the process to improve these fibres to increase the concentration further and to reduce the UL and ESA.

There are many other challenges, one of them is to find out the active state in Bi-doped fibres that is causing IR luminescence. Many hypotheses were reported based on the experimental facts but none of them confirmed all the properties seen in Bi-doped fibres. By knowing the active state of Bi it is easy to optimize the fabrication conditions and to develop efficient fibres for lasers and amplifiers. Researchers have to come forward to solve this problem which if resolved can revolutionize the field of next-generation Bi-doped fibre lasers and amplifiers.

Another one is the requirement of high pump power laser diodes in absorption bands of Bi-doped fibres. At present, the available laser diodes are still limited to half a Watt. As the available pump powers offered by laser diodes are low dual pumping is the only option to achieve high pump powers using laser diodes as pump sources. High power laser diodes in the absorption bands of Bi-doped fibres can lead to compact experimental setups to develop lasers and amplifiers. The passive components such as WDMS, isolators, circulators etc., are not available off the shelf in the Bi-doped emission wavelength bands. This leads to custom made components to be ordered and most of the time doesn't meet the required specifications.

One can study the above mentioned challenges in general to mature the field of Bi-doped fibre lasers and amplifiers. Below I gave my thoughts towards future work one can perform in advancing the area of Bi-doped fibre lasers and amplifiers.

Development of high gain (>20dB) amplifiers around 1180nm wavelength using efficient Bi-doped aluminosilicate fibres

At present, a maximum gain of 12dB was demonstrated at 1180nm [121]. Further improvements of gain values are necessary for applications such as laser guide star and visible lasers. By improving the preform fabrication with new precursors, solvents and by optimizing the atmosphere conditions and temperatures during preform fabrication one can develop efficient Bi-doped fibre lasers and amplifiers around 1180nm. UL and ESA are very important factors one need to focus when working with Bi-doped aluminosilicate

fibres. In this thesis we reduced UL and ESA by pump optimization. One can develop novel experimental techniques to reduce UL and ESA to improve the performance of Bi-doped fibre amplifiers and lasers.

Extend the amplification band of current Bi-doped fibres to cover complete band from 1280-1500nm by improving the fabrication of these fibres with phosphorous and germanium hosts

We demonstrated a Bi-doped fibre amplifier covering 1300-1360nm with a flat gain of 25±1dB in 40nm bandwidth [133]. The amplification bandwidth offered by these fibres can be extended further by studying them with different host material and by optimising the fabrication. In this thesis we only used phosphosilicate host to develop Bi-doped lasers and amplifiers in the O-band. It is possible to extend this wavelength band further up to 1500nm by studying the phosphogermanosilicate host to fabricate Bi-doped fibres. This can allow one to access the complete 1280-1500nm band for optical fibre communication.

It is well known that the gain of Er-doped fibre amplifiers are polarization independent. To the best of my knowledge there are no studies reported on polarization dependent gain characteristics of Bi-doped fibres. This kind of study can be performed in future as the main application of Bi-doped fibre amplifiers are for extended optical fibre communication.

Development of efficient Bi-doped germanosilicate fibres with high germania concentration to extend the Bi amplification band to longer wavelength side around 1700nm covering the gap between the erbium and thulium-doped fibre amplifiers

In recent studies, it was realized that by using Bi-doped fibres with high germania concentration (50mol%) it is possible to demonstrate lasers and amplifiers around 1700nm wavelength band [12]. The application of lasers and amplifiers developed in this wavelength band (1600-1800nm) are in medicine, sensing, military and telecommunications. Bi-incorporation in germanosilicate host with low GeO_2 content form Bi-related active centres associated with silicon (BACs-Si) with emission peak around 1450nm, whereas when increased the GeO_2 content to 50mol% it will form Bi-related active centres associated with germanium (BACs-Ge) with emission peak around 1700nm. The alternative techniques to produce 1700nm radiation is by using Tm-doped fibres. Tm-doped silica fibre gain bandwidth covers this wavelength band, but complex amplified spontaneous emission (ASE) suppression schemes at longer wavelengths are necessary to achieve high gain values ≤1700nm. Hence, Bi-doped germanosilicate fibres with high germania concentration can be a good candidate to offer the gain values of 30dB around 1700nm wavelength band without any complex ASE suppression methods. On the other hand

the required length in case of Bi-doped fibres is higher compared to Tm-doped fibres because of low Bi-concentration [100].

Cladding pumped Bi-doped fibre lasers for power scaling

Power scaling through cladding pumping was realised in rare earth dopants such as erbium, ytterbium, thulium and Holmium to achieve kilowatt (kW) power levels. Similar concepts can be applied to Bi-doped fibres for power scaling. However, the core absorption per unit length of current Bi-doped fibres is low. In order to implement the cladding pumping technique development of high Bi-concentration fibres with high gain are essential.

Study the Bi-doped pulsed fibre lasers and understand the underlying phenomenon

The wideband emission observed in Bi-doped fibres is a unique property useful for ultrafast fibre lasers. Especially, development of mode-locked fibre lasers around 1.3μm wavelength band is important for optical communication in the second telecommunication window [157]. Even after 10 years of first pulsed Bi-doped fibre laser demonstration, the pulse dynamics in Bi-doped fibres have not yet well understood. Systematic study needs to be performed to understand the underlying phenomenon. Various studies reported the soliton bunching formation in the anomalous dispersion regime of the cavity in Bi-doped pulsed fibre lasers. One has to optimise the dispersion and pump powers to avoid the formation of soliton bunching. Also it is possible to develop tunable pulsed fibre lasers using Bi-doped fibres as they have broad gain spectrum.

Establish proof of concept of O-band WDM optical fibre communication experiments

Extending the bandwidth is important to further increase the capacity of optical fibre communication link.The low water peak fibres with loss values of less than 0.4dB/km in the wavelength band from 1260-1625nm are of great advantage to extend the bandwidth. Due to the limited bandwidth of Er-doped fibres it is not possible to use this low loss window for optical fibre communication. Development of Bi-doped fibre amplifiers paved the way to open up the O-band by using the low water peak fibres offered by Corning or Lucent technologies. For example, The loss of Corning SMF 28e fibre was 0.32dB/km from 1300-1360nm. If we consider an input signal power of 10dBm, after travelling through the SMF 28e over a distance of 62.5km the output signal will be -10dBm with an induced loss of 20dB. If we use a Bi-doped fibre amplifier that we developed after the 62.5km SMF 28e we can amplify the -10dBm signal to approximately 25dB for an output signal of 15dBm. The 15dBm signal can be transmitted further to a distance of 31km to achieve an output signal of 5dBm. This way one can establish a communication link in the O-band. The other advantage of our amplifier is, it has flat gain within 40nm

bandwidth which is important when it is required to send the signals over CWDM or DWDM along the transmission link. This kind of experiments can show the importance of Bi-doped fibre amplifier to extend the optical fibre communication bandwidth.

7.2 MEF fibres for broadband amplifiers

7.2.1 Introduction

We opted the MEF to study the feasibility of its geometry to develop broadband fibre amplifiers covering both C and L bands. 3-MEF and 7-MEF fibres were characterised for gain and NF and demonstrated amplifiers in the wavelength range from 1520-1595nm. Further, a cladding-pumped configuration was used to study the 5-MEF which helps to reduce the required number of components compared to core pump configuration. A cladding-pumped MEF amplifier covering the wavelength band from 1545-1615nm with more than 20dB gain was demonstrated.

7.2.2 Future scope

In future, one can incorporate thulium and holmium as a dopant in MEFs and study the gain and NF characteristics to tailor the gain in the wavelength band from 1700-2200nm. The dopant concentration and fibre design of each element in MEF can be varied according to the required gain characteristics.

Appendix A

Publications

A.1 Journal Publications

1. **N. K. Thipparapu**, S. Jain, T. C. May-Smith, J. K. Sahu, *Wideband multi-element Er-doped fiber amplifier*, Laser Physics Letters 2014 Vol.11(9) pp.095104

2. S. Jain, **N. K. Thipparapu**, P. Barua, J. K. Sahu, *Cladding-pumped Er/Yb-doped multi-element fiber amplifier for wideband applications*, IEEE Photonics Technology Letters 2015 Vol.27(4) pp.356-358

3. **N. K. Thipparapu**, S. Jain, A. A. Umnikov, P. Barua, J. K. Sahu, *1120nm diode-pumped Bi-doped fiber amplifier*, Optics Letters 2015 Vol.40(10) pp.2441-2444

4. **N. K. Thipparapu**, A. A. Umnikov, P. Barua, J. K. Sahu, *Bi-doped fiber amplifier with a flat gain of 25dB operating in the wavelength band 1320-1360nm*, Optics Letters 2016 Vol.41(7) pp.1518-1521

5. **N. K. Thipparapu**, C. Guo, A. A. Umnikov, P. Barua, A. Taranta, and J. K. Sahu, *Bismuth-doped all fiber mode-locked laser operating at 1340nm"*, Optics Letters 2018 Vol.42(24) pp.5102-5105

A.2 Conference publications

1. J. K. Sahu, S. Jain, D. Jain, **N. K. Thipparapu**, T. C. May-Smith, *Novel geometry fibres for use in optical communications and high power lasers*, Sixth International Conference on Optical, Optoelectronic and Photonic Materials and Applications (ICOOPMA-2014), Leeds 27-31 Jul 2014 (Invited)

2. **N. K. Thipparapu**, S. Jain, T. C. May-Smith, J. K. Sahu, *Configurable Er-doped core-pumped multi-element fiber amplifier*, OECC/ACOFT-2014, Melbourne 6-10 Jul 2014

3. S. Jain, **N. K. Thipparapu**, P. Barua, J. K. Sahu, *Multi-element fiber for next generation optical communication*, IEEE 5th International Conference on Photonics (ICP), Kuala Lumpur, 2-4 Sep 2014 (Invited)

4. **N. K. Thipparapu**, S. Jain, A. A. Umnikov, P. Barua, J. K. Sahu, *1180nm Bi-doped aluminosilicate fiber amplifier*, CLEO/Europe 2015, Munich, 21-25 Jun 2015

5. **N. K. Thipparapu**, S. Jain, A. Umnikov, P. Barua, J. K. Sahu, *Progress towards development of efficient Bi-doped fiber lasers and amplifiers*, Siegman International School on Lasers, Amberg, Germany, 2-7 Aug 2015

6. **N. K. Thipparapu**, A. Umnikov, S. Jain, B. Pranabesh, J. K. Sahu, *Diode pumped Bi-doped fiber laser operating at 1360nm*, 4th Workshop on Specialty Optical Fibers and Their Applications (WSOF-2015), Hong Kong, 4-6 Nov 2015

7. J. K. Sahu, **N. K. Thipparapu**, A. Umnikov, P. Barua, *Progress towards efficient Bi fiber lasers and amplifiers*, The 24th international congress on glass, Shangai, 7-11 Apr 2016 (Invited)

8. **N. K. Thipparapu**, A. Umnikov, P. Barua, M. Nunez Velazquez, J. K. Sahu, *A review on our latest amplifier and laser demonstrations by Bi-doped fibers*, International Training School on Fiber Lasers and Optical Fiber Technology, Prague, 30 Aug-1 Sep 2016

9. **N. K. Thipparapu**, A. Umnikov, P. Barua, M. Nunez Velazquez, J. K. Sahu, *Bi-doped fiber amplifiers: optical properties, challenges and applications*, XXIst International Summer School Krutyn, Poland, 4-10 Sep 2016

10. J. K. Sahu, **N. K. Thipparapu**, A. A. Umnikov, P. Barua and M. Nunez Velazquez, *Amplifier and laser demonstrations in Bi-doped silica optical fibers*, Fiber Optics and Photonics-2016, Kanpur, 4-8 Dec 2016 (Invited)

11. J. K. Sahu, **N. K. Thipparapu**, A. A. Umnikov, P. Barua, and C. Guo , *Bismuth-doped all-fiber lasers and amplfiers: recent advances and future perspectives* , CLEO-Pacific Rim 2017, Singapore, 31 July - 4 Aug 2017 (Invited)

12. **N. K. Thipparapu**, C. Guo, A. A. Umnikov, P. Barua, A. Taranta, S. Alam, and J. K. Sahu, *Self-mode-locked Bismuth-doped Fiber Laser Operating at 1340nm*, CLEO/Europe 2017, Munich, 25-29 Jun 2017

13. **N.K.Thipparapu**, C. Guo, A. Umnikov, P. Barua, A. Taranta, R. Standish and J. Sahu, *Bi-doped fibre lasers and wideband amplifiers in the 1150-1500nm band*, Beyond state of the art optical communications, London, 2 Jun 2017

Bibliography

[1] K. Kao and G. A. Hockham, "Dielectric fibre surface waveguides for optical frequencies," in *Proceedings of the Institution of Electrical Engineers*, vol. 113, no. 7. IET, 1966, pp. 1151–1158.

[2] F. Kapron, D. Keck, and R. Maurer, "Radiation losses in glass optical waveguides," *Applied Physics Letters*, vol. 17, no. 10, pp. 423–425, 1970.

[3] OFS. All Wave One Fiber-Zero Water Peak. [Online]. Available: http://http://fiber-optic-catalog.ofsoptics.com/Asset/AllWave-One-Fiber-160-web.pdf

[4] T. Miya, Y. Terunuma, T. Hosaka, and T. Miyashita, "Ultimate low-loss single-mode fibre at 1.55μm," *Electronics Letters*, vol. 15, no. 4, pp. 106–108, 1979.

[5] R. J. Mears, L. Reekie, I. Jauncey, and D. N. Payne, "Low-noise erbium-doped fibre amplifier operating at 1.54μm," *Electronics Letters*, vol. 23, no. 19, pp. 1026–1028, 1987.

[6] D. Richardson, J. Fini, and L. Nelson, "Space-division multiplexing in optical fibres," *Nature Photonics*, vol. 7, no. 5, pp. 354–362, 2013.

[7] Internet use reaches 5 billion worldwide. [Online]. Available: http://www.futuretimeline.net/21stcentury/2020.htm#internet-2020

[8] L. Technologies. All Wave Single Mode Optical Fiber. [Online]. Available: https://www.usbid.com/datasheets/usbid/2000/2000-q3/5822-3.pdf

[9] L. Dong and B. Samson, *Fiber Lasers: Basics, Technology, and Applications*. CRC Press, 2016.

[10] P. C. Becker, A. A. Olsson, and J. R. Simpson, *Erbium-doped fiber amplifiers: fundamentals and technology*. Academic press, 1999.

[11] I. Bufetov and E. Dianov, "Bi-doped fiber lasers," *Laser Physics Letters*, vol. 6, no. 7, p. 487, 2009.

[12] S. Firstov, S. Alyshev, M. Melkumov, K. Riumkin, A. Shubin, and E. Dianov, "Bismuth-doped optical fibers and fiber lasers for a spectral region of 1600–1800nm," *Optics letters*, vol. 39, no. 24, pp. 6927–6930, 2014.

[13] S. Firstov, V. Khopin, I. Bufetov, E. Firstova, A. Guryanov, and E. Dianov, "Combined excitation-emission spectroscopy of bismuth active centers in optical fibers," *Optics express*, vol. 19, no. 20, pp. 19 551–19 561, 2011.

[14] E. M. Dianov, "Bismuth-doped optical fibers: a challenging active medium for near-IR lasers and optical amplifiers," *Light: Science and Applications*, vol. 1, p. e12, 2012.

[15] E. Dianov, "Fiber for fiber lasers: Bismuth-doped optical fibers: Advances in an active laser media," *Laser Focus World*, 2015.

[16] I. Bufetov, S. L. Semenov, V. V. Vel'miskin, S. V. Firstov, G. A. Bufetova, and E. M. Dianov, "Optical properties of active bismuth centres in silica fibres containing no other dopants," *Quantum Electronics*, vol. 40, no. 7, p. 639, 2010.

[17] Griscom and D. L, "Optical properties and structure of defects in silica glass," *Journal of the Ceramic Society of Japan*, vol. 99, no. 1154, pp. 923–942, 1991.

[18] M. Neff, V. Romano, and W. Lüthy, "Metal-doped fibres for broadband emission: Fabrication with granulated oxides," *Optical materials*, vol. 31, no. 2, pp. 247–251, 2008.

[19] I. Razdobreev, H. El Hamzaoui, V. Y. Ivanov, E. Kustov, B. Capoen, and M. Bouazaoui, "Optical spectroscopy of bismuth-doped pure silica fiber preform," *Optics letters*, vol. 35, no. 9, pp. 1341–1343, 2010.

[20] A. S. Zlenko, V. M. Mashinsky, L. D. Iskhakova, S. L. Semjonov, V. V. Koltashev, N. M. Karatun, and E. M. Dianov, "Mechanisms of optical losses in Bi: SiO2 glass fibers," *Optics express*, vol. 20, no. 21, pp. 23 186–23 200, 2012.

[21] S. V. Firstov, V. F. Khopin, V. V. Velmiskin, E. G. Firstova, I. A. Bufetov, A. N. Guryanov, and E. M. Dianov, "Anti-stokes luminescence in bismuth-doped silica and germania-based fibers," *Optics express*, vol. 21, no. 15, pp. 18 408–18 413, 2013.

[22] V. Neustruev, "Colour centres in germanosilicate glass and optical fibres," *Journal of Physics: Condensed Matter*, vol. 6, no. 35, p. 6901, 1994.

[23] Y. Arai, T. Suzuki, and Y. Ohishi, "Spectroscopic properties of bismuth-doped silicate glasses for ultra-broadband near-infrared gain media," *Glass Technology-European Journal of Glass Science and Technology Part A*, vol. 51, no. 2, pp. 86–88, 2010.

[24] L. Bulatov, V. Mashinsky, V. Dvoyrin, and A. Sukhorukov, "Spectroscopic study of bismuth centers in aluminosilicate optical fibers," *Journal of radio electronics*, no. 3, pp. 1–19, 2009.

[25] Y. Fujimoto and M. Nakatsuka, "Infrared luminescence from bismuth-doped silica glass," *Japanese Journal of Applied Physics*, vol. 40, no. 3B, p. L279, 2001.

[26] X. g. Meng, J. r. Qiu, M. y. Peng, D. p. Chen, Q. z. Zhao, X. w. Jiang, and C. s. Zhu, "Near infrared broadband emission of bismuth-doped aluminophosphate glass," *Optics Express*, vol. 13, no. 5, pp. 1628–1634, 2005.

[27] J. Ren, L. Yang, J. Qiu, D. Chen, X. Jiang, and C. Zhu, "Effect of various alkaline-earth metal oxides on the broadband infrared luminescence from bismuth-doped silicate glasses," *Solid state communications*, vol. 140, no. 1, pp. 38–41, 2006.

[28] S. Khonthon, S. Morimoto, Y. Arai, and Y. Ohishi, "Luminescence characteristics of Te-and Bi-doped glasses and glass-ceramics," *Journal of the Ceramic Society of Japan*, vol. 115, no. 1340, pp. 259–263, 2007.

[29] V. Sokolov, V. Plotnichenko, and E. Dianov, "Origin of broadband near-infrared luminescence in bismuth-doped glasses," *Optics letters*, vol. 33, no. 13, pp. 1488–1490, 2008.

[30] B. Denker, B. Galagan, V. Osiko, I. Shulman, S. Sverchkov, and E. Dianov, "The IR emitting centers in Bi-doped Mg-Al-Si oxide glasses," *Laser physics*, vol. 19, no. 5, pp. 1105–1111, 2009.

[31] M. Y. Sharonov, A. B. Bykov, V. Petricevic, and R. R. Alfano, "Spectroscopic study of optical centers formed in Bi-, Pb-, Sb-, Sn-, Te-, and In-doped germanate glasses," *Optics letters*, vol. 33, no. 18, pp. 2131–2133, 2008.

[32] G. Lakshminarayana, R. Yang, M. Mao, Y. Zhang, and J. Qiu, "Spectral analysis of optical centres formed in Bi-, Bi/Yb-, Pb-, Pb/Yb-, Sb-, Sb/Yb-and Sn-, Sn/Yb-co-doped germanate glasses," *Journal of Physics D: Applied Physics*, vol. 42, no. 14, p. 145108, 2009.

[33] M. Peng, G. Dong, L. Wondraczek, L. Zhang, N. Zhang, and J. Qiu, "Discussion on the origin of nir emission from Bi-doped materials," *Journal of Non-Crystalline Solids*, vol. 357, no. 11, pp. 2241–2245, 2011.

[34] V. Sokolov, V. Plotnichenko, and E. Dianov, "The origin of near-IR luminescence in bismuth-doped silica and germania glasses free of other dopants: First-principle study," *Optical Materials Express*, vol. 3, no. 8, pp. 1059–1074, 2013.

[35] E. M. Dianov, "On the nature of near-IR emitting Bi centres in glass," *Quantum Electronics*, vol. 40, no. 4, p. 283, 2010.

[36] A. Witkowska, J. Rybicki, J. Bosko, and S. Feliziani, "A molecular dynamics study of lead-bismuth-silicate glasses," *IEEE Transactions on Dielectrics and Electrical Insulation*, vol. 8, no. 3, pp. 385–389, 2001.

[37] X. g. Meng, J. r. Qiu, M. y. Peng, D. p. Chen, Q. z. Zhao, X. w. Jiang, and C. s. Zhu, "Infrared broadband emission of bismuth-doped barium-aluminum-borate glasses," *Optics express*, vol. 13, no. 5, pp. 1635–1642, 2005.

[38] M. Peng, J. Qiu, D. Chen, X. Meng, and C. Zhu, "Superbroadband 1310 nm emission from bismuth and tantalum codoped germanium oxide glasses," *Opt. Lett.*, vol. 30, no. 18, pp. 2433–2435, Sep 2005.

[39] M. Y. Sharonov, A. B. Bykov, V. Petricevic, and R. R. Alfano, "Spectroscopic study of optical centers formed in Bi-, Pb-, Sb-, Sn-, Te-, and In-doped germanate glasses," *Opt. Lett.*, vol. 33, no. 18, pp. 2131–2133, Sep 2008.

[40] V. Truong, L. Bigot, A. Lerouge, M. Douay, and I. Razdobreev, "Study of thermal stability and luminescence quenching properties of bismuth-doped silicate glasses for fiber laser applications," *Applied Physics Letters*, vol. 92, no. 4, p. 041908, 2008.

[41] M. Peng, B. Wu, N. Da, C. Wang, D. Chen, C. Zhu, and J. Qiu, "Bismuth-activated luminescent materials for broadband optical amplifier in WDM system," *Journal of Non-Crystalline Solids*, vol. 354, no. 12, pp. 1221–1225, 2008.

[42] V. Sokolov, V. Plotnichenko, V. Koltashev, and E. Dianov, "Centres of broadband near-IR luminescence in bismuth-doped glasses," *Journal of Physics D: Applied Physics*, vol. 42, no. 9, p. 095410, 2009.

[43] J. Wu, D. Chen, X. Wu, and J. Qiu, "Ultra-broad near-infrared emission of Bi-doped SiO2/Al2O3/GeO2 optical fibers," *Chin. Opt. Lett.*, vol. 9, no. 7, pp. 071 601–071 601, Jul 2011.

[44] B. I. Galagan, B. I. Denker, L. Hu, S. E. Sverchkov, I. L. Shulman, and E. M. Dianov, "Effect of variable valence impurities on the formation of bismuth-related optical centres in a silicate glass," *Quantum Electronics*, vol. 42, no. 10, p. 940, 2012.

[45] A. N. Romanov, Z. T. Fattakhova, A. A. Veber, O. V. Usovich, E. V. Haula, V. N. Korchak, V. B. Tsvetkov, L. A. Trusov, P. E. Kazin, and V. B. Sulimov, "On the origin of near-IR luminescence in Bi-doped materials (ii). subvalent monocation Bi+ and cluster Bi53+ luminescence in AlCl 3/ZnCl 2/BiCl3 chloride glass," *Optics express*, vol. 20, no. 7, pp. 7212–7220, 2012.

[46] I. Razdobreev, H. E. Hamzaoui, V. B. Arion, and M. Bouazaoui, "Photoluminescence in Ga/Bi co-doped silica glass," *Opt. Express*, vol. 22, no. 5, pp. 5659–5674, Mar 2014.

[47] B. Denker, B. Galagan, V. Osiko, I. Shulman, S. Sverchkov, and E. Dianov, "Factors affecting the formation of near infrared-emitting optical centers in Bi-doped glasses," *Applied Physics B: Lasers and Optics*, vol. 98, no. 2, pp. 455–458, 2010.

[48] M. A. Hughes, R. M. Gwilliam, K. Homewood, B. Gholipour, D. W. Hewak, T.-H. Lee, S. R. Elliott, T. Suzuki, Y. Ohishi, T. Kohoutek *et al.*, "On the analogy between photoluminescence and carrier-type reversal in Bi-and Pb-doped glasses," *Optics express*, vol. 21, no. 7, pp. 8101–8115, 2013.

[49] W. Fan, L. Htein, B. H. Kim, P. R. Watekar, and W. T. Han, "Upconversion luminescence in bismuth-doped germano-silicate glass optical fiber," *Optics & Laser Technology*, vol. 54, pp. 376–379, 2013.

[50] I. A. Bufetov, M. A. Melkumov, S. V. Firstov, K. E. Riumkin, A. V. Shubin, V. F. Khopin, A. N. Guryanov, and E. M. Dianov, "Bi-doped optical fibers and fiber lasers," *IEEE Journal of Selected Topics in Quantum Electronics*, vol. 20, no. 5, pp. 111–125, 2014.

[51] E. Dianov, "Fiber for fiber lasers: Bismuth-doped optical fibers: Advances in an active laser media," *Laser Focus World*, vol. 16, 2015.

[52] D. Evgeny, "Nature of bi-related near IR active centers in glasses: state of the art and first reliable results," *Laser Physics Letters*, vol. 12, no. 9, p. 095106, 2015.

[53] S. Firstov, S. Alyshev, V. Khopin, M. Melkumov, A. Guryanov, and E. Dianov, "Photobleaching effect in bismuth-doped germanosilicate fibers," *Opt. Express*, vol. 23, no. 15, pp. 19 226–19 233, Jul 2015.

[54] S. Colin, E. Contesse, P. Le Boudec, G. Stephan, and F. Sanchez, "Evidence of a saturable-absorption effect in heavily erbium-doped fibers," *Optics letters*, vol. 21, no. 24, pp. 1987–1989, 1996.

[55] S. Firstov, V. Khopin, F. Afanasev, A. Khegai, S. Alyshev, K. Riumkin, N. Vechkanov, A. Abramov, M. Melkumov, A. Guryanov, and E. Dianov, "Unsaturable absorption in various Bi-doped optical fibers," *26th Annual International Laser Physics Workshop*, 2017.

[56] M. P. Kalita, S. Yoo, and J. Sahu, "Bismuth doped fiber laser and study of unsaturable loss and pump induced absorption in laser performance," *Optics express*, vol. 16, no. 25, pp. 21 032–21 038, 2008.

[57] R. Laming, S. Poole, and E. Tarbox, "Pump excited-state absorption in Er-doped fibres," *Optics Letters*, vol. 13, pp. 1084–1086, 1988.

[58] S. Yoo, M. P. Kalita, J. Nilsson, and J. Sahu, "Excited state absorption measurement in the 900-1250 nm wavelength range for bismuth-doped silicate fibers," *Optics letters*, vol. 34, no. 4, pp. 530–532, 2009.

[59] E. M. Dianov, K. E. Riumkin, M. A. Melkumov, and I. A. Bufetov, "Excited state absorption in bismuth-doped fibers with various glass compositions," in *Optical Fiber Communication Conference*. Optical Society of America, 2014, pp. Tu2D–5.

[60] K. E. Riumkin, M. A. Melkumov, I. A. Varfolomeev, A. V. Shubin, I. A. Bufetov, S. V. Firstov, V. F. Khopin, A. A. Umnikov, A. N. Guryanov, and E. M. Dianov, "Excited-state absorption in various bismuth-doped fibers," *Opt. Lett.*, vol. 39, no. 8, pp. 2503–2506, Apr 2014. [Online]. Available: http://ol.osa.org/abstract.cfm?URI=ol-39-8-2503

[61] K. Murata, Y. Fujimoto, T. Kanabe, H. Fujita, and M. Nakatsuka, "Bi-doped SiO2 as a new laser material for an intense laser," *Fusion Engineering and Design*, vol. 44, no. 1, pp. 437–439, 1999.

[62] Y. Fujimoto, "New infrared luminescence from Bi-doped glasses," in *Advances in Solid State Lasers Development and Applications*. InTech, 2010.

[63] V. Dvoyrin, V. Mashinsky, E. Dianov, A. Umnikov, M. Yashkov, and A. Guryanov, "Absorption, fluorescence and optical amplification in MCVD bismuth-doped silica glass optical fibres," in *Optical Communication, 2005. ECOC 2005. 31st European Conference on*, vol. 4. IET, 2005, pp. 949–950.

[64] T. Haruna, M. Kakui, T. Taru, S. Ishikawa, and M. Onishi, "Silica-based bismuth-doped fiber for ultra broad band light source and optical amplification around at 1.1μm," in *Optical Amplifiers and Their Applications*. Optical Society of America, 2005, p. MC3.

[65] N. S. Sadick and R. Weiss, "The utilization of a new yellow light laser (578nm) for the treatment of class I red telangiectasia of the lower extremities," *Dermatologic surgery*, vol. 28, no. 1, pp. 21–25, 2002.

[66] C. F. Blodi, S. R. Russell, J. S. Pulido, and J. C. Folk, "Direct and feeder vessel photocoagulation of retinal angiomas with dye yellow laser," *Ophthalmology*, vol. 97, no. 6, pp. 791–797, 1990.

[67] C. E. Max, S. S. Olivier, H. W. Friedman, J. An, K. Avicola, B. V. Beeman, H. D. Bissinger, J. M. Brase, G. V. Erbert, D. T. Gavel *et al.*, "Image improvement from a sodium-layer laser guide star adaptive optics system," *Science*, vol. 277, no. 5332, pp. 1649–1652, 1997.

[68] E. M. Dianov, V. Dvoyrin, V. Mashinsky, A. Umnikov, M. Yashkov, and A. Gur'yanov, "CW bismuth fibre laser," *Quantum Electronics (Woodbury, NY)*, vol. 35, no. 12, pp. 1083–1084, 2005.

[69] E. M. Dianov, A. V. Shubin, M. A. Melkumov, O. I. Medvedkov, and I. A. Bufetov, "High power CW bismuth fiber lasers," *JOSA B*, vol. 24, no. 8, pp. 1749–1755, 2007.

[70] V. Dvoyrin, V. Mashinsky, and E. Dianov, "Efficient bismuth-doped fiber lasers," *IEEE Journal of Quantum Electronics*, vol. 44, no. 9, pp. 834–840, 2008.

[71] S. Yoo, M. P. Kalita, J. K. Sahu, J. Nilsson, and D. Payne, "Bismuth-doped fiber laser at 1.16μm," in *Conference on Lasers and Electro-Optics*. Optical Society of America, 2008, p. CFL4.

[72] I. Razdobreev, L. Bigot, V. Pureur, A. Favre, G. Bouwmans, and M. Douay, "Efficient all-fiber bismuth-doped laser," *Applied physics letters*, vol. 90, no. 3, p. 031103, 2007.

[73] E. Dianov, V. Dvoyrin, V. Mashinsky, and O. Medvedkov, "Yellow frequency-doubled bismuth fibre laser," in *Optical Communications, 2006. ECOC 2006. European Conference on*. IEEE, 2006, pp. 1–2.

[74] A. Rulkov, A. Ferin, S. Popov, J. Taylor, I. Razdobreev, L. Bigot, and G. Bouwmans, "Narrow-line, 1178nm CW bismuth-doped fiber laser with 6.4W output for direct frequency doubling," *Optics Express*, vol. 15, no. 9, pp. 5473–5476, 2007.

[75] B. Chapman, E. Kelleher, K. Golant, S. Popov, and J. Taylor, "Amplification of picosecond pulses and gigahertz signals in bismuth-doped fiber amplifiers," *Optics letters*, vol. 36, no. 8, pp. 1446–1448, 2011.

[76] E. M. Dianov, S. V. Firstov, V. F. Khopin, A. N. Gur'yanov, and I. Bufetov, "Bi-doped fibre lasers and amplifiers emitting in a spectral region of 1.3μm," *Quantum Electronics*, vol. 38, no. 7, pp. 615–617, 2008.

[77] S. Firstov, I. Bufetov, V. Khopin, A. Shubin, A. Smirnov, L. Iskhakova, N. Vechkanov, A. Guryanov, and E. Dianov, "2W bismuth doped fiber lasers in the wavelength range 1300-1500nm and variation of Bi-doped fiber parameters with core composition," *Laser Physics Letters*, vol. 6, no. 9, p. 665, 2009.

[78] I. A. Bufetov, S. V. Firstov, V. F. Khopin, O. I. Medvedkov, A. N. Guryanov, and E. M. Dianov, "Bi-doped fiber lasers and amplifiers for a spectral region of 1300–1470nm," *Optics letters*, vol. 33, no. 19, pp. 2227–2229, 2008.

[79] I. A. Bufetov, M. A. Melkumov, V. F. Khopin, S. V. Firstov, A. V. Shubin, O. I. Medvedkov, A. N. Guryanov, and E. M. Dianov, "Efficient Bi-doped fiber lasers and amplifiers for the spectral region 1300-1500nm," in *Proceedings of SPIE, the International Society for Optical Engineering*. Society of Photo-Optical Instrumentation Engineers, 2010.

[80] S. Firstov, S. Alyshev, K. Riumkin, M. Melkumov, O. Medvedkov, and E. Dianov, "Watt-level, continuous-wave bismuth-doped all-fiber laser operating at 1.7μm," *Optics letters*, vol. 40, no. 18, pp. 4360–4363, 2015.

[81] S. V. Firstov, S. V. Alyshev, K. E. Riumkin, V. F. Khopin, A. N. Guryanov, M. A. Melkumov, and E. M. Dianov, "A 23dB bismuth-doped optical fiber amplifier for a 1700-nm band," *Scientific Reports*, vol. 6, 2016.

[82] E. M. Dianov, A. A. Krylov, V. V. Dvoyrin, V. M. Mashinsky, P. G. Kryukov, O. G. Okhotnikov, and M. Guina, "Mode-locked Bi-doped fiber laser," *JOSA B*, vol. 24, no. 8, pp. 1807–1808, 2007.

[83] S. Kivistö, J. Puustinen, M. Guina, O. Okhotnikov, and E. Dianov, "Tunable mode-locked bismuth-doped soliton fibre laser," *Electronics Letters*, vol. 44, no. 25, pp. 1456–1458, 2008.

[84] S. Kivisto, R. Gumenyuk, J. Puustinen, M. Guina, E. M. Dianov, and O. G. Okhotnikov, "Mode-locked Bi-doped all-fiber laser with chirped fiber bragg grating," *IEEE Photonics Technology Letters*, vol. 21, no. 9, pp. 599–601, 2009.

[85] A. A. Krylov, P. G. Kryukov, E. M. Dianov, and O. G. Okhotnikov, "Picosecond pulse generation in a passively mode-locked Bi-doped fibre laser," *Quantum Electronics*, vol. 39, no. 10, pp. 882–886, 2009.

[86] B. H. Chapman, E. J. Kelleher, S. V. Popov, K. M. Golant, J. Puustinen, O. Okhotnikov, and J. R. Taylor, "Picosecond bismuth-doped fiber MOPFA for frequency conversion," *Optics letters*, vol. 36, no. 19, pp. 3792–3794, 2011.

[87] E. Kelleher, J. Travers, Z. Sun, A. Ferrari, K. Golant, S. Popov, and J. Taylor, "Bismuth fiber integrated laser mode-locked by carbon nanotubes," *Laser Physics Letters*, vol. 7, no. 11, p. 790, 2010.

[88] V. V. Dvoyrin, V. M. Mashinsky, and E. Dianov, "Yb-Bi pulsed fiber lasers," *Optics letters*, vol. 32, no. 5, pp. 451–453, 2007.

[89] R. Gumenyuk, J. Puustinen, A. V. Shubin, I. A. Bufetov, E. M. Dianov, and O. G. Okhotnikov, "1.32μm mode-locked Bi-doped fiber laser operating in anomalous and normal dispersion regimes," *Optics letters*, vol. 38, no. 20, pp. 4005–4007, 2013.

[90] T. Noronen, M. Melkumov, D. Stolyarov, V. F. Khopin, E. Dianov, and O. G. Okhotnikov, "All-fibre fiber system for femtosecond pulse generation, compression, and energy scaling," *Optics letters*, vol. 40, no. 10, pp. 2217–2220, 2015.

[91] A. Khegai, M. Melkumova, K. Riumkina, V. Khopinc, F. Afanasievc, D. Myasnikovd, and E. Dianova, "Figure-of-eight fibre doped fiber laser operating at 1.3microns in dissipative soliton regime," in *Proc. of SPIE Vol*, vol. 10083, 2017, pp. 100 830A–1.

[92] M. Jung, M. Melkumov, V. Khopin, E. Dianov, J. Kim, and J. Lee, "Self-Q-switching of a bismuth-doped germanosilicate fiber laser operating at 1.46μm," *Laser Physics Letters*, vol. 10, no. 12, p. 125104, 2013.

[93] M. Jung, J. Lee, M. Melkumov, V. Khopin, E. Dianov, and J. Lee, "Burst-mode pulse generation from a fibre-doped germanosilicate fiber laser through self Q-switched mode-locking," *Laser Physics Letters*, vol. 11, no. 12, p. 125102, 2014.

[94] R. Gumenyuk, M. Melkumov, V. Khopin, E. Dianov, and O. Okhotnikov, "Effect of absorption recovery in bismuth-doped silica glass at 1450nm on soliton grouping in fiber laser," *Scientific reports*, vol. 4, p. 7044, 2014.

[95] J. Rissanen, D. A. Korobko, I. O. Zolotovsky, M. Melkumov, V. F. Khopin, and R. Gumenyuk, "Infiltrated bunch of solitons in Bi-doped frequency-shifted feedback fibre laser operated at 1450nm," *Scientific Reports*, vol. 7, 2017.

[96] T. Noronen, S. Firstov, E. Dianov, and O. G. Okhotnikov, "1700nm dispersion managed mode-locked fibre fiber laser," *Scientific reports*, vol. 6, 2016.

[97] A. Khegai, M. Melkumov, K. Riumkin, V. Khopin, S. Firstov, and E. Dianov, "Nalm-based bismuth-doped fiber laser at 1.7 μm," *Opt. Lett.*, vol. 43, no. 5, pp. 1127–1130, Mar 2018. [Online]. Available: http://ol.osa.org/abstract.cfm?URI=ol-43-5-1127

[98] K. E. Riumkin, M. A. Melkumov, I. A. Bufetov, A. V. Shubin, S. V. Firstov, V. F. Khopin, A. N. Guryanov, and E. M. Dianov, "Superfluorescent 1.44μm fibre-doped fiber source," *Optics letters*, vol. 37, no. 23, pp. 4817–4819, 2012.

[99] K. E. Riumkin, M. A. Mel'kumov, A. V. Shubin, S. V. Firstov, I. Bufetov, V. F. Khopin, A. N. Gur'yanov, and E. M. Dianov, "Superfluorescent 1.34μm bismuth-doped fibre source," *Quantum Electronics*, vol. 44, no. 7, p. 700, 2014.

[100] S. V. Firstov, S. Alyshev, K. Riumkin, A. Khegai, A. Kharakhordin, M. Melkumov, and E. M. Dianov, "Laser-active fibers doped with bismuth for a wavelength region of 1.6-1.8 μm," *IEEE Journal of Selected Topics in Quantum Electronics*, 2018.

[101] R. Horley, S. Norman, and M. N. Zervas, "Progress and development in fibre laser technology," in *Proc. SPIE*, vol. 6738, 2007, p. 67380K.

[102] S. Jain, T. May-Smith, A. Dhar, A. Webb, M. Belal, D. Richardson, J. Sahu, and D. Payne, "Erbium-doped multi-element fiber amplifiers for space-division multiplexing operations," *Optics letters*, vol. 38, no. 4, pp. 582–584, 2013.

[103] S. Jain, N. K. Thipparapu, P. Barua, and J. K. Sahu, "Cladding-pumped Er/Yb-doped multi-element fiber amplifier for wideband applications," *IEEE Photonics Technology Letters*, vol. 27, no. 4, pp. 356–358, 2015.

[104] S. Jain, Y. Jung, T. May-Smith, S. Alam, J. Sahu, and D. Richardson, "Few-mode multi-element fiber amplifier for mode division multiplexing," *Optics express*, vol. 22, no. 23, pp. 29 031–29 036, 2014.

[105] S. Jain, V. Rancaño, T. May-Smith, P. Petropoulos, J. Sahu, and D. Richardson, "Multi-element fiber technology for space-division multiplexing applications," *Optics express*, vol. 22, no. 4, pp. 3787–3796, 2014.

[106] V. J. Rancaño, S. Jain, T. C. May-Smith, E. Hugues-Salas, S. Yan, G. Zervas, D. Simeonidou, P. Petropoulos, and D. J. Richardson, "Demonstration of space-to-wavelength conversion in SDM networks," *IEEE Photonics Technology Letters*, vol. 27, no. 8, pp. 828–831, 2015.

[107] S. Yan, E. Hugues Salas, V. J. Rancaño, Y. Shu, G. M. Saridis, B. R. Rofoee, Y. Yan, A. Peters, S. Jain, T. May-Smith *et al.*, "Archon: A function programmable optical interconnect architecture for transparent intra and inter data

center SDM/TDM/WDM networking," *Journal of Lightwave Technology*, vol. 33, no. 8, pp. 1586–1595, 2015.

[108] A. Ghatak and K. Thyagarajan, *An introduction to fiber optics*. Cambridge university press, 1998.

[109] Agilent Technologies. EDFA Testing with the Interpolation Technique. [Online]. Available: https://www.atecorp.com/ATECorp/media/pdfs/data-sheets/Agilent-8168C_Application_Note.pdf

[110] S. W. Rhee and S. W. Kang, "Yttrium-doped bismuth titanate thin film and preparation thereof," Jul. 31 2007, united States Patent 7,250,228.

[111] Y. Fujimoto and M. Nakatsuka, "Optical amplification in bismuth-doped silica glass," *Applied physics letters*, vol. 82, no. 19, pp. 3325–3326, 2003.

[112] K. Bizheva, A. Unterhuber, B. Hermann, B. PovazË, H. Sattmann, W. Drexler, A. Stingl, T. Le, M. Mei, R. Holzwarth *et al.*, "Imaging ex vivo and in vitro brain morphology in animal models with ultrahigh resolution optical coherence tomography," *Journal of biomedical optics*, vol. 9, no. 4, pp. 719–724, 2004.

[113] A. Shubin, I. Bufetov, M. Melkumov, S. Firstov, O. Medvedkov, V. Khopin, A. Guryanov, and E. Dianov, "Bismuth-doped silica-based fiber lasers operating between 1389 and 1538nm with output power of up to 22W," *Optics letters*, vol. 37, no. 13, pp. 2589–2591, 2012.

[114] Y. S. Seo, Y. Fujimoto, and M. Nakatsuka, "Optical amplification in a bismuth-doped silica glass at 1300nm telecommunications window," *Optics communications*, vol. 266, no. 1, pp. 169–171, 2006.

[115] E. M. Dianov, "Amplification in extended transmission bands using bismuth-doped optical fibers," *Journal of Lightwave Technology*, vol. 31, no. 4, pp. 681–688, 2013.

[116] M. Melkumov, I. Bufetov, A. Shubin, S. Firstov, V. Khopin, A. Guryanov, and E. Dianov, "Laser diode pumped bismuth-doped optical fiber amplifier for 1430nm band," *Optics letters*, vol. 36, no. 13, pp. 2408–2410, 2011.

[117] V. V. Dvoyrin, A. V. Kir'yanov, V. M. Mashinsky, O. I. Medvedkov, A. A. Umnikov, A. N. Guryanov, and E. M. Dianov, "Absorption, gain, and laser action in bismuth-doped aluminosilicate optical fibers," *IEEE Journal of Quantum Electronics*, vol. 46, no. 2, pp. 182–190, 2010.

[118] K. Riumkin, M. Melkumov, I. Varfolomeev, A. Shubin, I. Bufetov, S. Firstov, V. Khopin, A. Umnikov, A. Guryanov, and E. Dianov, "Excited state absorption

in various bismuth-doped fibers," *Optics letters*, vol. 39, no. 8, pp. 2503–2506, 2014.

[119] E. Martin and K. Wilhelm. Developing a new guide star laser system for the very large telescope. [Online]. Available: https://www.azooptics.com/Article.aspx?ArticleID=1129

[120] M. Enderlein and W. Kaenders. Using a guide star laser as an astronomical point of reference for increased image resolution. [Online]. Available: https://www.azooptics.com/Article.aspx?ArticleID=1059

[121] N. K. Thipparapu, S. Jain, A. Umnikov, P. Barua, and J. Sahu, "1120nm diode-pumped Bi-doped fiber amplifier," *Optics letters*, vol. 40, no. 10, pp. 2441–2444, 2015.

[122] N. K. Thipparapu, A. A. Umnikov, S. Jain, P. Barua, and J. K. Sahu, "Diode pumped Bi-doped fiber laser operating at 1360nm," in *Workshop on Specialty Optical Fibers and their Applications*. Optical Society of America, 2015, pp. WT1A–5.

[123] P. J. Winzer, "Making spatial multiplexing a reality," *Nature Photonics*, vol. 8, no. 5, pp. 345–348, 2014.

[124] Corning. Corning smf-28 ultra-low loss optical fiber. [Online]. Available: https://www.artisantg.com

[125] OFS. All wave low loss fiber (zero water peak). [Online]. Available: http://fiberopticcatalog.ofsoptics.com/Asset/AllWaveLowLossZWP153web.pdf

[126] Y. S. Seo, C. H. Lim, Y. Fujimoto, and M. Nakatsuka, "9.6dB gain at a 1310nm wavelength for a bismuth-doped fiber amplifier," *Journal of the Optical Society of Korea*, vol. 11, no. 2, pp. 63–66, 2007.

[127] S. Norizan, W. Chong, S. Harun, and H. Ahmad, "O-band bismuth-doped fiber amplifier with double-pass configuration," *IEEE Photonics Technology Letters*, vol. 23, no. 24, pp. 1860–1862, 2011.

[128] N. K. Thipparapu, S. Jain, A. Umnikov, P. Barua, and J. Sahu, "1120nm diode-pumped Bi-doped fiber amplifier," *Optics letters*, vol. 40, no. 10, pp. 2441–2444, 2015.

[129] E. M. Dianov, M. A. Mel'kumov, A. V. Shubin, S. V. Firstov, V. F. Khopin, A. N. Gur'yanov, and I. Bufetov, "Bismuth-doped fibre amplifier for the range 1300-1340nm," *Quantum electronics*, vol. 39, no. 12, p. 1099, 2009.

[130] D. J. Richardson, J. Nilsson, and W. A. Clarkson, "High power fiber lasers: current status and future perspectives," *J. Opt. Soc. Am. B*, vol. 27, no. 11, pp. B63–B92, Nov 2010.

[131] L. Nelson, D. Jones, K. Tamura, H. Haus, and E. Ippen, "Ultrashort-pulse fiber ring lasers," *Applied Physics B*, vol. 65, no. 2, pp. 277–294, 1997.

[132] A. B. Rulkov, A. A. Ferin, S. V. Popov, J. R. Taylor, I. Razdobreev, L. Bigot, and G. Bouwmans, "Narrow-line, 1178nm cw bismuth-doped fiber laser with 6.4w output for direct frequency doubling," *Opt. Express*, vol. 15, no. 9, pp. 5473–5476, Apr 2007.

[133] N. K. Thipparapu, A. A. Umnikov, P. Barua, and J. K. Sahu, "Bi-doped fiber amplifier with a flat gain of 25dB operating in the wavelength band 1320–1360nm," *Optics letters*, vol. 41, no. 7, pp. 1518–1521, 2016.

[134] G. P. Agrawal, *Nonlinear fiber optics*. Academic press, 2007.

[135] R. Gumenyuk and O. G. Okhotnikov, "Temporal control of vector soliton bunching by slow/fast saturable absorption," *JOSA B*, vol. 29, no. 1, pp. 1–7, 2012.

[136] Soliton. [Online]. Available: https://en.wikipedia.org/wiki/Soliton_(optics)

[137] L. Nelson, D. Jones, K. Tamura, H. Haus, and E. Ippen, "Ultrashort-pulse fiber ring lasers," *Applied Physics B: Lasers and Optics*, vol. 65, no. 2, pp. 277–294, 1997.

[138] R. Paschotta, *Field Guide to Laser Pulse Generation*. SPIE Press, 2008.

[139] *FR-103MN Autocorrelator Instruction Manual*.

[140] D. Korobko, R. Gumenyuk, I. Zolotovskii, and O. Okhotnikov, "Multisoliton complexes in fiber lasers," *Optical Fiber Technology*, vol. 20, no. 6, pp. 593–609, 2014.

[141] D. Noske, N. Pandit, and J. Taylor, "Source of spectral and temporal instability in soliton fiber lasers," *Optics letters*, vol. 17, no. 21, pp. 1515–1517, 1992.

[142] J. Lee, J. Koo, Y. M. Jhon, and J. H. Lee, "A femtosecond pulse erbium fiber laser incorporating a saturable absorber based on bulk-structured Bi2Te3 topological insulator," *Optics express*, vol. 22, no. 5, pp. 6165–6173, 2014.

[143] P. Winzer, "Spatial multiplexing: The next frontier in network capacity scaling," *IET Conference Proceedings*, 2013.

[144] M. A. Arbore, Y. Zhou, G. Keaton, and T. Kane, "34dB gain at 1500nm in S-band EDFA with distributed ASE suppression," in *Optical Communication, 2002. ECOC 2002. 28th European Conference on*, vol. 1. IEEE, 2002, pp. 1–2.

[145] S. W. Harun, K. Dimyati, K. K. Jayapalan, and H. Ahmad, "An overview on S-band erbium-doped fiber amplifiers," *Laser Physics Letters*, vol. 4, no. 1, p. 10, 2007.

[146] F. A. Flood, "L-band erbium-doped fiber amplifiers," in *Optical Fiber Communication Conference, 2000*, vol. 2. IEEE, 2000, pp. 102–104.

[147] S. W. Harun, N. M. Samsuri, and H. Ahmad, "Gain enhancement in partial double-pass L-band EDFA system using a band-pass filter," *Laser Physics Letters*, vol. 2, no. 1, p. 36, 2004.

[148] C. Jiang, W. Hu, Q. Zeng, and S. Xiao, "Novel split-band erbium-doped fiber amplifier," *Optics & Laser Technology*, vol. 35, no. 4, pp. 251–256, 2003.

[149] B. A. Hamida, X. Cheng, S. W. Harun, A. Naji, H. Arof, S. Khan, W. Alkhateeb, and H. Ahmad, "Wideband and compact erbium-doped fiber amplifier using parallel double-pass configuration," *Microwave and Optical Technology Letters*, vol. 54, no. 3, pp. 629–631, 2012.

[150] S. Chernikov, S. Lewis, and J. Taylor, "Broadband Raman amplifiers in the spectral range of 1480-1620nm," in *Optical Fiber Communication Conference, 1999, and the International Conference on Integrated Optics and Optical Fiber Communication. OFC/IOOC'99. Technical Digest*, vol. 2. IEEE, 1999, pp. 117–119.

[151] H. Kidorf, K. Rottwitt, M. Nissov, M. Ma, and E. Rabarijaona, "Pump interactions in a 100nm bandwidth Raman amplifier," *IEEE Photonics Technology Letters*, vol. 11, no. 5, pp. 530–532, 1999.

[152] H. Masuda, "Review of wideband hybrid amplifiers," in *Optical Fiber Communication Conference, 2000*, vol. 1. IEEE, 2000, pp. 2–4.

[153] S. Jain, T. C. May-Smith, and J. K. Sahu, "Cladding-pumped Er/Yb-doped multi-element fiber amplifier for C+L band operations," *Optical Fiber Communication Conference*, p. M2J.3, 2014.

[154] J. Saurabh, T. C. May-Smith, and J. K. Sahu, "Er/Yb-doped cladding pumped multi-element fiber amplifier," *Workshop on Specialty Optical Fibers and their Applications*, p. W5.4, 2013.

[155] S. Alam, A. Harker, R. Horley, F. Ghiringhelli, M. Varnham, P. Turner, M. Zervas, and S. Norman, "All-fibre, high power, cladding-pumped 1565nm MOPA pumped by high brightness 1535nm pump sources," *Lasers and Electro-Optics Conference*, pp. 1–2, 2008.

[156] N. Thipparapu, S. Jain, T. May-Smith, and J. Sahu, "Wideband multi-element er-doped fiber amplifier," *Laser Physics Letters*, vol. 11, no. 9, p. 095104, 2014.

[157] N. K. Thipparapu, G. Chunyun, A. A. Umnikov, P. Barua, A. Taranta, S. Alam, and J. K. Sahu, "Self-mode-locked bismuth-doped fiber laser operating at 1340nm," in *CLEO/Europe 2017*. Optical Society of America, 2017, p. 1.